Solar Mild Carbonization (Torrefaction) Characteristics of Solid Olive Mill Residue With a Solar Furnace

Nemika Cellatoğlu

Submitted to the
Institute of Graduate Studies and Research
in partial fulfillment of the requirements for the degree of

Doctor of Philosophy
in
Physics

Eastern Mediterranean University
September 2016
Gazimağusa, North Cyprus

ABSTRACT

Solar energy and biomass are two attractive renewable energy resources which gained special interest in recent years. However, problems like storage are preventing efficient and cheap utilization of solar energy and biomass. Mild carbonization which is also known as torrefaction; is a thermochemical pretreatment method for biomass which changes the structure of raw biomass and yields more energy denser solid fuel. Besides increasing the energy density, torrefaction results with a hydrophobic fuel that can be stored for longer periods without degradation. In this thesis, torrefaction characteristics of Solid Olive Mill Residue (SOMR) were investigated. Also, effect of torrefaction on carbonization characteristics of SOMR is studied. Results obtained from torrefaction experiments showed that SOMR is very suitable type of biomass for torrefaction process. SOMR is mainly produced in Mediterranean Basin which enjoys abundance of solar energy. This fact motivated solar torrefaction experiments with SOMR. A solar furnace; which named "parabolic dish solar torreffier" is designed and tested. Solar torrefaction experiments revealed that solar torrefaction results with more value added solid fuel similar to torrefaction process. This study is also important because of demonstrating that, solar energy can be used to produce a transportable solid fuel, rather than Hydrogen.

Keywords: Biomass, Solar Thermal Energy, Torrefaction, Carbonization, Pyrolysis

ÖZ

Güneş enerjisi ve biyokütle kullanım potansiyelleri oldukça yüksek yenilenebilir enerji kaynaklarıdır. Bununla birlikte güneş enerjisinin depolama problemi ve taşınamıyor oluşu etkin biçimde kullanımını engellemektedir. Aynı şekilde, biyokütlenin yapısı dolayısı ile düşük enerji yoğunluğuna sahip oluşu ve yüksek nem içeriği kullanımı ve depolanması açısından sıkıntı yaratmaktadır. Bu da uzun vadeli kullanımı engellemektedir. Termokimyasal bir ön işlem olan torifikasyon, biyokütlenin yapısını değiştirerek hem enerji yoğunluğu daha yüksek, hemde hidrofobik yapıda bir yakıt üretmektedir. Bu tezde bir biyokütle çeşidi olan pirinanın torifikasyon özellikleri incelenmiştir. Biyokütle seçimi elemental içerik, yüksek ısı değeri ve nem içeriği değerlerine göre yapılmıştır. Bu tezde ayrıca, pirinanın özellikle Akdeniz Bölgesinde üretilen bir tarımsal atık olması göz önünde bulundurularak, torifikasyon islemi için termal güneş enerjisi kullanılması önerilmiştir. Torifikasyon deneylerinin sonuçları, pirinanın bu proses için oldukça uygun bir biyokütle olduğunu göstermiştir.

Ayrıca güneş enerjisi kullanılarak gerçekleştirilen torifikasyon işlemi, değeri daha yüksek bir yakıt oluşturmaktadır. Bu çalışma, güneş enerjisinin bir güneş yakıtına (Hidrojen dışında) dönüştürülmesi ile dolaylı da olsa taşınabilien bir yakıta dönüştürülebileceğini göstermesi açısından önemlidir.

Anahtar Kelimeler: Biyokütle, Güneş Enerjisi, Torifikasyon, Karbonizasyon, Piroliz

To my family

ACKNOWLEDGMENT

I would like to sincerely thank my supervisor Assoc. Prof. Dr. Mustafa İlkan for his valuable guidance and continous encouragement during this work.

I wish to express my appreciation to the staff of Engineering Faculty of European University of Lefke and Physics Department of Eastern Mediterrenean University. I am grateful for their confidence to me.

Special thanks to my family for their support and patience. Thanks in advance to Ernur and Erciyas families for their kindness and invaluable support.

TABLE OF CONTENTS

LIST OF TABLES

LIST OF FIGURES

LIST OF ABBREVIATIONS

a	Radius of Receiver
b	Radius of Circular Parabolic Dish Collector
f	Focal Length
h	Height of Parabolic Dish Collector
m_F	Mass of Torrefied Biomass
r_s	Radius of Sun
K	Angular Acceptance Function
k	Reaction Rate Constant
F	Amount of Intercepted Solar Radiation
R	Distance From Sun to Collector
S	Surface Area of Parabolic Dish Collector
T	Temperature of Receiver
A_r	Area of Receiver
C_G	Geometric Concentration Ratio
C_o	Optical Concentration Ratio
E_a	Activation Energy
$E_{receiver \rightarrow sun}$	Radiation reaching from receiver to sun
$F_{sun \rightarrow collector}$	Radiation Captured by Collector
I_o	Incident Insolation
I_r	Incident Radiation on Receiver Area
M_F	Mass of Unreacted Biomass
R_{M_F}	Mass of unreacted biomass to initial mass
R_{m_F}	Mass of torrefied biomass to inital mass
T_s	Temperature of Sun

T_L	Ambient Temperature
$T_{stagnation}$	Stagnation Temperature
$Q_{concentrator \rightarrow Receiver}$	Radiation coming to receiver
Q_{sun}	Amount of Radiation emitted by Sun
$Q_{Receiver}$	Amount of Radiation emitted by Receiver
α	Absorption Coefficient
ε	Emittance
θ	Incidence Angle
σ	Stefan Boltzman Constant
θ_l	Major Axis
θ_s	Minor Axis
$\eta_{absorption}$	Absorption efficiency
η_{exergy}	Exergy efficiency
Φ	Rim Angle of Parabolic Dish Collector
CPC	Compound Parabolic Collector
CT	Carbonization Temperature
EPC	Flat Plate Solar Collector
ETC	Evacuated Tube Collector
FC	Fixed Carbon
HFC	Heliostat Field Reflector
HHV	Higher Heating Value
LFR	Linear Fresnel Reflector
ORC	Organic Rankine Cycle
PDC	Parabolic Dish Collector
PTC	Parabolic Trough Collector
TGA	Thermogravimetric Analysis
VM	Volatile Matter

SOMR	Solid Olive Mill Residue
T30	Solid Olive Mill Residue torrefied at 280^{o}C for 30 minutes
T120	Solid Olive Mill Residue torrefied at 280^{o}C for 120 minutes
S1	Solar Torrefied Sample 1
S2	Solar Torrefied Sample 2
S3	Solar Torrefied Sample 3

Chapter 1

INTRODUCTION

1.1 Fossil Fuel Consumption and Production

Energy is one of the most important factors, for economic development and for improving quality of life [1]. Providing adequate energy is important for overcoming poverty and rising life standards all around the world [2]. Currently, fossil fuels dominate the energy market and provide 78.4% of total energy demand [3]. Global rate of change in fossil fuel consumption and production between 2013 and 2015 are demonstrated in Figure 1 and Figure 2 respectively [4].

Figure 1 clearly indicates that, the coal production significantly reduced between 2013 and 2015. Similar behavior, in consumption of natural gas and oil was observed between 2013 and 2014. Contrary, statistics showed that the combustion of natural gas and oil have been risen by rate of 1.7% and 1.9% respectively in 2015.

Figure 2 shows that, the rate of fossil fuel production rise between 2013 and 2015, except coal. However, the rise in production rate was very close to rise in consumption rate. The finite structure of fossil fuels motivated researchers to calculate depletion time of fossil fuels. Calculations based on econometric model showed that depletion time of oil, gas and coal are 24, 26 and 96 years, respectively, which showed that coal will be available up to 2112[5].

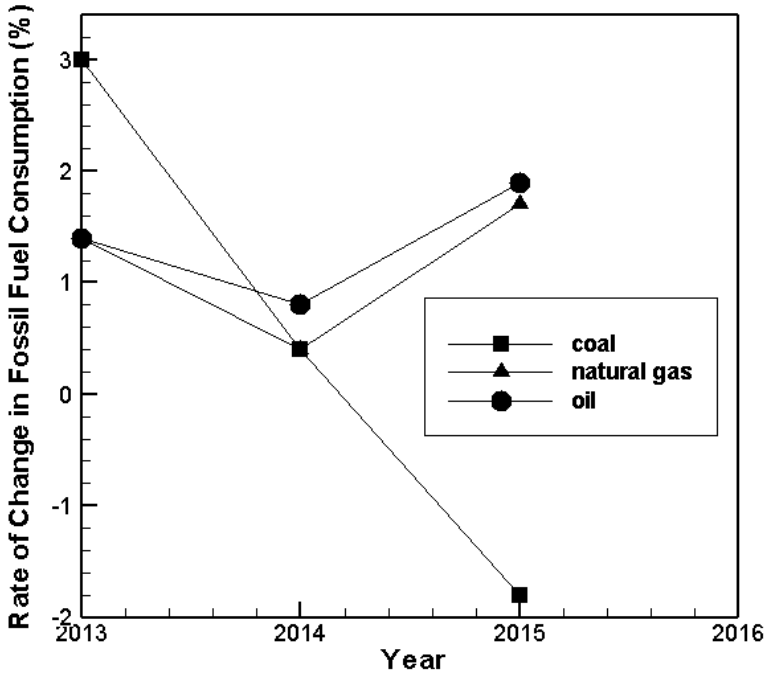

Figure 1. Rate of Change in Fossil Fuel Consumption between 2013 and 2015 [5].

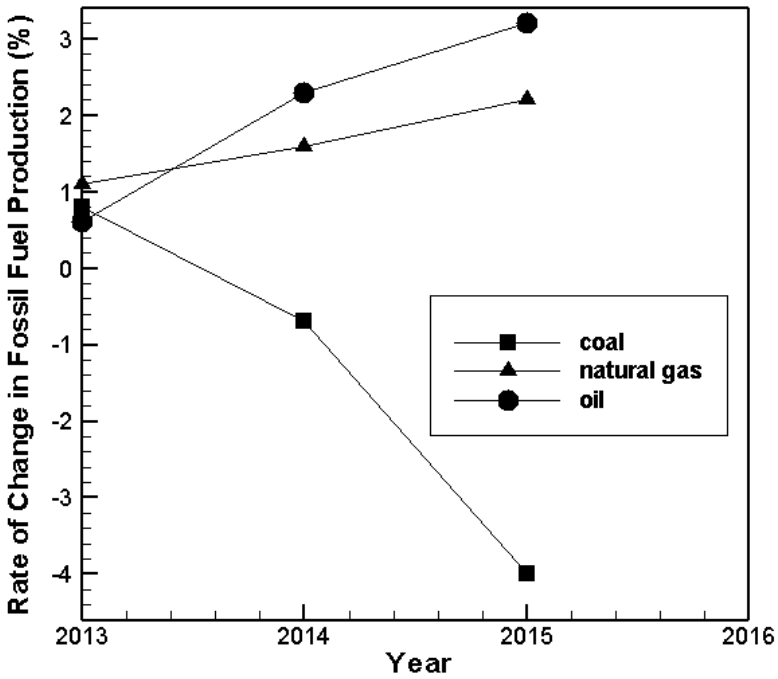

Figure 2. Rate of Change in Fossil Fuel Production between 2013 and 2015 [5].

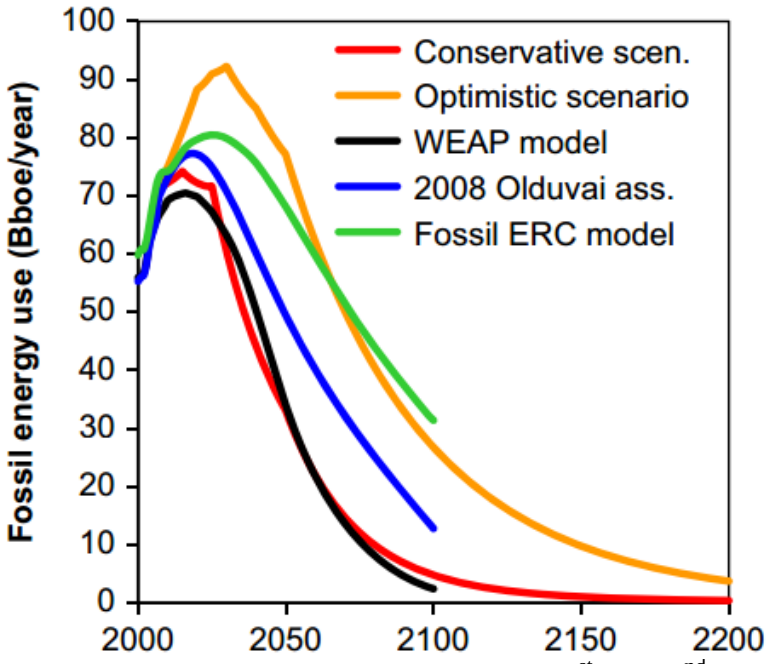

Figure 3. The projections of fossil energy use for the 21st and 22nd centuries [6].

Besides econometric model, other models based on Hubert's peak theory were also used for calculation of the depletion time of fossil fuels [6]. Figure 3, demonstrates the projection of fossil fuel use; computed by different researchers and different models. All models, shown in Figure 3, are indicating that the fossil fuels will deplete around 2100-2200 with current reserves and alternative energy resources are emerging.

1.2 Environmental Problems Associated with Fossil Fuel Consumption

The population of world is increasing exponentially [7], with increasing demand of energy. Main problems, associated with the consumption of current fossil fuels are their finite structure and environmental problems they caused. Gaseous pollutants; Carbon Dioxide (CO_2), Sulphur Dioxide (SO_2), Carbon Monoxide (CO), Nitrogen Oxides (NO_x) and Volatile Organic Compounds are emitted during the combustion of fossil fuels. Emission of those gaseous pollutants, results with environmental

problems; global climate change, acid rain and ozone depletion. The contribution of each pollutant to listed environmental problems is given in Table 1 [8].

The contribution of each gas to associated environmental problem is illustrated by "✓". The "✓/-" represents that; effect depends on the rate of increase in atmospheric concentration. Table 1 shows that, fossil fuel consumption remarkably contributes to greenhouse effect which results to global climate change. Most harmful greenhouse gasses are listed in Table 2 [9]. Carbon dioxide is considered as the reference greenhouse gas. Table 2, shows that Methane (CH_4) and Nitrogen Dioxide (N_2O) are much powerful greenhouse gases compared to Carbon Dioxide (CO_2). However, rise in atmospheric concentration of carbon dioxide, makes it the most hazardous greenhouse gas. Şen [8] stated that; CO_2 provides 60% of anthropogenic greenhouse effect because of its significant rise in concentration [8]. Statistics showed that, the global mean temperature increased by about 0.8^oC in the last century and resulted to 0.20 m rise in sea level [9, 10].

Table 1. Gaseous pollutants emitted from combustion of fossil fuels and their contribution on environmental problems [8].

Gaseous pollutants	**Greenhouse effect**	**Ozone depletion**	**Acid rain**
Sulphur Dioxide (SO_2)	-	✓	✓
Carbon Monoxide (CO)	✓	✓ /-	-
Carbon Dioxide (CO_2)	✓	✓ /-	-
Nitrogen Oxides (NO_x)	✓ /-	✓	✓

Table 2. Rise in atmospheric concentration and greenhouse gas effect of major greenhouse gases [8].

Greenhouse gas	Rise inConcentration (ppm)	Greenhouse effect
CO_2	90	1
CH_4	1	25
N_2O	0.04	300

It is also estimated that the temperature of earth will increase by rate of 2-4^oC in coming century, if the emission of greenhouse gases, mainly from combustion of fossil fuels, will continue to increase with current rate [9].

1.3 Alternative Energy Resources

Finite structure of fossil fuels and environmental problems associated with their combustion emerges long term, clean and sustainable energy resources with following properties [11]:

- Being available and sustainable for future.
- Having acceptable cost limits for economic growth.
- Being politically reliable.
- Being environment friendly and do not contribute climate change.

Renewable energy sources fulfill all above properties, by providing clean, environmental friendly fuel with emission of no or less amount of greenhouse gases. Renewable energy provided 19% of global final energy consumption in 2012, and it is expected to grow in coming years [3]. The most important concerns, which prevent higher contribution of renewables to total energy consumption, are the cost

effectiveness [8] and transfer-storage difficulties /impossibility. However, the cost of renewable energy systems is becoming competitive with conventional forms of energy in recent years [8] but transfer-storage difficulty still prevents efficient utilization of renewable energy.

1.4 Biomass and Solar Energy

Solar energy is the fundamental source of all types of energy including fossil fuels, except nuclear. Solar energy is used in several systems such as cooking, hot water generation, electricity generation, hydrogen production and etc. Although several technologies exist for utilization of solar energy, storage difficulty prevents its more efficient usage.

Biomass is the only source of renewable energy which can be directly transported from one place to another. As mentioned earlier, the high moisture content of biomass results with rapid degradation and prevents its long term storage. Also, low bulk density, hydrophilic nature and low energy density are important drawbacks associated with biomass usage.

1.5 Mild Carbonization (Torrefaction) of Solid Olive Mill Residue and Solar Mild Carbonization of Solid Olive Mill Residue

Biomass treatment and pretreatment methods aim to produce more valuable solid, liquid and gas energy carriers from biomass. Mild Carbonization is a thermochemical biomass pretreatment method which upgrades the fuel properties of raw biomass. The process is also named as torrefaction. Mild Carbonization provides more energy denser and hydrophobic fuel. The process is conducted at 200-300^{o}C under inert conditions.

SOMR is an attractive source of biomass especially for Mediterranean Basin. SOMR is a seasonally produced biomass. It contains high amount of carbon and has high Higher Heating Value (HHV). Long-term storage of raw SOMR is difficult due to its high moisture content (around 40%-three phase systems). An upgrading pretreatment is required in order to provide long term and efficient utilization of SOMR.

In this study, torrefaction characteristics of SOMR were investigated at three different torrefaction temperatures (210^{o}C, 240^{o}C and 280^{o}C) and three different holding times (30, 60 and 120 minutes). The properties of torrefied SOMR were compared with carbonized SOMR (400^{o}C, 30 minutes). Also, the effect of torrefaction on carbonization characteristics of SOMR was investigated at three different carbonization temperatures 350^{o}C, 400^{o}C and 450^{o}C.

SOMR is mainly produced in Mediterranean Basin, which enjoys the abundance of solar energy. Relatively low process temperature of torrefaction, and available solar energy in Mediterranean Basin, makes solar thermal energy an attractive source of energy for conducting mild carbonization process (solar torrefaction). Advantages of solar torrefaction can be listed as:

- Inefficient combustion of biomass will be prevented.
- Indirectly, transportation of solar energy will be possible.
- The process results with almost 100% renewable solid fuel.

Above listed merits of solar torrefaction, motivated the design of a solar furnace, for conducting the process. The solar furnace was constructed by using a parabolic dish collector and named as “parabolic dish solar torrefier”. The ultimate and proximate

analysis of solar torrefaction products showed that, more qualified fuel than raw SOMR can be produced by solar torrefaction.

Chapter 2

SOLAR COLLECTORS AND CURRENT APPLICATIONS

2.1 Solar Thermal Energy

The sun is source of almost all renewable energy, which occurrences can be listed as wind energy, wave energy, hydropower through the hydrological cycle and biomass [8]. The hydrogen is converted to helium at rate of; 4×10^6 tons per second by sun [9] with total energy output of 3.8×10^{20} MW [12]. Earth intercepts a very small amount of radiation, 1.7×10^{14} kW, emitted by sun [13].

Solar thermal energy can be utilized with different methods, and converted to electricity or solar fuels (hydrogen) with different routes as shown in Figure 4. The main component of solar thermal conversion systems is the solar collector. Solar collectors transform solar thermal radiation to internal energy of transport medium [9].

2.2 Solar Collectors

A solar collector absorbs incident radiation and converts it to thermal energy by using a heat transfer medium [10] or concentrate solar radiation to a smaller absorber area. Solar collectors can be classified in two groups as;

- Stationary Collectors
- Concentrating Collectors

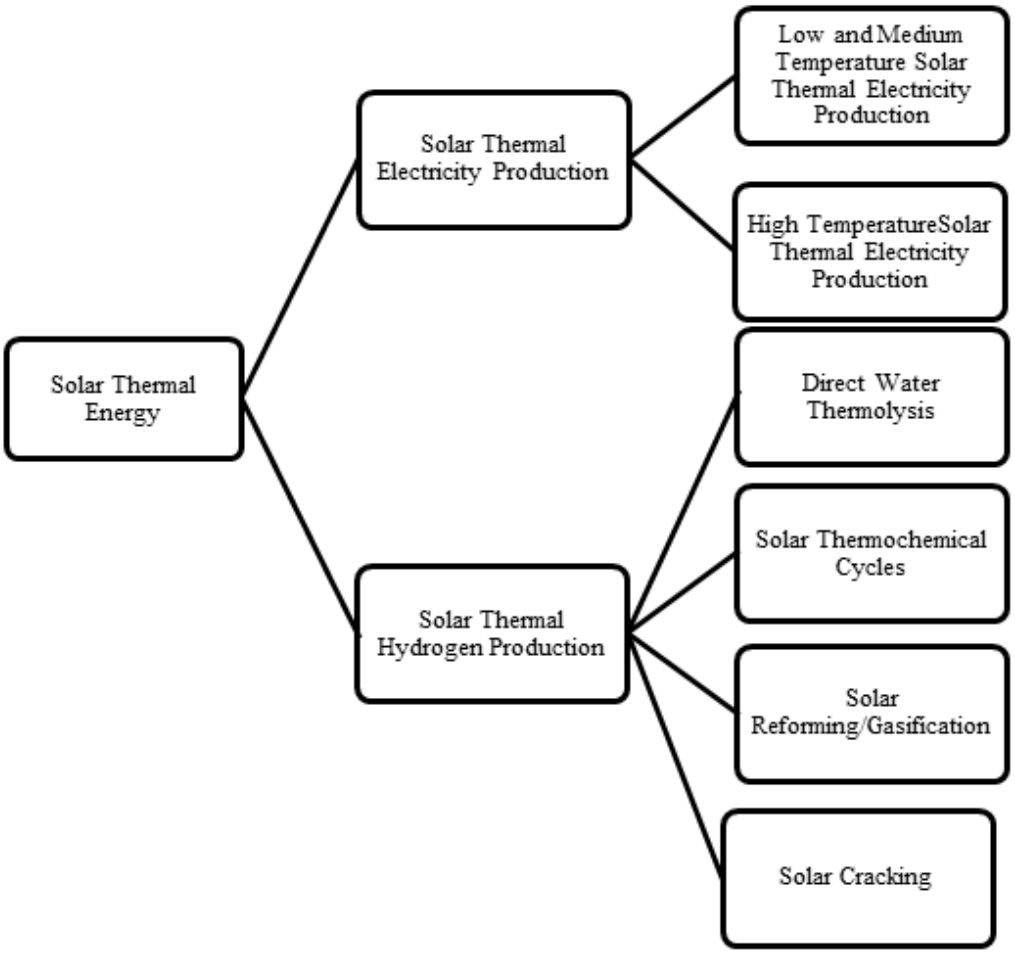

Figure 4. Routes of solar thermal energy conversion.

2.2.1 Stationary Collectors

Stationary collectors have fixed position. These collectors are used for conducting any low temperature process or for hot water generation. Stationary collectors can be listed as Flat Plate Collectors (FPC), Evacuated Tube Collectors (ETC), and Compound Parabolic Collectors (CPC). Schematic representation of FPC, ETC and CPC are given in Figure 5 (a), (b) and (c) respectively. The FPC has a black base which absorbs the solar radiation and a glazing cover to keep thermal energy inside the collector [8]. The glazing cover is made up of glass with high transmissivity of short-wave radiation and low transmissivity of long-wave radiation [14]. ETC is made up of two glass tubes one inside another. The inner tube is inside a vacuum.

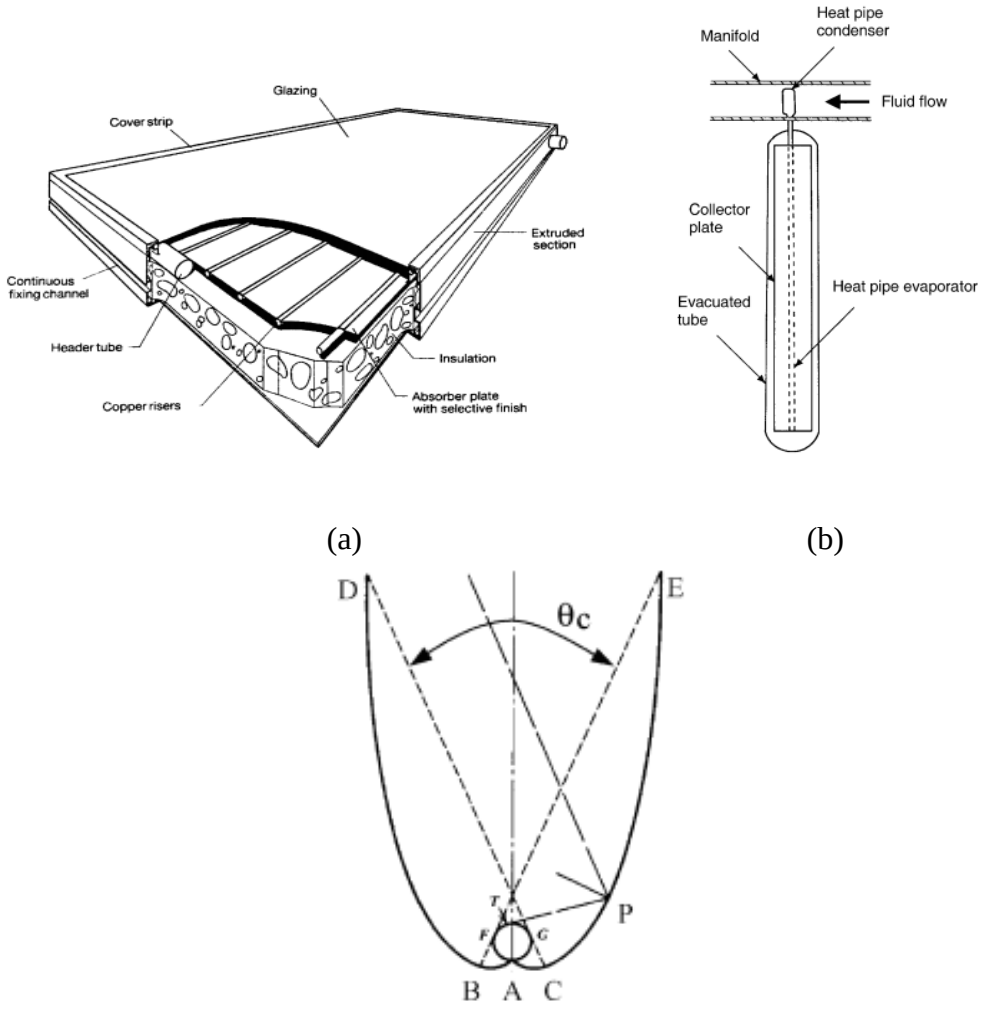

Figure 5. Schematic illustration of (a) FPC, (b) ETC, (c) CPC [9].

The inner tube is coated with a special coating for absorbing maximum solar heat and the outer tube is able to stand different climatic conditions [15]. ETCs are more suitable for cold and windy climates compared to FPT [16].

CPC consists of two sections of parabola. CPC concentrates solar radiation on to linear receiver of small transverse width [17]. The incoming radiation on CPC, is concentrated on the absorber by multiple internal reflections [9].The absorber is located at bottom of CPC as shown in Figure 5(c).

2.2.2 Concentrating Collectors

Concentrating collectors are generally used for high temperature process heat generation or electricity generation. Concentrating collectors use reflection or refraction principles to concentrate solar radiation on to a smaller area by use of mirrors and lenses [12]. There exist several different designs for concentrating collectors. However, main concentrating collectors can be listed as; Parabolic Trough Collectors (PTC), Parabolic Dish Collectors (PDC), Linear Fresnel Reflector (LRF) and Heliostat Field Collector (HFC). Schematic illustration of PTC, PDC, LRF and HFC are given in Figure 6 (a), (b), (c) and (d) respectively. PTC are manufactured by curving reflective sheet into a parabolic shape, and also known as line focus collectors [12]. The reflecting surface of PTC concentrates solar energy to linear receiver tube continuously, by tracking sun [18]. PTC can achieve temperature between 50^{o}C to 400^{o}C and can be used for process heat applications besides electricity production [9]. PDC concentrates solar energy to a point receiver, at focus of collector by tracking sun in two axes [12]. PDC can achieve temperatures higher than 1,500°C [19].

Parabolic dish collectors have important advantages compared to other collectors [12];

- Modular structure of parabolic dish collector receiver systems allow functioning independently as part of a large system of dishes.
- The concentration ratio of PDC is ranging from 600 to 2,000, with high efficient thermal energy absorption.

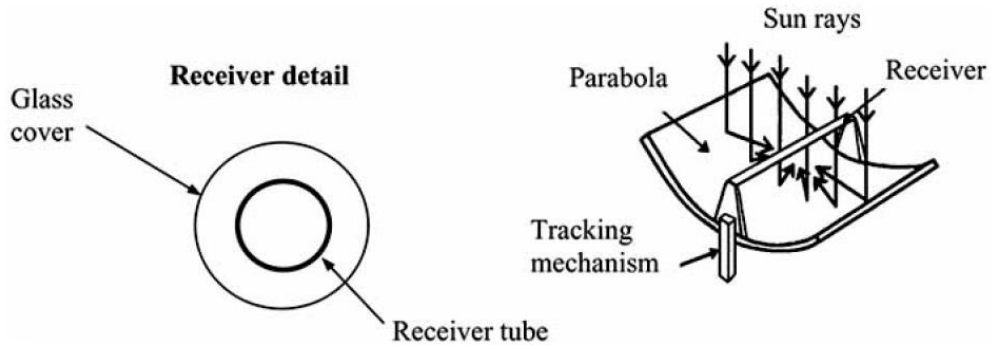

(a)

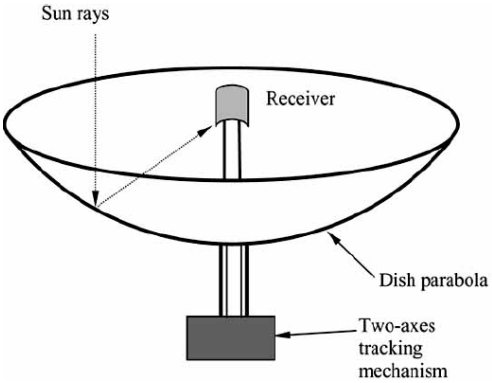

(b)

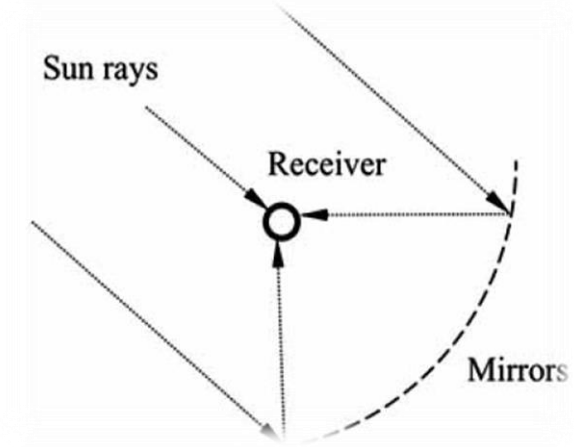

(c)

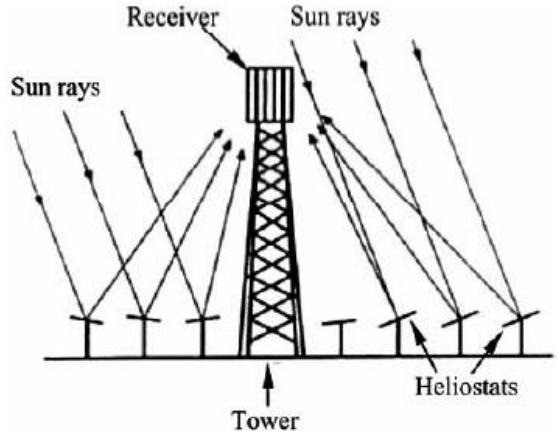

(d)

Figure 6. Schematic illustration of (a) PTC (b) PDC (c) LRF (d) HFC [12].

LFR consist of, array of linear mirror strips which all concentrates solar radiation to a fixed receiver, placed on a tower [12]. LFR can achieve temperature ranging from 60^{o}C to 250^{o}C [9], and has several merits compared to other concentrating solar power technologies, especially in industrial applications [20].

HFC Systems use multiple flat mirrors (heliostats), and reflect incident solar radiation to a common receiver [12]. HFC have high efficiencies in collecting solar energy and can reach concentration ratios ranging from 300 to 1500 [10]. HFC can reach temperatures around 1,500^{o}C [12].

2.3 Solar Thermal Collector Applications

2.3.1 Solar Thermal Electricity Production

Solar Thermal Electricity Systems (STES) generate electricity by using solar thermal energy. The electricity production route with STES is shown in Figure 7 [21]. Solar thermal energy directed to absorber by a solar collector drives a heat engine; where the mechanical energy produced by heat engine is followed electricity production.

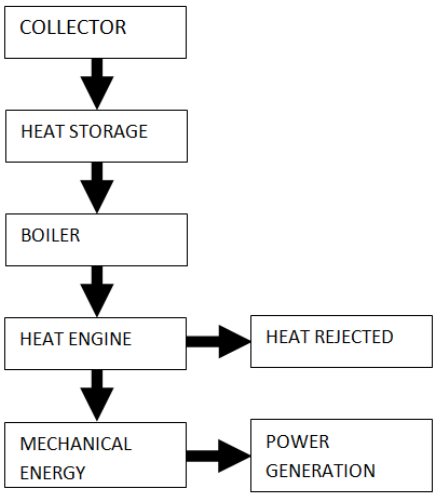

Figure 7. Solar thermal electricity production route [21].

STES can produce electricity with different collectors by using different heat engines. Schematic view of solar thermal electricity production by different collectors and with different heat engines are shown in Figure 8 [22]. Rankine Cycle can be driven by all Fresnel Reflector, Parabolic Dish, Parabolic Trough and Central Tower Receiver systems. Besides Rankine Cycle, Strling and Brayton Cycles can also be driven by parabolic dish and central power systems respectively.

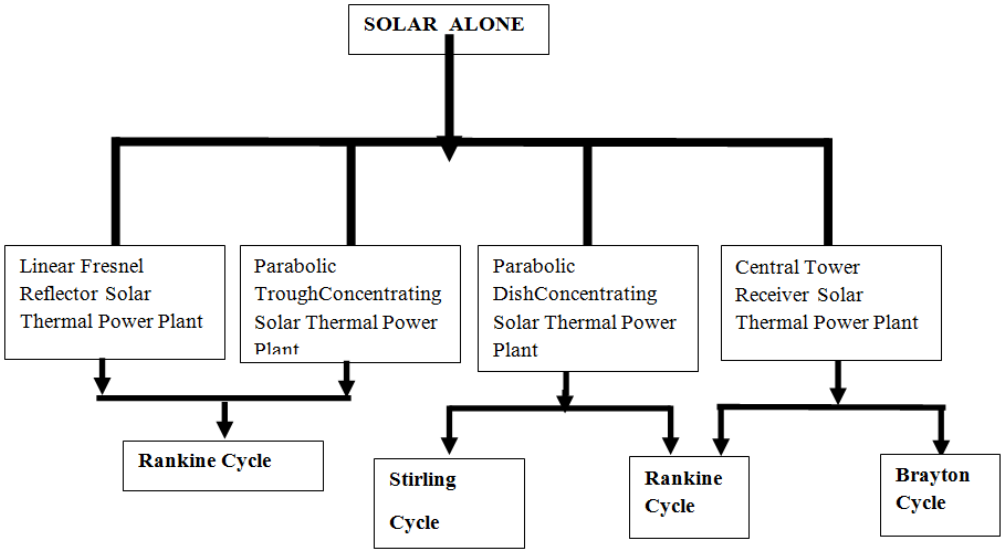

Figure 8. Schematic view of Solar Thermal Electricity Production [22].

2.3.2 Solar Thermal Hydrogen Production

Hydrogen, naturally presents on Earth in organic and inorganic compounds; in form of hydrocarbons, water and other substances. However, Hydrogen rarely presents in molecular form. The elemental hydrogen can be artificially produced; where its environmental friendly production is important [23]. As an environmental friendly method, Hydrogen can be produced by using solar energy. Methods of producing Hydrogen by using solar energy can be listed as; solar thermolysis, solar thermochemical cycles, solar reforming, solar cracking and solar gasification as

shown in Figure 9. Also, Table 3 shows the chemical reactions during these processes. Among all, solar thermochemical production is the most promising method for hydrogen production. Using solar energy as input energy, for hydrogen production is important by means of both; producing hydrogen by using clean energy and also converting solar energy to a transportable and storable fuel.

Table 3. Solar thermal Hydrogen Production methods.

Solar Thermal Hydrogen Production Method	**Reaction**
Solar Thermochemical Cycles	$\mathrm{M_xO_y} \rightarrow \mathrm{xM} + \frac{\mathrm{y}}{2}\mathrm{O_2}$ $xM + yH_2O \rightarrow yH_2$
Solar Reforming/Gasification	$C_xH_y + xH_2O \rightarrow xCO + \left(\frac{y}{2} + x\right)H_2$
Solar Cracking	$CH_4 \rightarrow C(solid) + 2H_2$
Direct Water Thermolysis	$H_2O \rightarrow H_2 + \frac{1}{2}O_2$

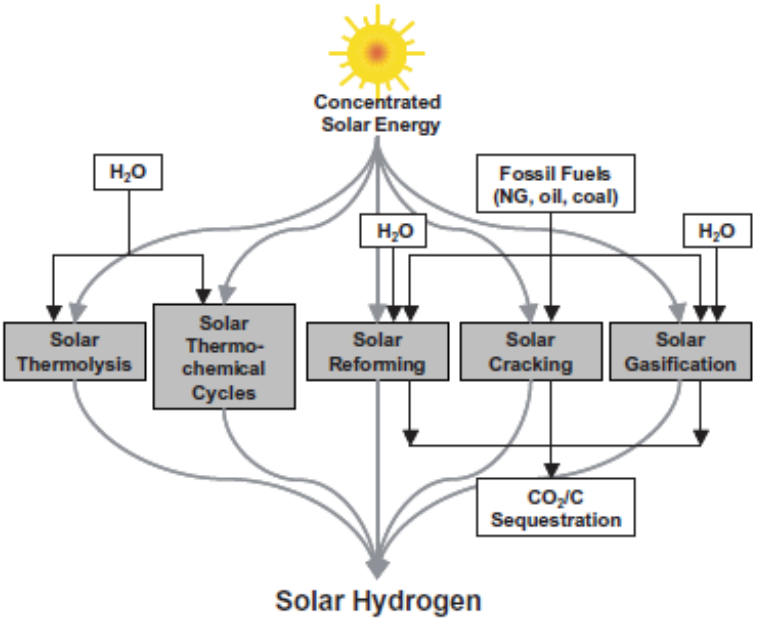

Figure 9. Schematic diagram of solar thermochemical hydrogen production [25].

Özalp et al. [24] summarized advantages of producing hydrogen by using concentrated solar energy;

- Conducting process by using solar energy results with no fossil fuel consumption during process.
- Emission of greenhouse gases during process is prevented.
- Process has high thermal efficiency.

Chapter 3

CHARACTERIZATION OF A SOLAR COLLECTOR

3.1 Characterization of a Solar Collector

A parabolic dish solar collector is used for designing “parabolic dish torrefier”. Any collector is characterized by its geometrical, optical and thermal analysis. In this section, the geometrical analysis, optical analysis and thermal analysis methods of parabolic dish collector are given in detail.

3.2 Geometrical Characterization of a Parabolic Dish Collector

A parabolic dish, given in Figure 10, is obtained from revolution of a circular paraboloid ; which, in cartesian coordinates can be defined as;

$$x^2 + y^2 = 4fz \tag{3.1}$$

Also the surface area of parabolic dish is defined as;

$$S = \frac{8\pi}{3} f^2 \left\{ \left[1 + \left(\frac{d}{4f} \right)^2 \right]^{3/2} - 1 \right\} \tag{3.2}$$

The cross-sectional area of parabola is given by;

$$S_O = \frac{\pi d^2}{4} \tag{3.3}$$

Also, the focal distance of a parabolic dish is given by;

$$f = \frac{d^2}{16\,h} \tag{3.4}$$

The focal length (f), aperture diameter (d) and height of parabolic dish (h) are illustrated in Figure 10. A parabolic dish collector is generally described by its aperture area (S), aperture diameter (d), the rim angle (φ) and the focal length. However, the focal length and the rim angle of a parabolic dish collector are sufficient to describe the shape of collector [26]. Figure 11 illustrates the effect of focal length and rim angle on the shape of solar collector.

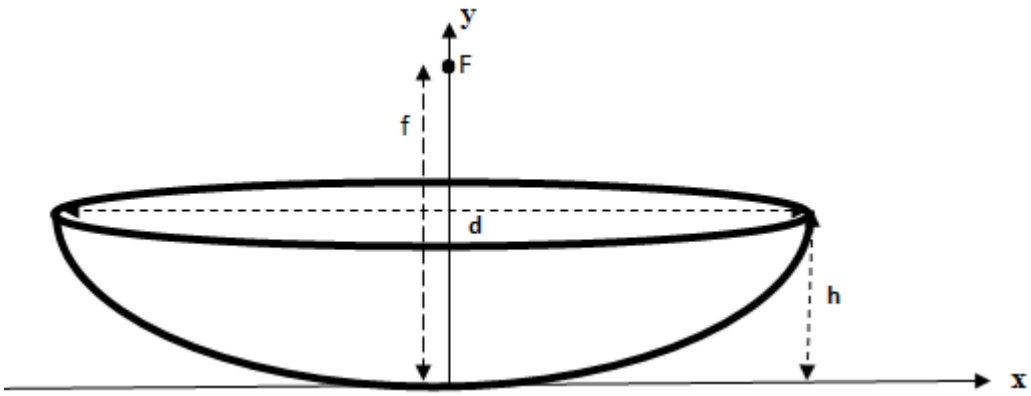

Figure 10.Geometrical parameters of parabolic dish collectors.

The rim angle affects the ratio of the aperture diameter, to the focal length. The parabolic dish, given in Figure 12, has the algebraic representation, so that the following relation holds, $y=\frac{x^2}{4f}$, and;

$$tan\Phi = \frac{x_0}{f-\frac{x_0^2}{4f}} \tag{3.5}$$

Which can be transformed into;

$$tan\Phi = \frac{{}^{d}/_{f}}{2-\frac{1}{8}\left({}^{d}/_{f}\right)^2} \tag{3.6}$$

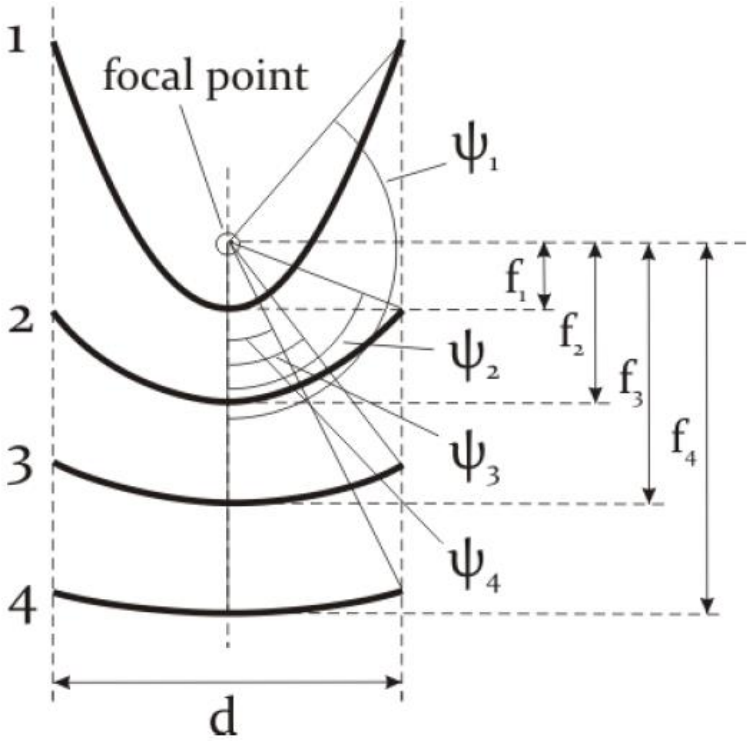

Figure 11. Changes associated to focal length and rim angle for a constant reflector diameter [26].

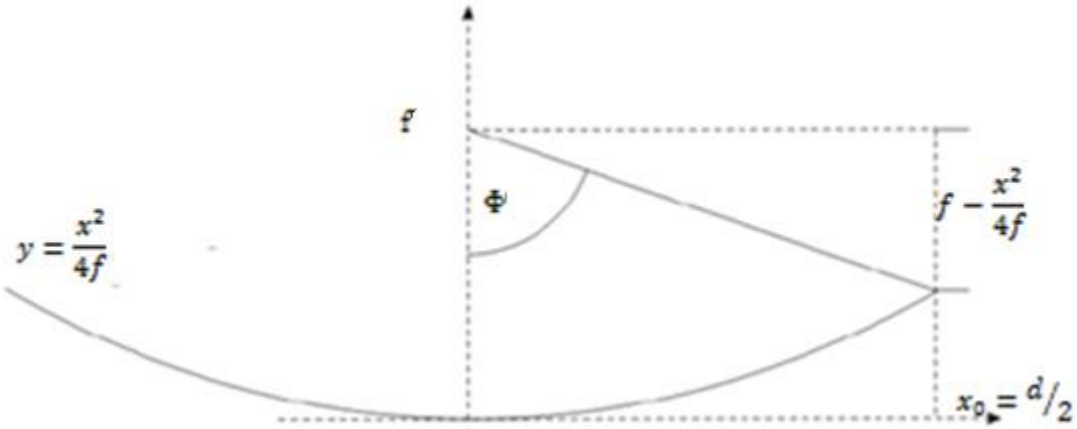

Figure 12. Representation of the rim angle in a cross-section of a paraboloid [26].

Equation (3.6) indicates, the relation between the rim angle and ratio of the aperture diameter to the focal length and can be transformed to;

$$\frac{d}{f} = -\frac{4}{\tan \Phi} + \sqrt{\frac{16}{tan^2 \Phi} + 16} \tag{3.7}$$

3.3 Optical Analysis of a Parabolic Dish Collector

Optical performance of a solar collector is defined by its optical and geometrical concentration ratio. The optical concentration ratio (C_O) can be represented by [27, 28]:

$$C_O = \frac{1}{A_R} \int I_r dA_r \Big/ I_O \tag{3.8}$$

Where (I_r) represent integration over the receiver area (A_r) and (I_o) the radiation incident on the collector aperture. Also the geometric concentration ratio (C_G) can be defined as:

$$C_G = \frac{A_a}{A_r} \tag{3.9}$$

Performance of a parabolic dish collector system can be analyzed by two methods which are ray tracing method and analytical optimization of system. Ray tracing method is a practical method which can be used most of the cases [29]; however, analytical optimization is important for design optimization [30]. Figure 16 shows the geometric parameters used for geometric optimization of parabolic dish. Rabl and Bendth [30] proposed a point acceptance function, $K_P(\theta, \Phi, \rho, \alpha)$, for geometrical optimization of parabolic dish collector- flat receiver system.

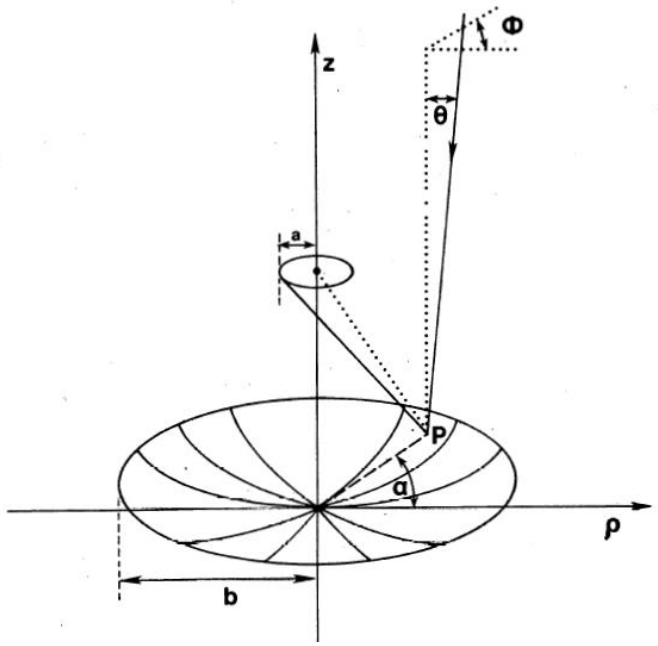

Figure 13. Geometric parameters of parabolic dish collector [30].

They define a point acceptance function, $K_P(\theta, \Phi, \rho, \alpha)$ as;

$$\left.\begin{aligned} K_P(\theta, \Phi, \rho, \alpha) = 1 \text{ , if incident ray reaches to receiver} \\ K_P(\theta, \Phi, \rho, \alpha) = 0 \text{ , if incident ray does not reach to receiver} \end{aligned}\right\} \quad (3.10)$$

The angular acceptance function, $K(\theta, \Phi)$, of parabolic dish collector is the average of point acceptance function $K_P(\theta, \Phi, \rho, \alpha)$ and defined as ;

$$K(\theta, \Phi) = \frac{1}{\pi b^2} \int_0^b d\rho\rho \int_0^{2\pi} d\alpha \, K_P(\theta, \Phi, \rho, \alpha) \quad (3.11)$$

For particular $\gamma = -\alpha$, $K_P(\theta, \Phi, \rho, \alpha) = K_P(\theta, \Phi - \gamma, \rho, 0)$ and by defining $\beta = \Phi - \gamma$, the angular acceptance function $K(\theta, \Phi)$ can be written as;

$$K(\theta, \Phi) = \frac{1}{\pi b^2} \int_0^b d\rho\rho \int_0^{2\pi} d\alpha \, K_P(\theta, \beta, \rho, 0) \quad (3.13)$$

According to azimuthal symmetry of parabolic dish; $K(\theta, \Phi) = K(\theta)$. Although the point acceptance angle $K_P(\theta, \Phi, \rho, \alpha)$ was defined with respect to radiation incident

on the receiver, reversing the path does not change the path. It can be treated as; the receiver is the emitter of any ray, coming from the receiver by leaving the aperture at point P in the direction(θ, β). For the case of flat receiver, rays emitted by receiver and reaching P, form an elliptical cone as demonstrated in Figure 13. The angular principal axes of the elliptical cone are given by;

$$\left.\begin{array}{l} \theta_s = \frac{a}{r}\cos\psi \quad \text{and} \quad \theta_l = \frac{a}{r} \\ \\ \cos\psi = \frac{3-r}{r} \quad \text{and}\, r = \sqrt{\rho^2 + (1-z)^2} = 1 + z \end{array}\right\} \tag{3.14}$$

With $z = \frac{\rho^2}{4}$ Figure 14 illustrates the geometrical relations, necessary for calculating angular acceptance function of a parabolic dish with flat receiver. The boundaries of elliptical cone are defined by θ_e and Φ_e and defined as;

$$\theta_e(\rho, \Phi_e) = {\theta_s\theta_l}\Big/{\sqrt{\theta_s^2 sin^2\Phi_e + \theta_l^2 cos^2\Phi_e}} \tag{3.15}$$

The rays emitted from receiver will hit to ellipse if θ is less than the $\theta_e(\rho, \Phi_e)$ and the point acceptance angle is described as;

$$K_P(\theta, \Phi, \rho, \alpha) = 1\,,\ \theta < \theta_e \tag{3.16}$$

$$K_P(\theta, \Phi, \rho, \alpha) = 0\ \ , otherwise \tag{3.17}$$

It is obvious that all rays with, less than θ_s are within the ellipce and the rays θ larger than the major axis are outside the ellipse. The azimuthal part of integration has the form of;

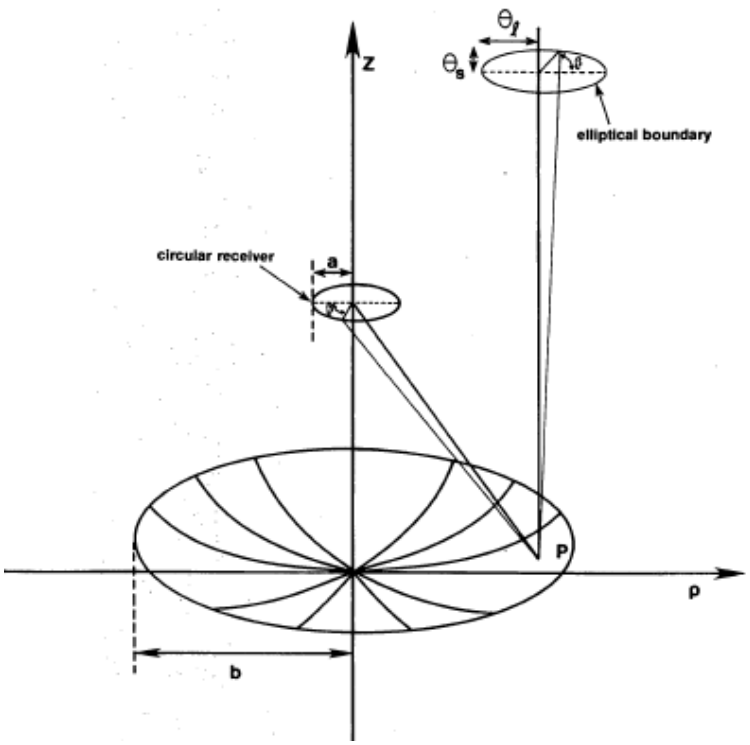

Figure 14. Geometrical relations for the calculation of the angular acceptance function of parabolic dish with flat receiver [30].

$$\int_0^{2\pi} d\beta K_P(\theta,\beta,\rho,0) = 2\pi\,,\ for\theta < \theta_s(\rho) \tag{3.18}$$

and

$$\int_0^{2\pi} d\beta K_P(\theta,\beta,\rho,0) = 0\,,\ for\theta > \theta_l(\rho) \tag{3.19}$$

For portion $\theta_s<\theta<\theta_l$; the azimuthal part of integration can be computed by considering the reflection symmetry of ellipse and restrict Φ in the first quadrant of $0 < \beta < {}^{\pi}/_{2}$ as;

$$\int_0^{2\pi} \mathrm{d}\beta\, \mathrm{K_P}(\theta,\beta,\rho,0) = 4\int_0^{\pi/4} \mathrm{d}\beta\, \mathrm{K_P}(\theta,\beta,\rho,0) \tag{3.20}$$

Considering the elliptical boundary $\theta_e(\beta,\rho)$ and letting $\beta \to \beta(\theta,\rho)$;

$$\int_0^{2\pi} \mathrm{d}\beta \mathrm{K_P}(\theta,\beta,\rho,0) = 4\arcsin\left(\sqrt{({}^{a}/_{r\theta})^2 - 1}\cot\psi\right) \tag{3.21}$$

So this brings the result that the angular acceptance function $f(\theta, \Phi)$ shows three different behavior according to θ. Noting that;

$$\theta_s = \frac{a(2-r)}{r^2} \tag{3.22}$$

and θ_s is minimum when r is maximum ;

$$r_{max} = 1 + \frac{b^2}{4} \tag{3.23}$$

The rim angle can be written as ;

$$\sin \Phi = \frac{\mathrm{b}}{1+\left(\mathrm{b}^2/_4\right)} \tag{3.24}$$

and the minimum value of θ_s can be represented by;

$$\theta_{\mathrm{s,min}} = \frac{\mathrm{a}}{\mathrm{b}} \sin \Phi \cos \Phi \tag{3.25}$$

and obviously the maximum value of θ_l corresponds to r_{min} and; $\theta_{\,l,max} = a$. For angles between $\theta_{s,min}$ and $\theta_{l,max}$ using the relation $r = 1 + \frac{\rho^2}{4}$ for changing the variable of integration , the boundaries of r which is defined by , $\theta > \theta_l(\rho) = \frac{a}{r}$ and can be written as $r > \frac{a}{\theta} = r_2$ and also; $\theta \leq \theta_s(\rho) = \frac{a(2-r)}{r^2}$ and can be written as $r^2 \leq \frac{a}{\theta}(2-r) = r_2(2-r)$. Solution of this quadratic equation noting that $r \geq 1$,

$$r \leq r_1 = -\frac{r_2}{2} + \sqrt{\frac{r_2^2}{4} + 2r_2} \tag{3.26}$$

By using the Equations from (3.23) to (3.26), the results can be summarized to obtain the angular acceptance function as;

$$\left.\begin{array}{c} K(\theta) = \ 1 \ for\ \theta \le \theta_1 = \frac{\sin\Phi cos\Phi}{\sqrt{C}} \\ K(\theta) = \frac{2}{\pi b^2}\int_1^{1+b^2/4} drg(\theta,r), \ \ for\theta_1 \le \theta \le \theta_2 \\ K(\theta) = \ 0 \ for\theta \le \theta_2 = \frac{2}{\sqrt{C}} tan\frac{\Phi}{2} \end{array}\right\} \quad (3.27)$$

where

$$\left.\begin{array}{c} g(\theta,r) = 2\pi, \quad ifr < r_1 = -\frac{r_2}{2} + \sqrt{\frac{r_2^2}{4} + 2r_2} \\ g(\theta,r) = 4\ arcsin\left[\frac{2-r}{2\sqrt{r-1}}\sqrt{\left(\frac{b}{r\theta\sqrt{C}}\right)^2 - 1}\right] if r_1 < r < r_2 \\ g(\theta,r) = 0\,, \qquad ifr > r_2 \ = \frac{b}{\theta\sqrt{C}} \qquad .... \end{array}\right\} \quad (3.28)$$

Where the geometric concentration ratio is defined by $C = \frac{b^2}{a^2}$. The angular acceptance function $K(\theta)$; depends only the combination $\theta\sqrt{C}$ and the rim angle Φ. If the $K(\theta)$ in the intermediate region is expanded by a polynomial expansion in the variable $\sqrt{C}$. The angular acceptance function can be written as ;

$$\left.\begin{array}{c} K(\theta) = 1, for\theta \le \theta_1 = \frac{sin\Phi cos\Phi}{\sqrt{C}} \\ K(\theta) = a + (b\theta^2) + c(b\theta^2)^2 + \ ...., \ \ for\ \theta_1 \le \theta \le \theta_2 \\ K(\theta) = 0, \quad for\theta \le \theta_2 = \frac{2}{\sqrt{C}}\tan\frac{\Phi}{2} \end{array}\right\} \quad (3.29)$$

3.4 Thermal Characterization of a Parabolic Dish Collector

Thermal analysis of a solar collector must be done for characterization of solar collectors. The geometric concentration ratio (C_G) is given in Equation (3.9). It must be pointed out that the source Sun is a sphere of radius r, and the collector has an

aperture area of A, The collector is at distance of R from the center of the Sun as shown in Figure 15. Solar radiation emitted by Sun, as a blackbody, can be calculated by;

$$Q_{Sun} = 4\pi {r_{sun}}^2 \sigma T_{Sun}^4 \tag{3.30}$$

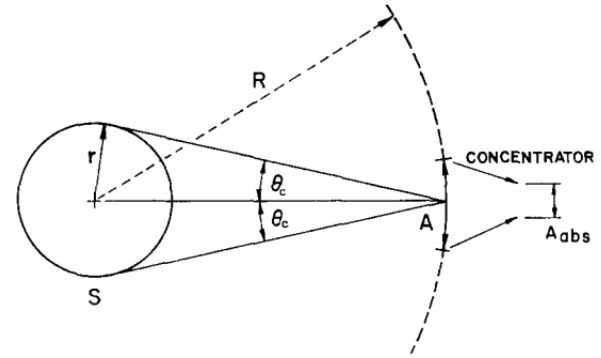

Figure 15. Schematic representation of radiation coming from a source with radius r, to collector with aperture area of A [31].

Amount of radiation captured by collector can be written as [31];

$$F_{Sun \to Collector} = \frac{A}{4\pi R^2} \tag{3.31}$$

If no collector losses exist between aperture and receiver, the heat radiated from the Sun and reaching to the absorber is;

$$Q_{Sun \to Receiver} = Q_{Sun} F_{Sun \to Receiver} = \frac{A}{4\pi R^2} \sigma T_{Sun}^4 \tag{3.32}$$

Similarly the receiver radiates by rate of;

$$Q_{Receiver} = A_{Receiver} \sigma T_{Receiver}^4 \tag{3.33}$$

The radiation transfer from receiver to source can be written as [31];

$$Q_{Receiver \to Sun} = E_{receiver \to Sun} A_{Receiver} \sigma T_{Recevier}^4 \tag{3.34}$$

$$(E_{Receiver \to Sun} \leq 1)$$

$E_{Receiver \rightarrow Sun}$, represents the radiation reaching to source. If both receiver and source have same temperature then;

$$Q_{Sun \rightarrow Receiver} - Q_{Receive \rightarrow Sun} = 0$$

$$\text{if} \qquad T_{RECEIVER} = T_{SOURCE} \tag{3.35}$$

Combination of Equations (3.33) and (3.35) gives:

$$A\frac{r^2}{R^2} = E_{Receiver \rightarrow Sun} A_{Receiver} \tag{3.36}$$

and provides that

$$C = \frac{A}{A_{Receiver}} = \frac{R^2 E_{Receiver \rightarrow Sun}}{r^2} = \frac{E_{Receiver \rightarrow Sun}}{sin^2\theta_c} \tag{3.37}$$

and

$$C \leq \frac{1}{sin^2\theta_c} \tag{3.38}$$

Equation (3.38) is a general expression for all collectors and gives maximum possible concentration ratio for any collector [31]. However, practical applications of solar collectors have been shown that, it is very difficult to reach this maximum concentration ratio. The efficiency of a solar thermal system strongly depends on thermal efficiency of solar collector and the thermal efficiency of receiver. Solar thermal energy is directed on a receiver of solar collector and it must be absorbed by receiver efficiently in order to conduct any solar thermal process or engine efficiently.

The efficiency of a receiver is determined by its absorbed and lost solar thermal energy. Absorbed solar thermal energy is associated with absorption coefficient of

receiver material (α) and lost solar thermal energy is associated with emittance of material (ε). Net absorbed solar thermal energy can be expressed as;

$$Q_{net} = Q_{Absorbed} - Q_{Lost} \tag{3.39}$$

Which can be formulated by;

$$Q_{net} = \alpha Q_{aperature} - \varepsilon A_{aperture} \sigma T^4 \tag{3.40}$$

The efficiency of receiver can be expressed as;

$$\eta_{absorption} = {\alpha Q_{aperature} - \varepsilon A_{aperture} \sigma T^4} \Big/ {Q_{collector}} \tag{3.41}$$

Where $Q_{collector}$ is the solar thermal energy coming from collector, $A_{aperture}$ is the total area of receiver aperture, σ is the Stefan-Boltzman constant and T is the temperature of receiver. The capability of the collection system to concentrate solar energy is often expressed interms of its mean flux concentration ratio over an aperture normalized with respect to the incident beam insolation as [32];

$$C = \frac{Q_{aperture}}{I A_{aperture}} \tag{3.42}$$

An ideal receiver has absorption and emittence coefficient are 1 and also, total solar thermal energy coming from sun and incoming solar power intercepted by the reactor aperture equal ($Q_{aperture} = Q_{concentor}$). So the ideal absorption efficiency can be expressed as;

$$\eta_{absorption} = 1 - \left(\frac{\sigma T^4}{IC}\right) \tag{3.43}$$

Solar collector- receiver systems are used for conducting an endothermic reaction.The ideal exergy efficiency is limited by Carnot efficiency and maximum absorption efficiency. The ideal exergy efficiency is given as [32;]

$$\eta_{exergy,ideal} = \eta_{ansorption} \times \eta_{carnot}$$

$$= \left[1 - \left(\frac{\sigma T^4}{IC}\right)\right] \times \left[1 - \left(\frac{T_L}{T_H}\right)\right] \quad (3.44)$$

T_H and T_L are the maximum and minimum operating temperatures of the Carnot heat engine. In order to have high Carnot efficiency the process must be conducted at highest possible temperature, which is stagnation temperature ($T_{stagnation}$). At stagnation temperature $\eta_{exergy,ideal} = 0$. The receiver must be driven at temperatures below stagnation temperature and there exists an optimum working temperature for each receiver. The optimum working temperature of receiver is obtained by;

$$\frac{\partial \eta_{exergy,ideal}}{\partial T} = 0 \quad (3.45)$$

Equation (3.45) yields to;

$$T_{optimum}^5 - (0.75\ T_L) T_{optimum}^4 - \left(\frac{\alpha T_L IC}{4\varepsilon\sigma}\right) = 0 \quad (3.46)$$

Steinfeld and Schubnell [33] solved Equation (3.46) and the change of $\eta_{exergy,ideal}$ according to operating temperature (T_H) is demonstrated in Figure16. The optimum temperature for maximum efficiency is ranging between 1100 and 1800 K with concentrations between 1000 and 13,000. In practice, the contribution of convection, conduction and radiation losses results with observing peak efficiency at lower temperatures.

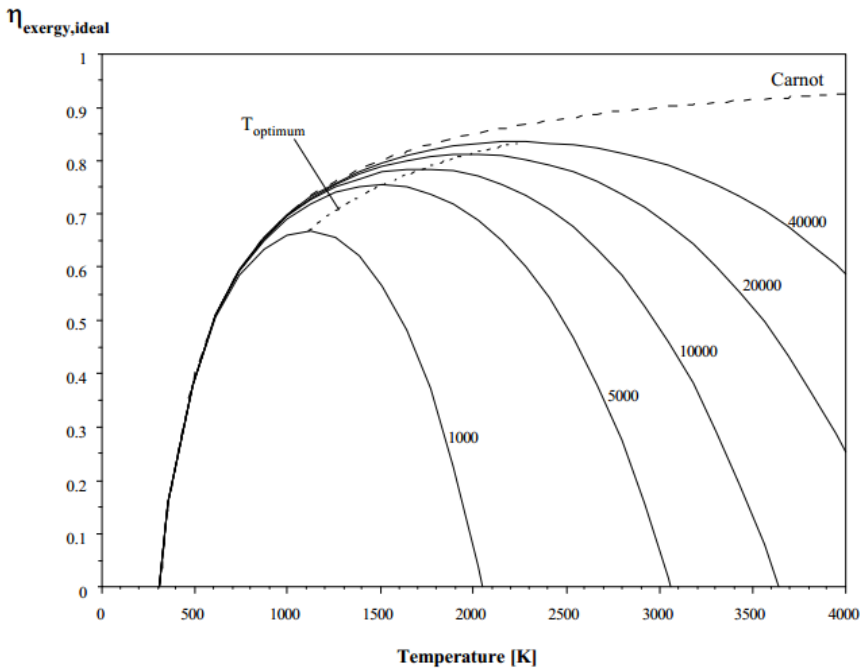

Figure 16. $\eta_{exergy,ideal}$ as a function of operating temperature[32].

Chapter 4

BIOMASS

4.1 Biomass Energy

Lignocellulosic biomass can be defined as; solar energy which is converted to organic material by plants (with photosynthesis) [34]. Biomass has great potential to replace fossil fuels. Currently, biomass contributes almost 14% of worlds total energy consumption [35], where this consumption reaches from 50% to 90% of total energy demand in developing countries [34]. Besides being an alternative to fossil fuels, biomass contributes stabilization of the concentrations of greenhouse gasses [36]. The biomass fuels are classified in four main groups as [37]:

1. Woody biomass
2. Herbaceous materials
3. Agricultural residues
4. Refuse-Derived Fuels (RDF)

The contribution of each group of biomass, listed above, to global energy consumption is given with different ratios by different researchers. Demirbaş [38] indicated that, 64% of biomass energy is mainly produced from wood, where the World Energy Council [39] stated that, woody biomass accounts for 87% of global biomass consumption. Biomass has remarkable potential as a fuel. Also, it must be pointed out that biomass have reasonable cost level [40].

The merits of biomass compared to other renewables can be listed as [41];

1. Remarkable contribution for reducing poverty in developing countries.
2. Being used as energy source from ancient time for different purposes.
3. Being CO_2- neutral.
4. Being transportable renewable fuel.

Furthermore; it is also important to prevent natural degradation of biomass in nature. The degradation of biomass results with emission of Methane, which is the most hazardous greenhouse gas, during its natural degradation [42].

4.2 Composition of Biomass

Biomass has been defined to be "any material, except fossil fuels, which was a living organism, that can be used as a fuel either directly or after a conversion process" [43]. Biomass mainly consists of cellulose, hemicellulose and lignin polymers which bounded together and form a complex structure [44]. The amount of each compound in lingocellulosic biomass changes according to type of plant and growing conditions [37]. The cellulose, hemicelluloses and lignin composition of some lignocellostic biomass is given in Table 4 [45].

Table 4. Concentration of cellulose, hemicellulose and lignin in different lignocellulostic biomass (dry basis) [45].

Lignocellulosic Biomass	Cellulose (%)	Hemicellulose (%)	Lignin(%)
Hardwood Stems	40-55	24-40	18-25
Softwood Stems	45-50	25-35	25-35
Nut Shells	25-30	25-30	30-40
Corn Cobs	45	35	15
Grasses	25-40	35-50	10-30
Paper	85-90	0	0-15
Wheat Straw	30	50	15
News Paper	40-55	25-40	18-30
PrimaryWaste Solids	8-15	NA	24-29
SolidCattle Manure	1.6-4.7	1.4	3.3
Switchgrass	45	31.4	12.0

4.2.1 Cellulose

Cellulose is the main structural component of cell walls [46]. The empirical formula of cellulose is $H(C_6H_{10}O_5)_nOH$ [47]. The chemical composition of cellulose is given in Figure 17.

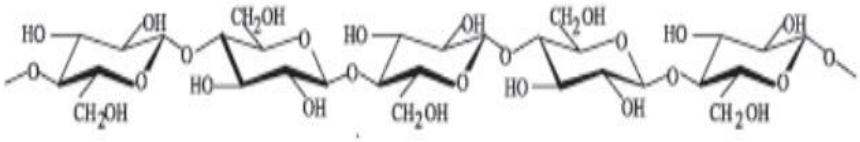

Figure 17. Chemical composition of cellulose [48,49].

4.2.2 Hemicellulose

Hemicellulose is mainly found in the plant cell wall [46]. Hemicellulose is linked to cellulose by physical intermixing and also connected to lignin with covalent bonds [47]. Hemicellulose has a non-homogenous chemical structure [50]. The chemical structure of main hemicellulose components is given in Figure 18. Hemicellulose is not soluble in water and its decomposition starts at lower temperature compared to cellulose and lignin [46].

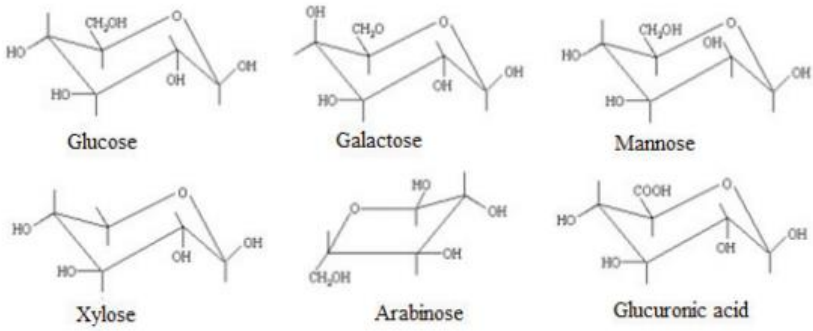

Figure 18. Chemical structure of of hemicelluloses [48,49].

4.2.3 Lignin

Lignin is the most complex aromatic polymer. Lignin provides a protective layer for the plant walls [46]. The chemical structure of lignin is given in Figure 19. Lignin is

the most difficult decomposing component of biomass [51]. Lignin decomposes in temperature range of 100–900^{o}C [47].

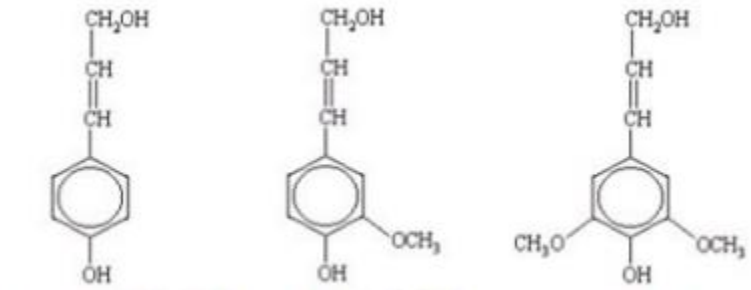

Figure 19. Chemical structure of lignin [48, 49].

4.3 Biomass Pretreatment and Treatment Methods

Although, biomass is clean energy source, it is important to overcome drawbacks like high oxygen content, low calorific value, high moisture content, collection-storage difficulties and low bulk density. Listed drawbacks prevent efficient energy generation from direct combustion of biomass. However, several methods exist for upgrading biomass and converting it more valuable energy carriers. These methods are classified in two groups as biomass pretreatment and biomass upgrading treatments methods.

Biomass pretreatment methods generally aim to convert biomass in to a form which can be stored longer period of time without degradation. Also pretreatment methods provide several advantages for upgrading treatments; like reducing the energy consumption. Upgrading treatments convert raw biomass to more energy denser solid, liquid and gas biofuels than pretreatment methods.

4.3.1 Biomass Pretreatment Methods

Biomass pretreatment methods are classified in four main groups as mechanical biological and thermo-chemical pretreatments [52, 53]. All pretreatment methods aim to damage the structure of lignocellulose and remove lignin [54].

4.3.1.1 Mechanical Pretreatment

Mechanical pretreatment methods can be listed as; grinding, chipping, shredding or milling [55]. Mechanical pretreatments mainly aim to reduce degree of polymerization and also to increase the available specific area for further treatment [45]. It must be stated that; mechanical pretreatment results to lignin depolymerization [56].

Several studies in literature have shown that; mechanical pretreatment results with increased biogas, bioethanol and bio-hydrogen yields during biomass upgrading treatments [57]. However, high energy consumption during mechanical pretreatment is the main challenging point about process [58].

4.3.1.3 Chemical Pretreatment

Chemical pretreatment methods of biomass can be listed as; pretreatment of biomass under acidic conditions, alkaline conditions and treatment by oxidative delignification. Chemical pretreatment of biomass, under acidic conditions, occurs treatment with different acids, where treatment with alkali conditions involves treatment with chemicals like sodium or ammonium [54]. Also, Oxidative delignification is conducted with an oxidizing agent [59, 60].

4.3.1.3 Biological Pretreatment

Biological pretreatment of biomass is cheap and efficient alternative for energy generation [61]. The biological pretreatment of biomass is performed by microorganisms which synthesize cellulolytic enzymes during hydrolysis [54].

4.3.1.4 Thermo-chemical Pretreatment

Main thermochemical pretreatment methods are pelletization and mild carbonization (torrefaction). The pelletization process includes; reception of raw material, screening, grinding, drying, pelleting, cooling, sifting and packaging [62, 63]. Typical pelletizing process is shown in Figure 20. The advantages of the biomass densified by pelletization can be listed as [64, 65];

- An increased bulk density.
- High energy density.
- Lower moisture content.
- More homogeneous composition than raw biomass.

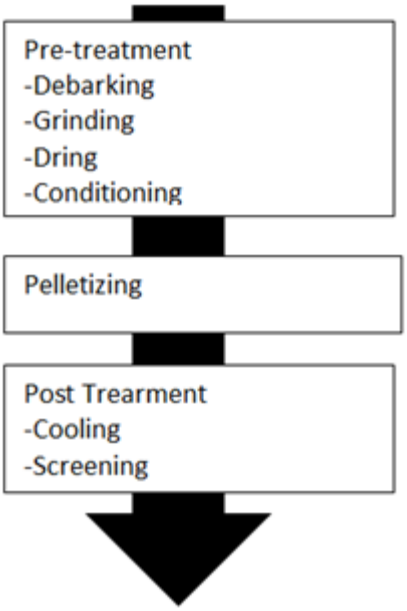

Figure 20. Typical pelletizing process [66].

Torrefaction is a low temperature thermochemical pretreatment of biomass conducted at 200-300^{o}C under inert atmosphere. The advantages of the torrefied biomass compared to raw biomass can be listed as [67];

1. Less moisture content.
2. Reduced H/C and O/C ratios.
3. Higher energy density and Higher Heating Value.
4. Hydrophobic nature.
5. Improved ignitability, reactivity and grindability.

4.3.2 Thermo Chemical Biomass Upgrading Treatments

Thermochemical Upgrading Methods can be listed as; pyrolysis and gasification. Although these methods yield valuable solid, liquid and gas energy carriers, processes require high heat energy input.

4.3.2.1 Pyrolysis

Pyrolysis is thermal degradation of biomass in the absence of oxygen without complete combustion. Pyrolysis has products in three phases; solid (char), liquid (bio-oil) and gas. The amount or fraction of the products depends on pyrolysis conditions.

Table 5. Operating conditions of pyrolysis processes [68].

Pyrolysis Type	**Residence Time (s)**	**Heating Rate ($^{o}C\ s^{-1}$)**	**Particle Size (mm)**	**Temperature (K)**
Conventional	250-550	01-1	5-50	550-950
Fast	0.5-10	10-200	<1	850-1250
Flash	<0.5	>1000	<2	1050-1300

Pyrolysis is classified in three categories as; slow pyrolysis (carbonization), fast pyrolysis and flash pyrolysis. Each pyrolysis process is characterized by own process conditions. The process parameters of each pyrolysis process are given in Table 5, by means of temperature, heating rate, particle size and solid residence time. As shown in Table 5, beside the temperature, heating rate, solid residence time and the particle size of each process is different and smaller particles are required for conducting fast and flash pyrolysis processes. The pyrolysis parameters can be arranged according to desired end product and other by products can be used as auxiliary fuel for the process.

4.3.3.2 Gasification

Gasification is a thermo-chemical conversion process for materials like coal, petroleum coke and biomass for producing a gas fuel called "producer gas" [69]. Gasification occurs at 750–850^{o}C [70]. Although the chemistry of gasification is complex, the processes consist of following stages [71];

1. Drying
2. Devolastilisation
3. Oxidation
4. Reduction

The main product of gasification is high amount of gaseous energy carriers and smaller amounts of char and ash.

Chapter 5

TORREFACTION PROCESS AND TORREFACTION OF SOLID OLIVE MILL RESIDUE (SOMR)

5.1 Literature Review

Torrefaction is a thermo-chemical process for upgrading cellulosic biomass. Torrefaction converts biomass into a more homogeneous fuel, that can be utilized in other conversion processes for energy purposes aswell [72]. Torrefaction was first studied in France in the early 1930s for upgrading fuel properties of biomass[73]. The process is also known as mild pyrolysis or mild carbonization. Torrefaction occurs at 200 to 300°C under inert atmosphere with slow heating rates of less than $50^{o}C\ min^{-1}$ [74]. Although there exists torrefaction studies conducted with heating rate $50^{o}C\ min^{-1}$ [75], slow heating rate is important for the homogeneity of products [76].

Torrefaction can be divided into two categories according to torrefaction temperature, namely light torrefaction and severe torrefaction. Light torrefaction occurs at temperatures less than 240°C, where as severe torrefaction occurs above 270°C [77]. Wood is the fundamental source of biomass all over the world and, like all other thermo-chemical processes; its torrefaction has been a topic of major research interest [78,79,80]. Besides wood, torrefaction of several biomass have been studied extensively.

Chen and Kuo [67] investigated the torrefaction properties of basic constituents of biomass in thermogravimetry. They tested the torrefaction properties under three different temperatures of 230^{o}C, 260^{o}C and 290^{o}C. Authors summarize the effect of temperature on the biomass as;

- At the light torrefaction conditions (230^{o}C) the moisture and the light volatiles are removed from the biomass and the heating value is increased to a small extent.
- At severe torrefaction conditions (290^{o}C) the contribution of lignin to energy plays important role than cellulose.

Uemura *et al*. [84] torrefie oil palm wastes at 220^{o}C, 250^{o}C and 300^{o}C for 30 minutes. Authors investigated the effect of torrefaction conditions on mass yield, calorific value, elemental composition and energy yield of products. Their results showed that the mass yield decreases with increased torrefaction temperature. Also, Uemura *et al*.[81] concluded that, torrefaction results in a higher calorific value and a higher carbon content.

Phanphanich and Mani [82], investigated the grindability and fuel characteristics of pine chips and logging residues at four different torrefaction temperatures. The study showed that, the torrefaction temperature affects the ability of absorbing moisture, when torrefied samples are stored in room temperature.

Bridgeman *et al*.[83] studied the effect of torrefaction on pulverization behavior of two energy crops. They conducted torrefaction experiments at different torrefaction conditions. Their experiments demonstrated that; the orders of the parameters

affecting the mass yield are torrefaction temperature, reaction time and particle size respectively. The authors concluded that; besides the mass yield; the torrefaction temperature, strongly influences the elemental composition and ease of grindability of the solid product.

Chen *et al.* [84] investigated the torrefaction behavior of woody biomass (Lauan) under three different torrefaction temperatures and residence times. Their results showed that the torrefaction temperature contributes more to mass loss and HHV than the residence time.

Chen and Kuo [84] investigated the torrefaction behaviors of bamboo, willow, coconut shell and wood by using thermogravimetry. They classified the torrefaction process as light (at range of 200-250^{o}C) and severe (at range of 250-300^{o}C) torrefaction. Authors concluded that the impact of torrefaction conditions(light or severe) varies according to type of biomass.

Bridgeman *et al.* [86] investigated the torrefaction of reed canary grass , short rotation willow coppice (SRC) and wheat straw. The oxygen content of the torrefied samples decreased as the torrefaction temperature increased, where carbon content and HHV rised with increased torrefaction temperature.

Arias *et al.* [87] investigated the torrefaction of eucalyptus (wood). They focused on the effect of torrefaction on grindability and combustibility of woody biomass (eucalyptus). Their results showed that torrefaction increases grindability of biomass. Also their study resulted that gross calorific value of biomass increases with increased residence time.

Chen *et al.* [88] studied the torrefaction properties of pulverized biomass. Their aim was evaluating the potential of biomass as a solid fuel for boilers and blast furnaces. The authors resulted that the properties of the torrefied samples tend to become uniform.

Above listed studies showed that; solid product of torrefaction reaction could be utilized as fuel for domestic heating, fuel for barbeques and food stoves. Also, the torrefaction reaction as a pre-treatment for gasification and fast pyrolysis process is investigated.

Couhert *et al.* [89] investigated effect of torrefaction on gasification characteristics of biomass by using wood. Results showed that the torrefied samples produced 7% more H_2 and 20% more CO, than the un-torrefied wood. It is observed that the CO_2 yields of all samples were similar.

Neupane *et al*. [90] showed that; bio-oils produced from torrefied biomass have lower oxygen content and enhanced aromatic yield . Also, results of Zheng *et al.* [91] showed that torrefaction improves quality of products obtained from fast pyrolysis of corn crobs. Torrefaction studies have shown that, torrefaction is suitable for wide range of biomass. However, wet biomass such as animal litter and sludges are not directly suitable for torrefaction because of their high moisture content (around 75 wt%) [92].

Table 6. Some biomass material for torrefaction and possible utilization market of products [93].

Suitable materials for torrefaction process:	***Possible utilization method-market***
• **Timber, wood, sawdust**	• Wood pellet replacement
• **Grass and straw**	• Barbeque substitutes
• **Municipal solid waste**	• Space heating(commercial and domestic)
• **Fruit plantation waste**	• Direct industrial use
• **Rubber and tire waste**	• Industrial power production

5.2 Torrefaction Reaction Kinetics

Torrefaction reaction kinetics are generally explained by two models which are one step and two step reaction models. One step reaction model is a simple model for explaining

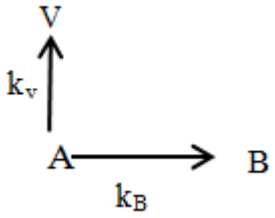

Figure 21. Schematic representation of one step reaction model.

torrefaction kinetics. In one step reaction model, raw biomass (A) is converted to solid biochar (B) and volatiles (V) as shown in Figure 21. In one step reaction model; the reaction rate equations are defined as;

$$\frac{d[A]}{dt} = -K_1[A] = -(k_B + k_v)[A] \tag{5.1}$$

$$\frac{d[B]}{dt} = k_B[B] \tag{5.2}$$

The mass of unreacted biomass after torrefaction can be shown by M_F and can be obtained by integration of Equation (5.1);

$$M_F = M_i\, exp(-((k_B + k_v)t) \tag{5.3}$$

And the mass of torrefied biomass (m_F) can be obtained from integration of (5.2);

$$m_F = M_i \left(\frac{k_B}{k_B + k_v}\right) [1 - \exp(-((k_B + k_v)t)] \tag{5.4}$$

The ratio of unreacted biomass and torrefied biomass to initial mass of biomass can be described as;

$$R_{M_F} = {}^{M_F}/_{M_\text{i}} = \exp(-((k_B + k_v)t) \quad (5.5)$$

$$R_{m_F} = {}^{m_F}/_{M_\text{i}} = \left(\frac{k_B}{k_B+k_v}\right)\ [1 - \exp(-((k_B + k_v)t)] \quad (5.6)$$

The total ratio (R_T) of torrefied and untorrefied biomass can be written as;

$$R_T = R_{M_F} + R_{m_F} =$$

$$\exp(-((k_B + k_v)t) + \left(\frac{k_B}{k_B+k_v}\right)\ [1 - \exp(-((k_B + k_v)t)] \quad (5.7)$$

or R_T can be written as;

$$R_T = \frac{k_B}{(k_B+k_v)} + \frac{k_v}{(k_B+k_v)}\exp(-((k_B + k_v)t) \quad (5.8)$$

In equation (5.8) if $t \to \infty$ (or sufficiently long);

$$R_\infty = \frac{k_B}{(k_B+k_v)} \quad (5.9)$$

and;

$$R_T = R_\infty + \frac{k_v}{(k_B+k_v)}\exp(-((k_B + k_v)t) \quad (5.10)$$

If we define; A = $\frac{k_v}{(k_B+k_v)}$ and $k = (k_B + k_v)$, then equation (5.10) can be rewritten as;

$$R_T = R_\infty + A\exp(-kt) \quad (5.11)$$

Where the reaction rate constant $k = k_o \exp(^{-E_a}/_{RT})$ can be defined by Arrhenius equation. Equation (5.11) can be used to determine mass loss behavior during torrefaction.

Two step reaction model explains torrefaction process in two steps contrary to one step model. According to two step model; biomass is converted into an intermediate solid; which characteristics are between biochar and raw biomass. Then within the second step, intermediate solid is converted into biochar. Figure 22, is the schematic representation of two step model.

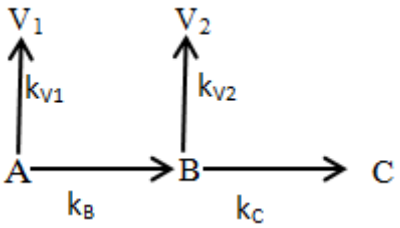

Figure 22. Schematic representation of two step reaction model for torrefaction.

In two step reaction model; the reaction rate equations are defined as;

$$\frac{d[A]}{dt} = -(k_B + k_{V1})[A] = k_1[A] \tag{5.12}$$

$$\frac{d[B]}{dt} = k_B[A] - (k_C + k_{V2})[B] \tag{5.13}$$

$$\frac{d[C]}{dt} = k_c[C] \tag{5.14}$$

Equation (5.12) to (5.14) can be solved as shown in one step reaction model and; R can be written as;

$$R_T = \frac{k_B.k_C}{k_1.K_2} + \left(1 + \frac{(k_B K_1 - k_B k_C}{K_1(K_2 - K_1)}\right) \exp(-K_1 t) + \left(\frac{(-k_B K_2 - k_B k_C}{K_2(K_2 - K_1)}\right) exp(-K_2 t) \quad (5.15)$$

For $t \rightarrow \infty$ or sufficiently long;

$$R_\infty = \frac{k_B.k_C}{K_1.K_2} \quad (5.16)$$

and

$$R_T = R_\infty + \left(1 + \frac{(k_B K_1 - k_B k_C}{K_1(K_2 - K_1)}\right) \exp(-K_1 t) + \left(\frac{(-k_B K_2 - k_B k_C}{K_2(K_2 - K_1)}\right) exp(-K_2 t)$$

$$= R_\infty + A_1 exp(-K_1 t) + A_2 \exp(-K_2 t) \quad (5.17)$$

with;

$$A_1 = \left(1 + \frac{(k_B K_1 - k_B k_C}{K_1(K_2 - K_1)}\right), \qquad A_2 = \left(\frac{(-k_B K_2 - k_B k_C}{K_2(K_2 - K_1)}\right). \quad (5.18)$$

5.3 Torrefaction of Solid Olive Mill Residue

5.3.1 Solid Olive Mill Residue (SOMR) as Fuel and Torrefaction Experiments

Solid Olive Mill Residue (SOMR) is an agricultural solid residue left after olive oil extraction. SOMR is an attractive source of biomass for energy generation especially for Mediterranean Basin. SOMR is attractive for energy generation because of being produced in bulk in associated mills and factories. Besides being produced in bulk; merits of using SOMR for energy generation can be listed as;

- SOMR has high carbon content.
- HHV of raw SOMR is high compared to many other agricultural residues.
- The collection and transportation costs are low because of being produced in bulk.

In this study, torrefaction of SOMR has been studied at three different temperatures and three different holding times. The SOMR used in torrefaction experiments was supplied by local Aydın Olive Mill Company, which is based in Akçay, Cyprus. Torrefaction temperature is set for clarifying effect of both light and severe torrefaction conditions on raw SOMR. Also, the holding times were set to 30, 60 and 120 minutes by considering the fact that reactivity of biomass slows around 1-2 hours [73] for any thermochemical process. It must be pointed out that the holding time does not include the heating time. The torrefaction experiments were conducted in a glass tube which is placed in to an electric heater. The schematic representation of used torrefaction equipment is shown in Figure 23. The glass tube has height of 0.29 m and radius 0.02 m. The glass tube was heated with heating rate of less than 15^{o}C/min. Internal temperature of biomass samples was measured by K-type thermocouple for assuring torrefaction temperature during process. Each torrefaction experiment was conducted with 3 gr of SOMR. The particle size of used raw SOMR was varying between 1mm and 2mm. Nitrogen was used as inert gas for providing the inert medium. Torrefaction processes were carried out under the flow of 20 mL/min nitrogen.

Table 7. Ultimate analysis of raw SOMR.

	C (wt%)	**H (wt%)**	**N (wt%)**	**S (wt%)**	**O (%)**
SOMR	47.62	6.50	1.86	0	39.82

Table 8. Proximate Analysis of raw SOMR.

	VM (wt%)	**Ash(wt%)**	**FC (wt%)**	**HHV (MJ/kg)**
SOMR	88.84	4.20	6.96	18.8

Also, 50 mL/min nitrogen was flowed for 10 minutes inside the glass tube before each torrefaction experiment, for taking out the oxygen from glass tube.Each torrefaction experiment was repeated twice and average of analysis results was presented.

In this study the optimum torrefaction condition (between studied torrefaction temperatures and holding times) have also been investigated. The optimum torrefaction condition is determined by considering the changes in ultimate and proximate composition, changes in HHV and energy yield. Additionally, thermogravimetric analysis (TGA) and the derivative thermogravimetric analysis (DTG) of raw SOMR were conducted in order to clarify the decomposition characteristics of SOMR with increased temperature. The Termogravimetric Analysis (TGA) and the Derivative Termogravimetric Analysis (DTG) of raw SOMR were conducted by Mettler Toledo TGA/DSC 1 Star System (Switzerland).

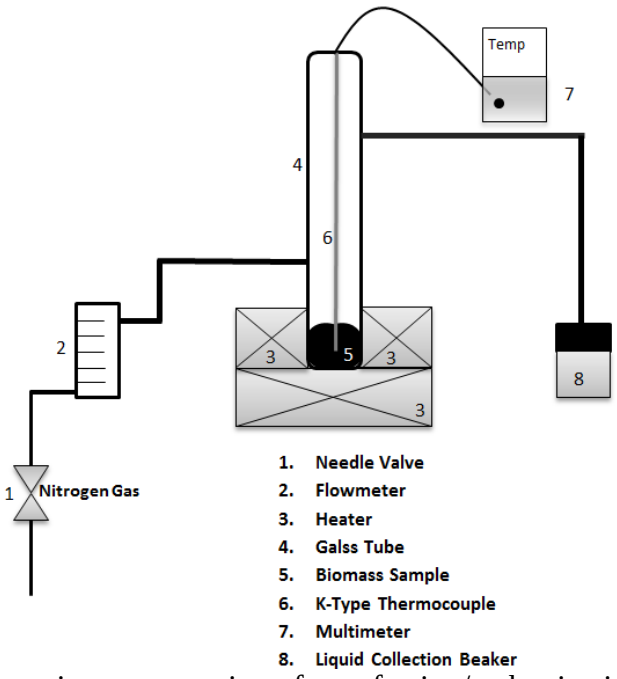

Figure 23. Schematic representation of torrefaction/carbonization equipment.

The ultimate analysis, which measures Carbon(C), Hydrogen (H), Nitrogen(N), Sulphur(S) and Oxygen(O) content, of torrefaction products were driven with Thermo Finnegan Flash EA 1112 Series Element Analyzer (Italy). For each ultimate analysis 2 mg sample were used and combusted rapidly in pure oxygen.

Proximate analysis of torrefaction products, were conducted in a muffle furnace. Torrefied samples were dried at 105^{o} C (until their mass reached to a stable point) before proximate analysis. Volatile matter, ash and fixed carbon content of torrefied SOMR were determined by proximate analysis. Volatile matter content of moisture free samples was measured by heating in a moisture free closed crucible up to 950^{o}C and keeping at that temperature for 6 minutes. Volatile matter content of products were calculated according to;

$$VM = 100 \times \frac{m_{products} - m_{vm}}{m_{products}} \quad (5.19)$$

$m_{products}$ is the mass of moisture free products SOMR before heating up to 950^{o}C and m_{vm} is the mass of left sample after heating up to 950^{o}C in a closed crucible and keeping at that temperature for 6 minutes. Ash content was measured after the measurement of volatile matter content. Volatile and moisture free torrefied samples were heated up to 750^{o}C and held at that temperature for 6 hours in an open crucible. Ash content was calculated according to;

$$Ash = 100 \times \frac{m_{ash}}{m_{products}} \quad (5.20)$$

m_{ash} is the remained mass after heating up to 750^{o}C and keeping at that temperature for 6 hours. Fixed carbon (FC) content of torrefied SOMR was calculated according to;

$$FC\% = 100 - VM\% - Ash\% \quad (5.21)$$

Beside ultimate and proximate analysis, mass yield, energy yield and HHV (MJ/kg) [97] were calculated by following equations:

$$Mass\ Yield = \frac{Mass\ of\ Products}{MassofrawSOMR} \times 100 \quad (5.22)$$

$$Energy\ Yield = \frac{Mass\ of\ Products}{MassofrawSOMR} \times \frac{(HHV)_{products}}{(HHV)_{RawSOMR}} \times 100 \quad (5.23)$$

$$HHV\left(\frac{MJ}{kg}\right) = 0.335\ C(wt\%) + 1.42H(wt\%)$$
$$-0.154\ O(wt\%) - 0.145\ N(wt\%) \quad (5.24)$$

5.3.2 Appearance of Torrefaction Products

The appearance of torrefied SOMR; at 210^{o}C, 240^{o}C and 280^{o}C are given in Figure 24 (a), (b), (c), Figure 25 (a), (b), (c) and Figure 26 (a), (b), (c) respectively. Figure 24, 25 and 26 clearly demonstrates that; the color of torrefied SOMR becomes darker. Torrefaction experiments showed that the torrefied SOMR becomes darker with increased torrefaction temperature and holding time. In this work, although no analysis is done for grindability of torrefaction products; it is observed that the torrefied SOMR becomes much more brittle after torrefaction.

5.3.3 Mass Yield of Torrefied Solid Olive Mill Residue

The effects of the torrefaction temperature and the holding time on mass yield are demonstrated in Figure 27 in dry basis.

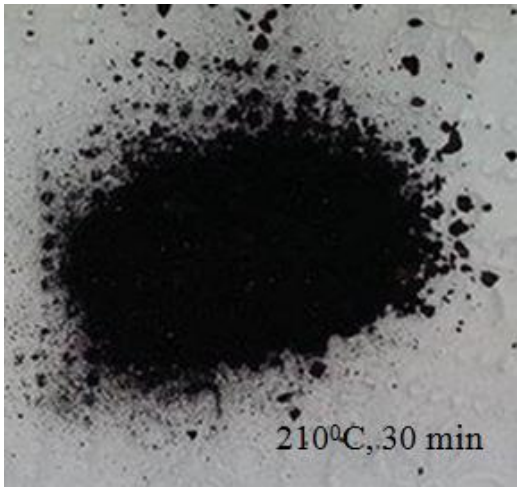

(a)

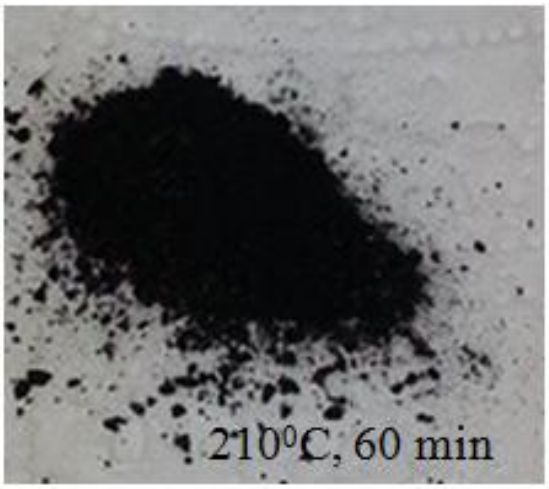

(b)

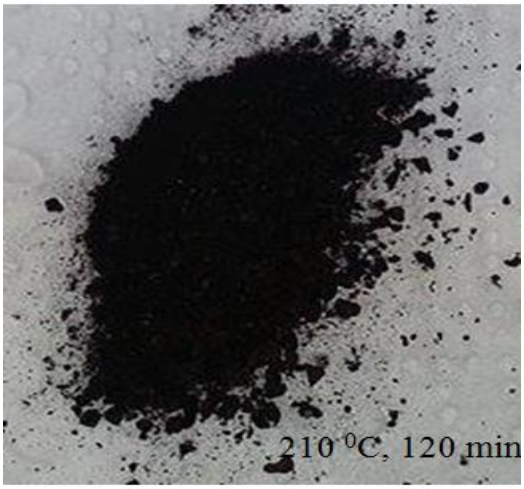

(c)

Figure 24. Torrefaction products obtained at 210^{o}C for holding times of (a) 30 minutes (b) 60 minutes (c) 120 minutes.

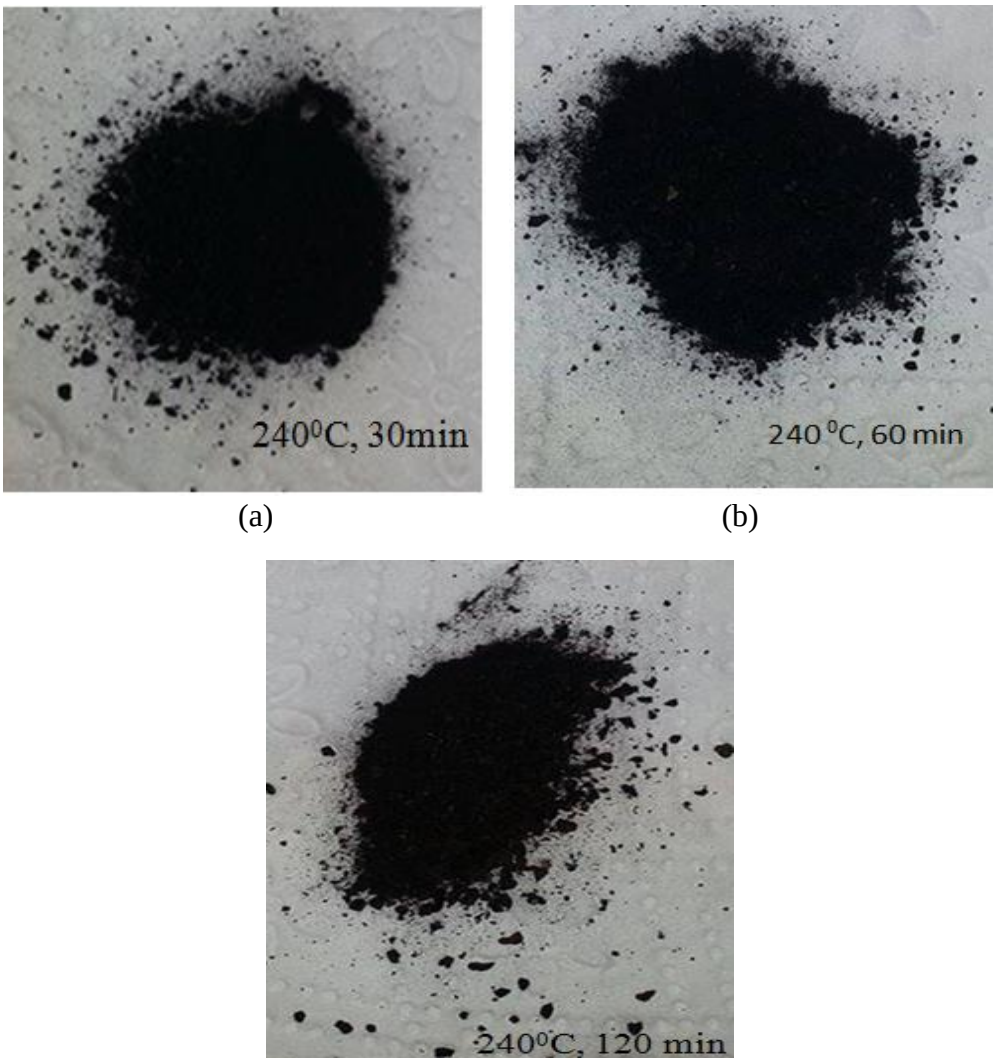

(a) (b)

(c)

Figure 25. Torrefaction products obtained at 240^{o}C for holding times of (a) 30 minutes (b) 60 minutes (c) 120 minutes.

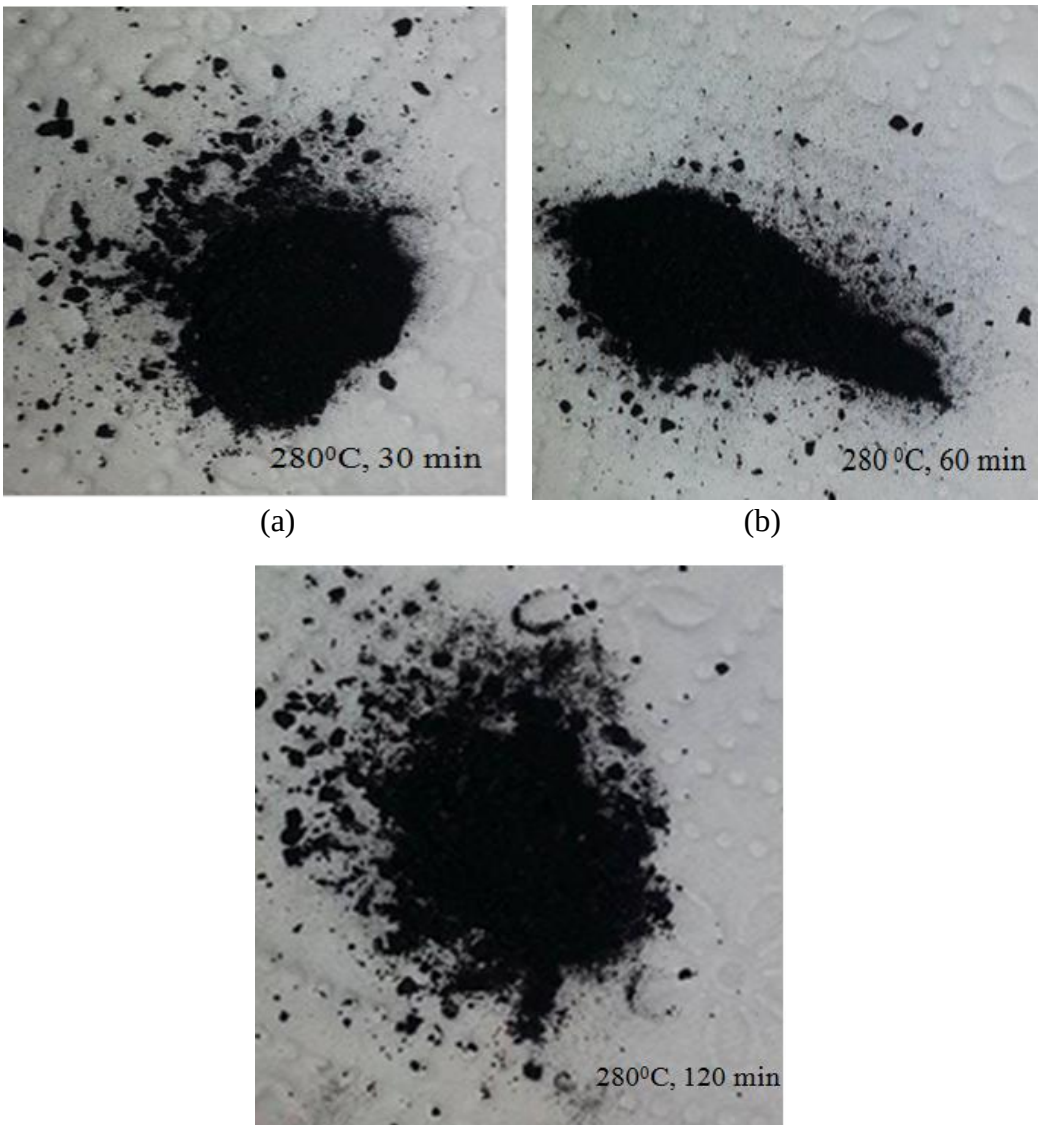

(a) (b)

(c)

Figure 26. Torrefaction products obtained at 280^{0}C for holding times of (a) 30 minutes (b) 60 minutes (c) 120 minutes.

Mass yield decreases with increased. and holding time. Results indicated that, at torrefaction temperature of 210^{o}C, increasing holding time from 30 minutes to 60 minutes did not alter the mass yield. However, at torrefaction temperature of 240^{o}C mass yield significantly reduced when holding time is rised from 30 to 60 minutes.

In contrast, at 240^{o}C mass yield of torrefied SOMR is not remarkably affected when holding time is 120 minutes. Figure 27 clearly indicated that holding time did not remarkably alter the mass yield at severe torrefaction conditions i.e., at 280^{o}C.The deviation in the mass yield of the torrefaction products is no more than 5% at 280^{o}C for all holding times.

Reduced mass yield during the torrefaction process is mainly based on bounded moisture removal and thermal degradation; to form volatile products such as H_2O, CO, CO_2, H, acetic acid, and other organics [98]. Studies on isothermal[99] and non-isothermal torrefaction [67] of cellulose, hemicellulose, lignin and xylan revealed that hemicellulose degrades at torrefaction temperatures as low as 230°C, whereas lignin does not degrade even at high torrefaction temperatures. However, these studies showed that xylan is the most reactive constituent of biomass and depleted prior whatever the type of performed torrefaction process.

In this study, mass loss during torrefaction of SOMR at 210°C was mainly due to the removal of bounded water which evaporates around 160^{o}C [100]. The removal of bound water is significantly observed in TGA curve as well, around 162^{o}C. Additionally mass loss at 210°C is associated with removal of the light volatiles and decomposition of xylan. Increased mass loss at 240°C was associated with the degradation of hemicellulose and degradation of cellulose also contributed to mass

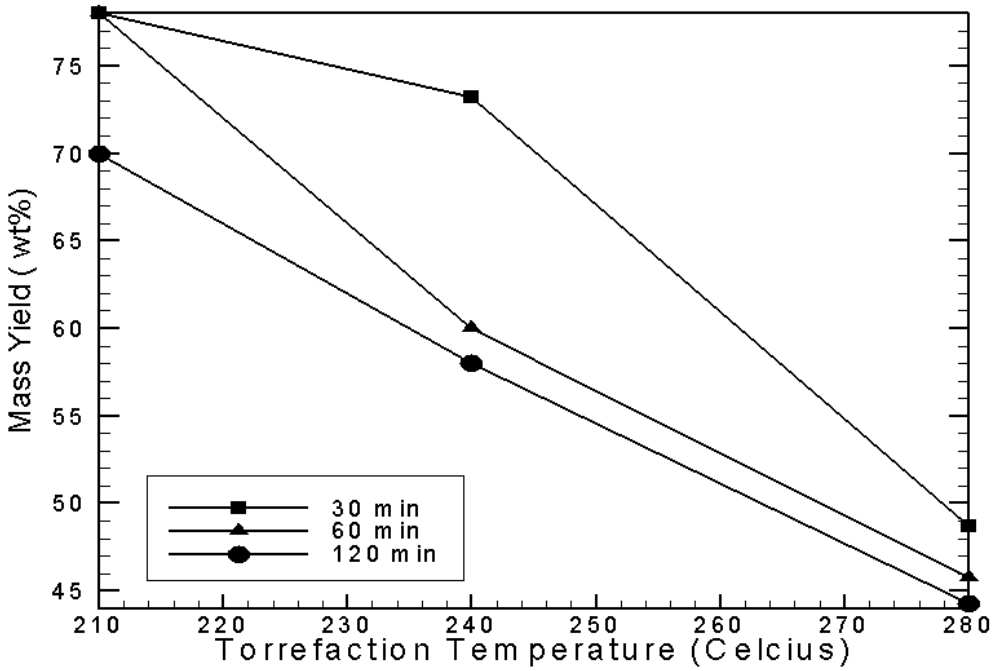

Figure 27. Effect of torrefaction temperature and holding time on mass yield.

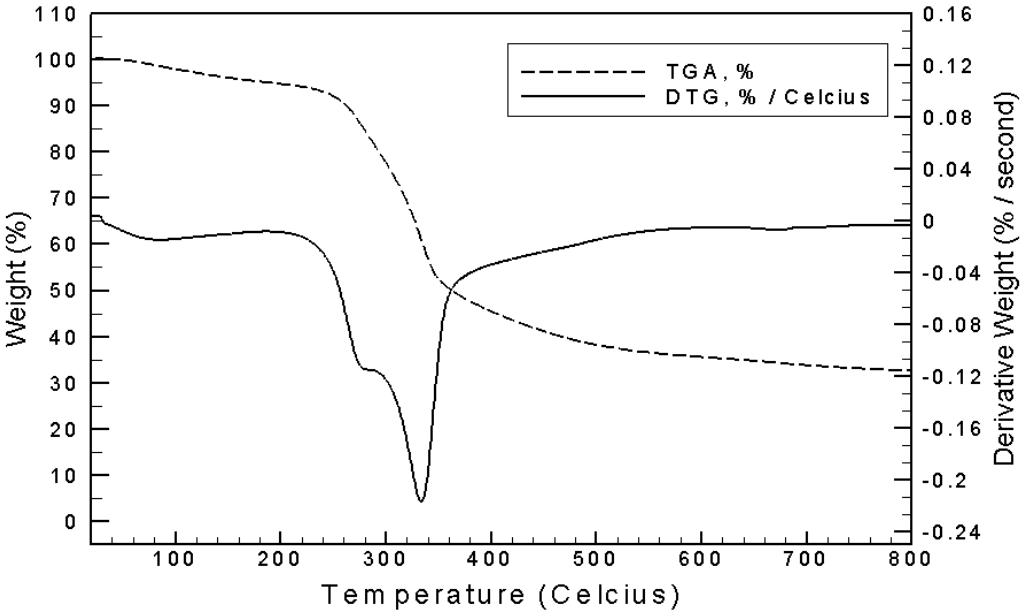

Figure 28. The TGA and DTG diagrams of raw SOMR.

loss at 280°C. The results from the analyses of TGA and DTG is shown in Figure 28. Results showed that mass of raw SOMR reduces in range of 200-280^{o}C remarkably. TGA results revealed that 84% of SOMR remains when temperature reached 280^{o}C. However, Chen and Kuo [99] showed that when cellolose and hemicellulose were torrefied isothermally, increasing holding time up to 60 minutes remarkably reduces the mass yield. In this work lowest mass yield was obtained when SOMR was torrefied at severe torrefaction conditions for 120 minutes. However, consistent with the work of Chen and Kuo[99] increasing holding time from 60 minutes to 120 minutes did not alter the mass yield more than 2% at severe torrefaction conditions.

5.3.4 Carbon (C), Hydrogen (H), Nitrogen (N) and Oxygen (O) Content of Torrefied Solid Olive Mill Residue

The ultimate analysis results of solid torrefaction products for studied torrefaction conditions are listed in Table 9 and changes in Carbon(C), Hydrogen (H) and Oxygen(O) content of the solid torrefaction products are demonstrated in Figure 29, 30 and 31 respectively. Ultimate analysis results have shown that torrefaction yields to solid fuel with higher carbon, less hydrogen and less oxygen content.

Reduced hydrogen and oxygen content is mainly associated with destroyed hydroxyl group (-OH) of the biomass during the torrefaction process [101, 82]. Loss of the hydroxyl group (-OH) results in a solid hydrophobic fuel with decreased hydrogen and oxygen contents. Besides changes in elemental composition, it is important to detect changes in H/C and O/C atomic ratios of solid torrefaction products. Figure 32 and 33 shows the effect of the torrefaction temperature and holding time on H/C and O/C atomic ratio of torrefied and raw SOMR respectively. H/C and O/C atomic ratios are measure of pyrolysis efficiency and degree of oxidation respectively [102,103].

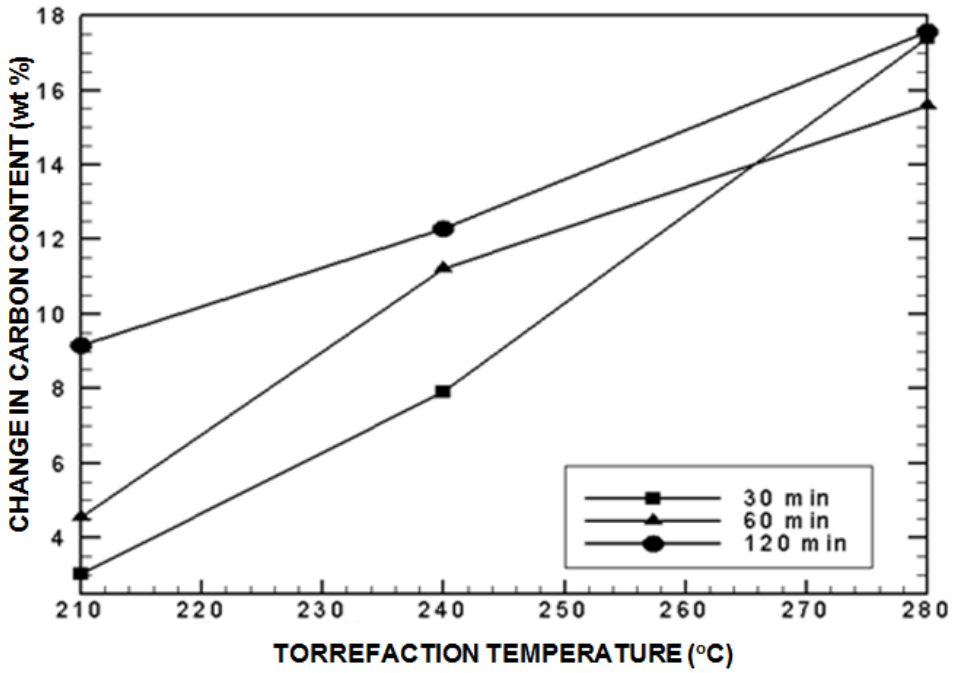

Figure 29. Change in Carbon content of SOMR at various torrefaction conditions.

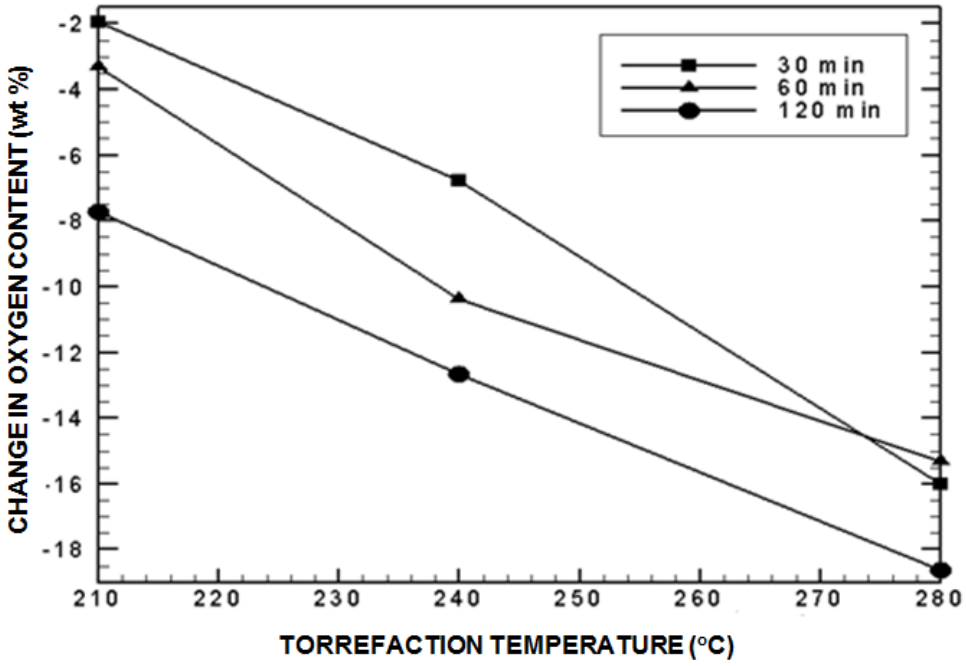

Figure 30. Change in Oxygen content of SOMR at various torrefaction conditions.

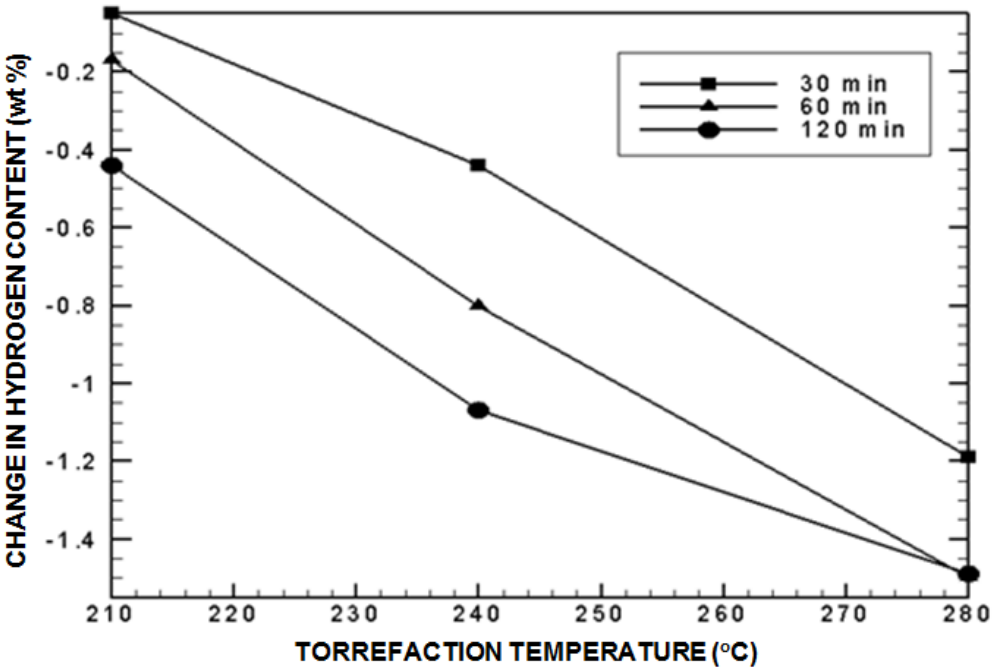

Figure 31. Change in Hydrogen content of SOMR at various torrefaction conditions.

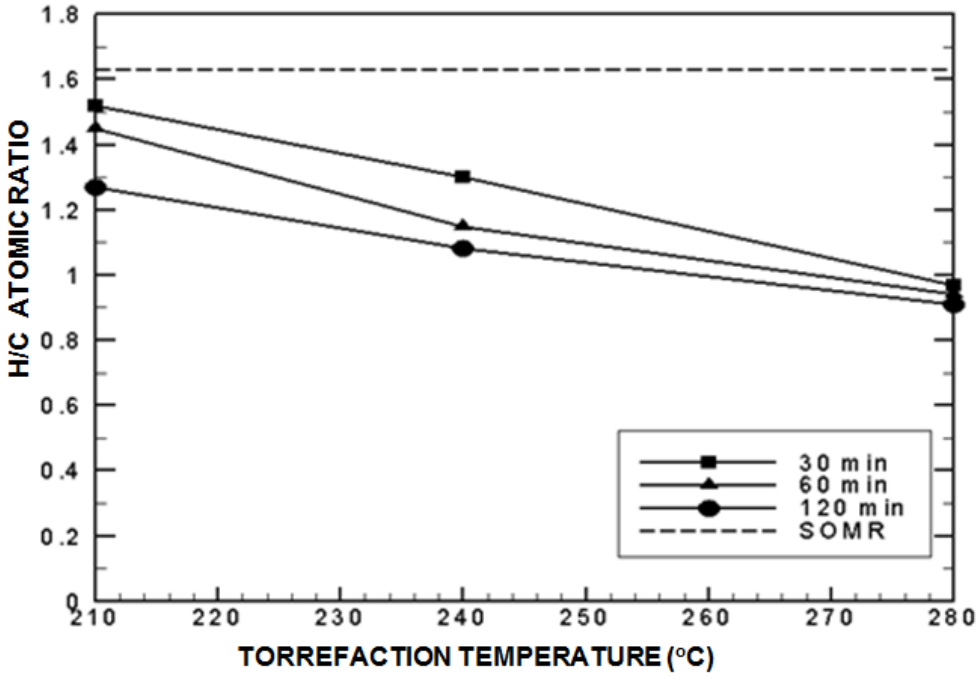

Figure 32. H/C Atomic ratio of SOMR at various torrefaction conditions.

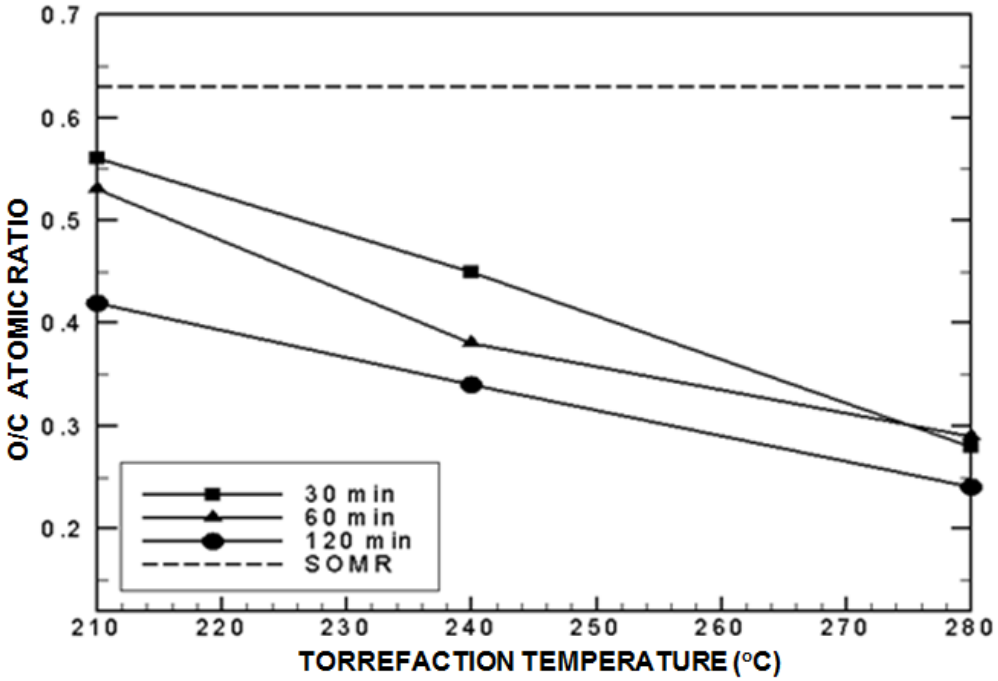

Figure 33. O/C Atomic ratio of SOMR at various torrefaction conditions.

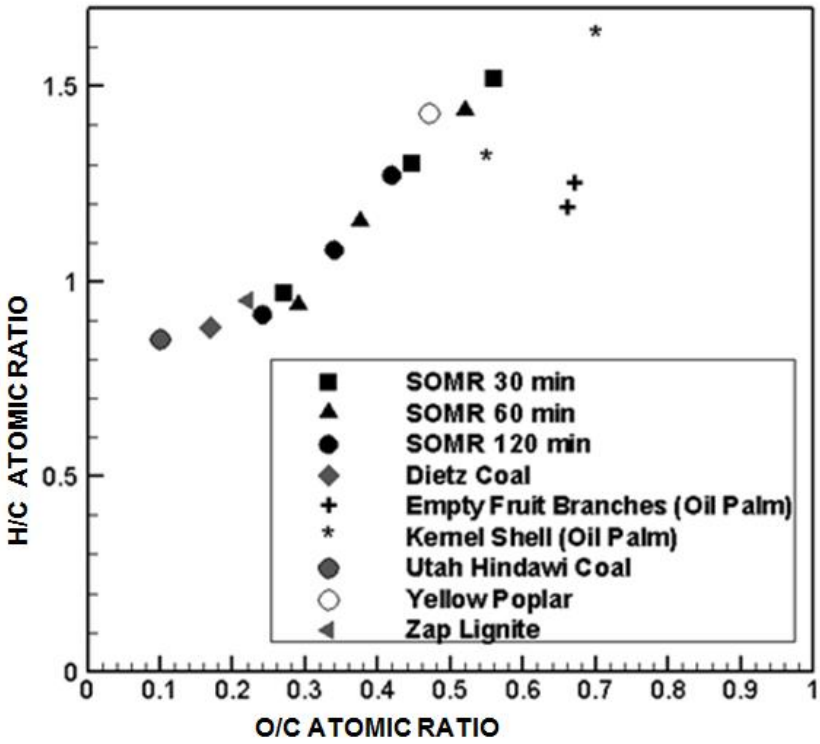

Figure 34. Van-Krevelen diagram of torrefied SOMR, and various torrefied biomass[105,101,81,106].

Table 9. Ultimate analysis of torrefied SOMR. (* db).

Holding Time (min)	Temperature (°C)	C (wt%)	H (wt%)	N (wt%)	O* (wt%)	HHV (MJ/kg)
	210	50.65	6.45	1.68	37.89	**20.06**
30	240	55.53	6.06	1.68	33.06	**21.96**
	280	65.02	5.31	1.14	23.8	**25.50**
	210	52.15	6.33	1.51	36.51	**20.65**
60	240	58.82	5.70	1.38	29.44	**23.08**
	280	63.19	5.00	0.77	24.49	**24.40**
	210	56.77	6.06	0.79	32.09	**22.59**
120	240	59.92	5.43	1.64	27.17	**23.37**
	280	65.18	5.01	1.40	21.21	**25.50**

Also, reduced O/C ratio is an indicator of both hydrophobicity and polarity, which results with reduction of fuel affinity with water molecules [104]. It can be evidently seen that both the degree of oxidation and pyrolysis efficiency rises with increased torrefaction temperature. Although, similar results were obtained with risen holding time, the effect of the holding time is less remarkable than the effect of torrefaction temperature especially at 280^{o}C.

The Van-Krevelen diagram, which shows H/C atomic ratio of solid fuel as function of O/C atomic ratio, is important for characterization of solid fuel. The Van-Krevelen diagram of torrefaction products is presented in Figure 34. Besides torrefied SOMR, other torrefied biomass samples and three different coal types (Zap Lignite, Dietz, and Utah Hindawi coal) were also included in the diagram.

In this work, the Van-Krevelen diagram is used to identify similarities and differences between torrefaction characteristics of SOMR and other types of biomass. Torreffied biomass used for comparing torrefaction behavior of SOMR were all torrefied for 30 minutes. Also, torrefaction temperatures of those biomass were not deviate more than 10^{o}C from torrefaction temperatures used for torrefaction of SOMR. Figure 34 illustrates that, torrefied SOMR behaves similarly to other types of torrefied biomass by means of reduction in both H/C and O/C ratios [105,101,81,106]. The results point out that SOMR torrefied much more efficiently compared to other types of biomass and less oxygenated fuel was obtained. It is estimated that relatively less oxygen content of torrefied SOMR is a result of high volatile content of raw SOMR. An important difference in the torrefaction characteristics of SOMR compared to other biomass was also detected. Results revealed that torrefaction of SOMR provides a solid fuel of which the H/C and O/C

atomic ratios are very close to low rank zap lignite coal when torrefied at 280°C for 120 minutes.

5.3.5 Volatile Matter (VM), Fixed Carbon (FC) and Ash Content of Torrefied Solid Olive Mill Residue

The proximate analysis of torrefaction products of SOMR is given in Table 10. Also changes in VM, FC and ash content are given in Figure 35, 36 and 37 respectively. The experimental results show that FC and ash content increases with increasing torrefaction temperature and holding time, whereas VM content shows a different trend. High ash content inhibits the combustion of fuel because oxygen may not penetrate through the ash easily for burning [108]. The non-homogenous structure of SOMR results in lower ash content at the torrefaction temperatures 210°C (for 30 and 60 min) and 240°C (for 30 min).

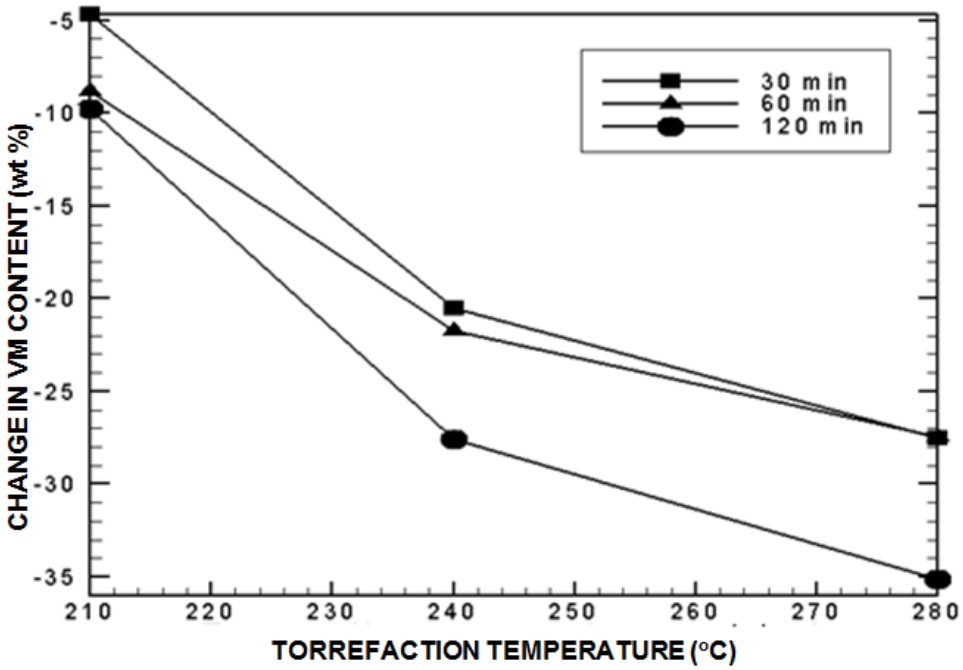

Figure 35. Change in VM of torrefied SOMR at various torrefaction conditions.

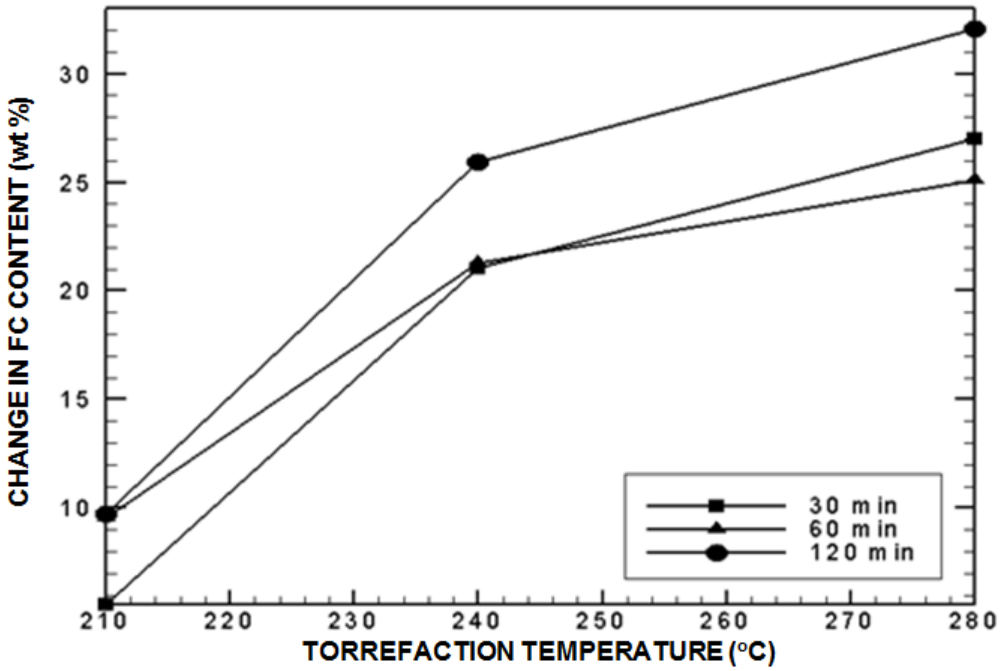

Figure 36. Change in FC of torrefied SOMR at various torrefaction conditions.

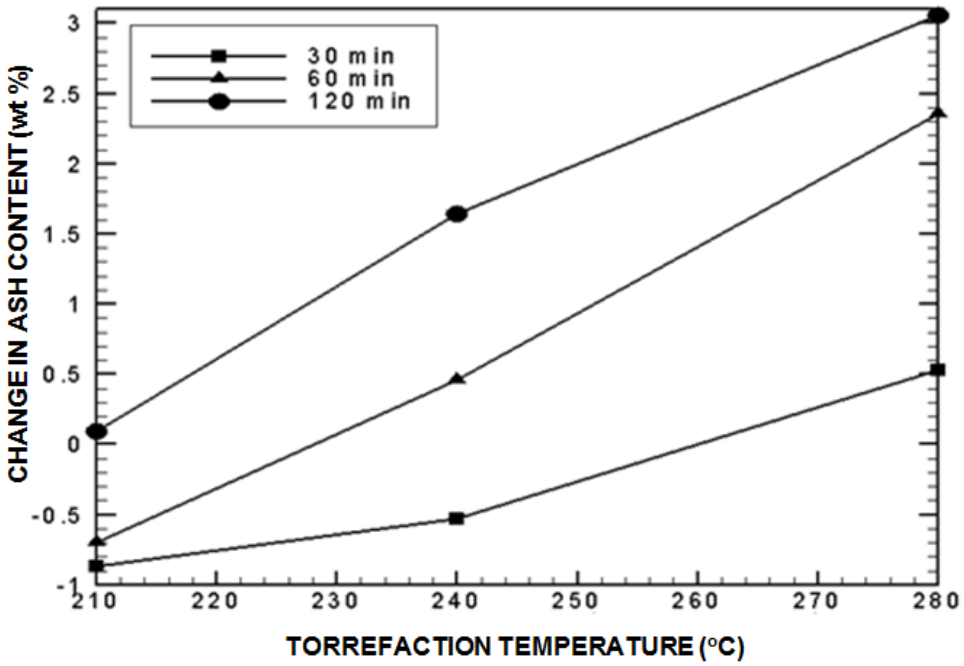

Figure 37. Change in ash content of torrefied SOMR at various torrefaction conditions.

Table 10. Proximate analysis of torrefied SOMR.

Holding Time (min)	Temperature (^{o}C)	VM (wt%)	Ash (wt%)	FC (wt%)	HHV (MJ/kg)
30	210	84.14	3.33	12.53	20.06
	240	68.35	3.67	27.98	21.96
	280	61.33	4.73	33.94	25.5
60	210	80.01	3.5	16.49	20.65
	240	67.11	4.66	28.23	23.08
	280	61.39	6.55	32.06	24.4
120	210	79.05	4.29	16.66	22.59
	240	61.28	5.84	32.88	23.37
	280	53.71	7.2	39.09	25.50

5.3.6 Energy Yield

The HHV of all solid torrefaction products are given in Table 2 in dry basis. Results revealed that the HHV of solid torrefaction samples increased with increasing torrefaction temperature and holding time. This phenomenon can be linked to reduced number of C-O bonds and increased number of C-C bonds during the torrefaction process [111].

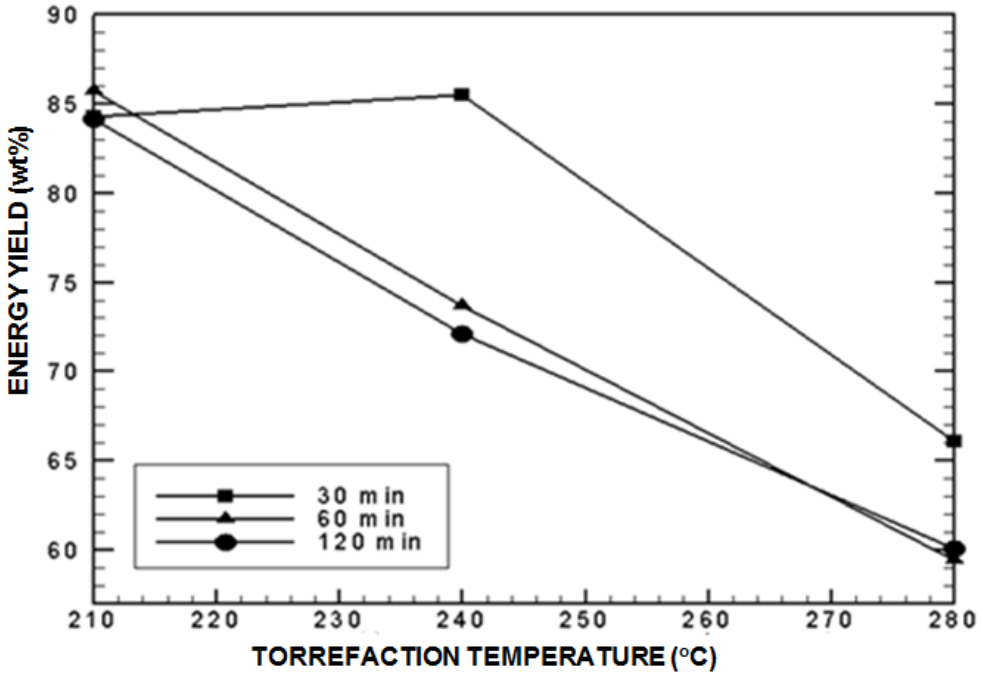

Figure 38. Energy yield of torrefied SOMR at various torrefaction conditions.

Finally, the energy yield calculation was performed in dry basis. Energy yield is the measure of the amount of energy lost after torrefaction [112]. The energy yield of torrefaction products strongly depends on mass yield, which is directly linked to biomass type [81, 106]. The effect of change in torrefaction temperature and holding time on energy yield obtained from the torrefaction products is shown in Figure 38 in dry basis. Energy yielded by torrefied SOMR ranges from 60.09% to 85.68%. It can be seen that energy yield gradually decreases with increasing torrefaction

temperature and drops below 60% at 280°C. However, an unexpected increase in energy yield was observed due to the non-homogenous chemical composition of SOMR when torrefied at 240°C for 30 minutes. Similar behaviors have also been observed during the torrefaction of sawdust [75], mesocarp fiber of oil palm waste, and kernel shell of oil palm waste [81].

5.3.7 Kinetics Model for Torrefaction of SOMR

One step reaction model is used for modeling torrefaction kinetics of SOMR. Total ratio of solids left after torrefaction is calculated according to;

$$R_T = (1 - \frac{m_i - m_f}{m_i}) \tag{5.25}$$

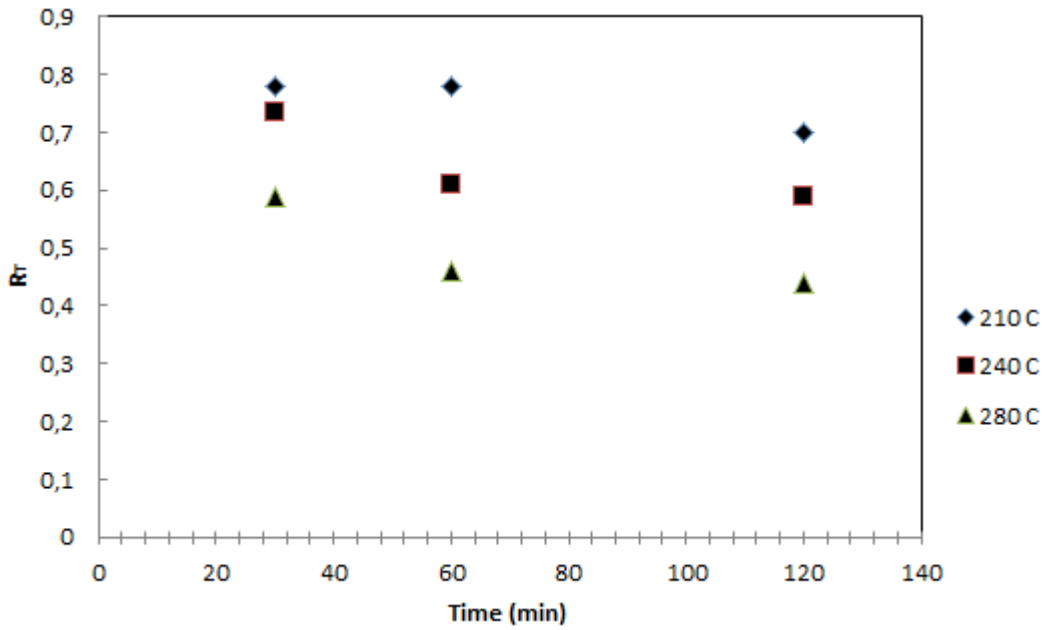

Figure 39. Change of R_T according to holding time.

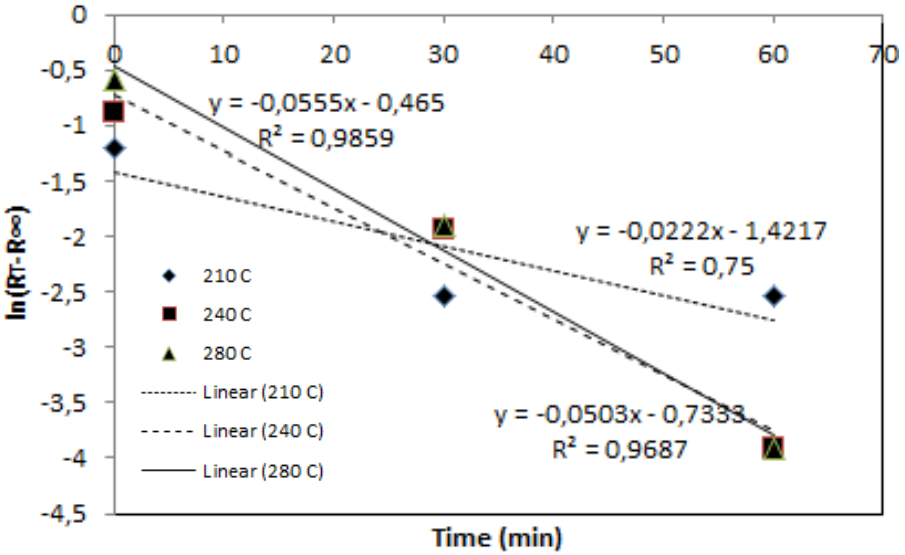

Figure 40. Change in $\ln(R_T - R_\infty)$ according to time.

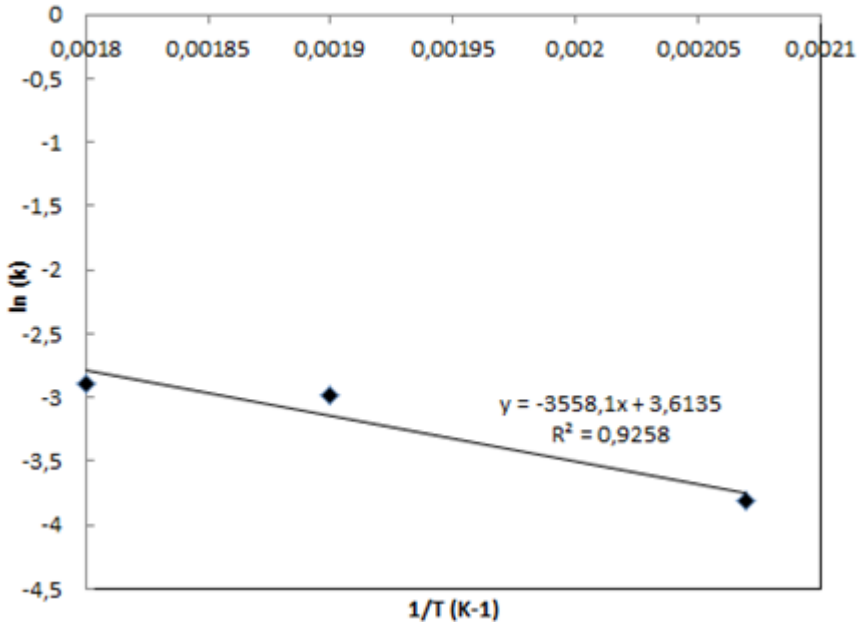

Figure 41. Change in ln(k) according to 1/T.

Figure 39 shows the change in total solids according to three different torrefaction temperature and three different holding times.

$$\ln(R_T - R_\infty) = \ln A - k\,t \qquad (5.26)$$

Equation (5.26) can be used for determination of "*k*". Equation (5.26) indicates a linear relation with holding time. The slope of $ln(R_T - R_\infty)$ vs t graph, gives the reaction rate constant "k". Figure 40 shows the change in $\ln(R_T - R_\infty)$ with respect to holding time.The slope of each line, which is "k", for each torrefaction temperature is shown in Figure 40. The Arrenihus Equation; $k = k_o \exp({}^{-E_a}/_{RT})$ can be rewritten as;

$$\ln k = \ln k_o - ({}^{E_a}/_{RT}) \qquad (5.27)$$

Equation (5.27) can be used to determine the activation energy E_a. By plotting, the graph of $\ln k$ vs ${}^{1}/_{T}$ graph the $({}^{E_a}/_{R})$ can be obtained as slope, where R is the universal gas constant (8.314 J mol^{-1} K^{-1}). The activation energy, E_a, is obtained as 29.58 kJ/mol and the Arrhenius Equation which gives the reaction rate, can be written as;

$$k = 36.97 * \exp({}^{-29582}/_{(R * T)}) \qquad (5.28)$$

where the reaction rate constants are; 0.022 min^{-1}, 0.050 min^{-1} and 0.056 min^{-1} at 210°C, 240°C and 280°C respectively.

5.3.8 Optimum Torrefaction Conditions for SOMR

The properties of torrefaction products were used for specifiying optimum torrefaction conditions of SOMR. The parameters evaluated for the optimization of torrefaction conditions can be listed as HHV, rate of change in carbon content, oxygen content, H/C ratio, O/C ratio, energy yield, and also proximate analysis results. Experimental results indicate that the effect of temperature is much more significant than the effect of holding time, especially on elemental composition.

The greatest changes in HHV, O/C ratio, H/ C ratio, carbon content, and oxygen content of torrefaction products were obtained at 280°C, where all contribute to upgrade the quality of SOMR as fuel. However, results showed that at 280°C, HHV, carbon content, and oxygen content were very similar for all torrefaction products at holding times of 30, 60, and 120 minutes. Similarly, a comparison of H/C ratios of torrefaction products revealed that process efficiencies were very similar for all holding times at 280°C. H/C ratio of products was only 5% less at 120 minutes compared to 30 and 60 minutes. The O/C ratio of products at 280°C was approximately 10% lower at 120 minutes, than that obtained at 30 and 60 minutes.

Proximate analysis results showed that torrefaction at 280 °C for 30 and 60 minutes yield solid fuel which has very similar volatile matter, fixed carbon, and ash contents. Volatile matter, fixed carbon, and ash content of torrefied SOMR do not deviate more than 3% for all holding times. For the holding time of 120 minutes at 280°C, changes in volatile matter, fixed carbon, and ash content of the products were 7.61%, 2.47%, and 5.15%, respectively, compared to 30 minutes. The energy yield of the process is a measure of chemical energy stored in the solid products of the

process. It is detected that 40% of the chemical energy is lost when the holding time exceeds 30 minutes at 280°C.

This study revealed that more qualified solid fuel is produced at severe torrefaction conditions from SOMR. Also, holding times which are not exceeding 30 minutes is sufficient to obtain qualified, energy dense, and hydrophobic solid fuel from SOMR.

5.4 Comparison of Torrefied and Carbonized Solid Olive Mill Residue

Carbonization or slow pyrolysis is a thermochemical upgrading treatment which mainly yields to solid fuel similar to torrefaction. The main difference between two process is the process temperature. It must be pointed out that carbonization is the unique biomass thermochemical upgrading treatment that yields a solid fuel(main product) and occurs at temperature range of 350-500^{o}C. Similar to torrefaction; carbonization occurs in inert atmosphere with slow heating rates. Carbonization occurs at higher temperature range compared to torrefaction

In this study, torrefied SOMR and carbonized SOMR are compared for clarifying the necessity of high process temperature for upgrading fuel properties of SOMR. According to results, torrefaction experiments demonstrated that optimum torrefaction temperature is 280^{o}C. In this section, torrefaction products produced at 280^{o}C with holding times of 30 minutes and 120 minutes are compared with carbonization products.

5.4.1 Carbonization Process

Carbonization process was carried out at 400^{o}C for 30 minutes with heating rate of less than 15^{o}C min^{-1} under the flow of nitrogen gas, with the equipment shown in Figure 23. Similar to torrefaction experiments, the particle size of raw SOMR was ranging 1-2mm during carbonization experiments. The flow rate of nitrogen gas was

20mL/ min also, 50 mL/min Nitrogen was flowed inside glass tube 10 minutes before each experiment. Each carbonization experiment was repeated twice and averages of analysis results are presented. SOMR torrefied at 280^{o}C for 30 minutes is represented by T30, SOMR torrefied at 280^{o}C for 120 minutes is represented by T120 and SOMR carbonized at 400^{o}C for 30 minutes is represented by CSOMR in figures.

5.4.2 Carbon(C), Hydrogen (H), Nitrogen (N) and Oxygen Content of Torrefied and Carbonized Solid Olive Mill Residue

Figure 42 shows carbon content of raw SOMR, SOMR torrefied at 280^{o}C for 30 minutes (T30), SOMR torrefied at 280^{o}C for 120 minutes (T120) and SOMR carbonized at 400^{0}C for 30 minutes (CSOMR). Analysis results showed that carbon content of both torrefied and carbonized SOMR is almost same and do not deviate more than 1.08%.

Hydrogen content of raw, torrefied and carbonized SOMR are given in Figure 43. The hydrogen content of carbonized SOMR was expected to be less compared to torrefied SOMR due to higher process temperature. Results demonstrated that, torrefied SOMR contains approximately 0.75% more hydrogen than carbonized SOMR. Figure 44 shows that both carbonization and torrefaction significantly contributes to reduce the oxygen content of SOMR. Experimental results revealed that solid fuel obtained by torrefaction at 280^{o}C for 30 minutes contains 5.19% more oxygen relative to CSOMR. However, torrefied SOMR at 280^{o}C for 120 minutes has 2.60% higher oxygen content compared to CSOMR. Similarly H/C and O/C ratios of raw, torrefied and carbonized SOMR are illustrated in Figure 45 and Figure 46 respectively. It is well known that pyrolysis efficiency increases with increased process temperature and results with lower H/C ratio. Nonetheless, H/C ratio of CSOMR is 0.15 lower than the H/C ratio of both torrefied SOMR.

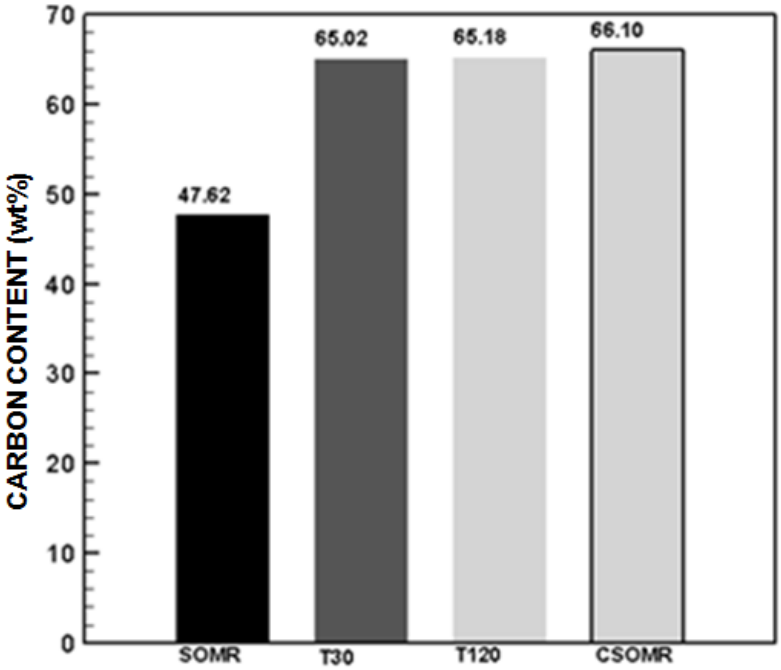

Figure 42. Carbon content of raw, torrefied and carbonized SOMR.

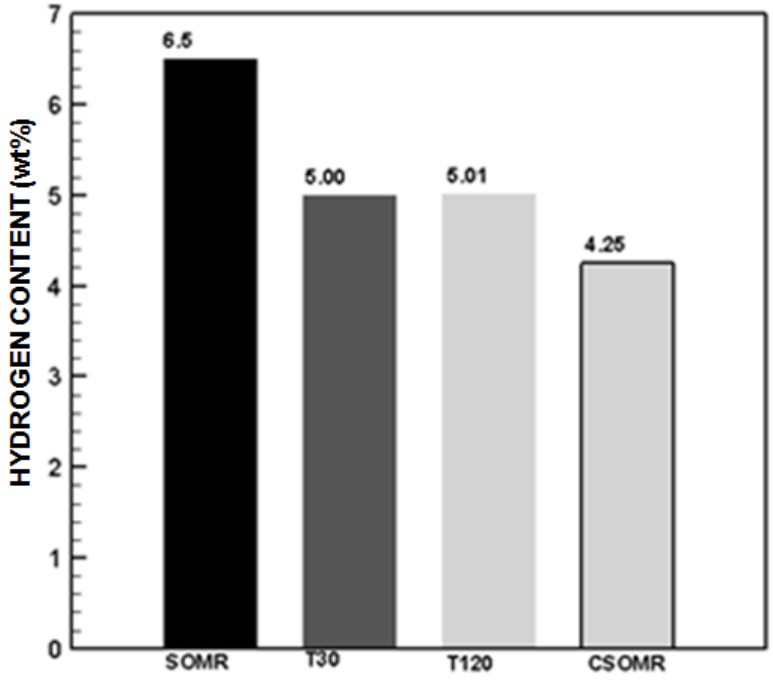

Figure 43. Hydrogen content of raw, torrefied and carbonized SOMR.

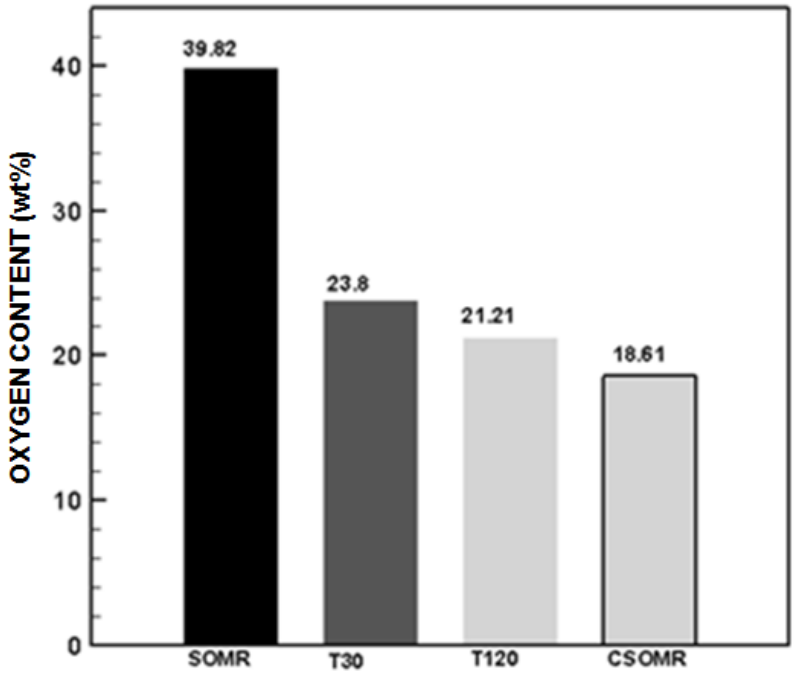

Figure 44. Oxygen content of raw, torrefied and carbonized SOMR.

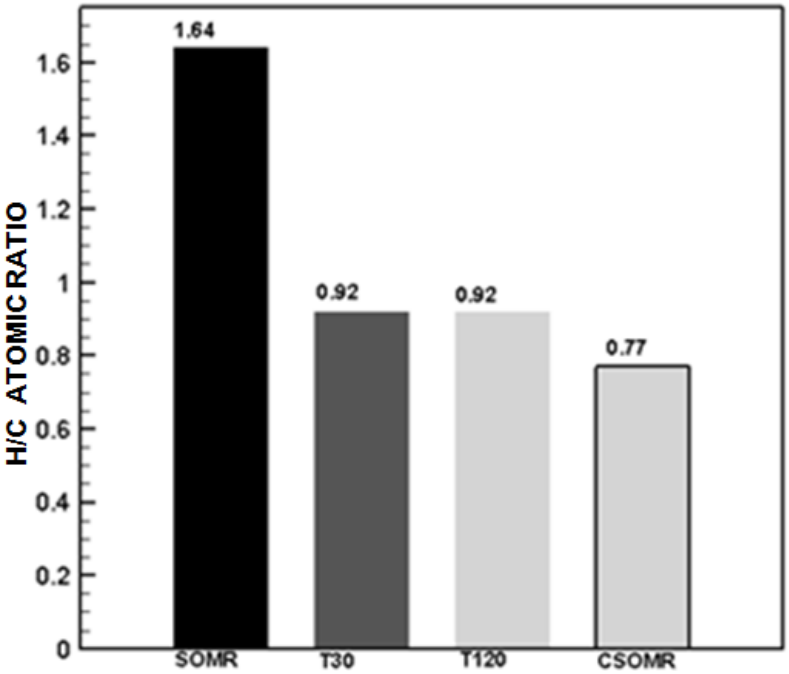

Figure 45. H/C ratio of raw, torrefied and carbonized SOMR.

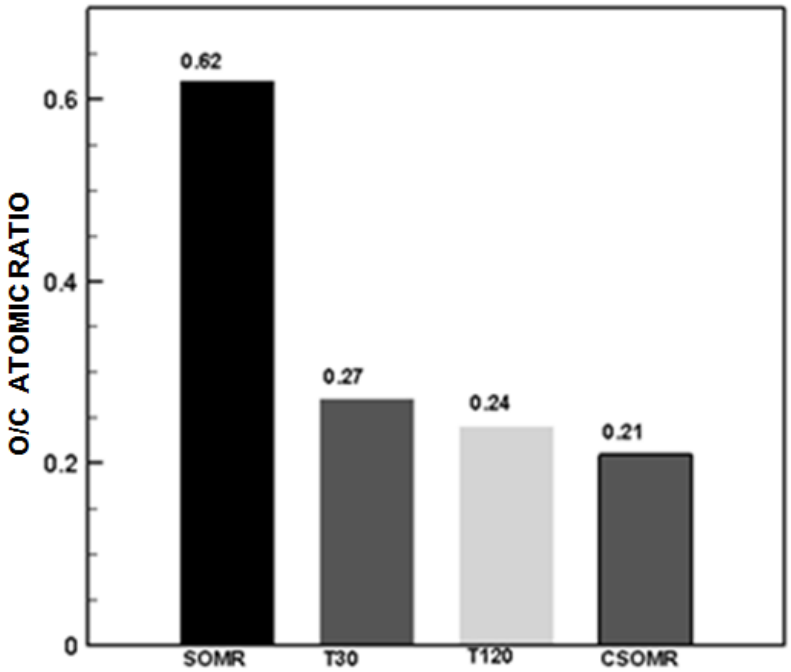

Figure 46. O/C Ratio of raw, torrefied and carbonized SOMR.

Oxygen content is one of parameters which was significantly affected from process temperature during thermochemical processes. Consistent with this fact, carbonization experiments results with less oxygenated solid fuel. That fact also results with less O/C ratio from carbonization of SOMR. The experimental results indicated that O/C ratio of T30 is 0.06 higher than CSOMR, where O/C Ratio of T120 is 0.03 higher than CSOMR.

5.4.3 Volatile Matter (VM), Fixed Carbon (FC) and Ash Content of Torrefied and Carbonized Solid Olive Mill Residue

Proximate analysis is conducted for comparing effect of carbonization and torrefaction on ash, volatile matter and fixed carbon composition of produced solid fuels. Figure 47 illustrates ash content of raw, torrefied and carbonized SOMR. It is well known that ash content of both torrefaction and carbonization products increases with increased process temperature.

Experimental results well agreed with the fact that, carbonized SOMR has highest ash content. However, torrefaction of SOMR revealed that ash content of solid torrefaction products are affected from holding time and T120 has higher ash content compared to T30. Results showed that torrefied SOMR at 280^{o}C has 2% less ash content compared carbonized SOMR. Qualified solid fuels are always associated with low ash content because of less combustion problems.

Ash content measurement of SOMR, T30 , T120 and CSOMR revealed that, torrefaction of SOMR at 280^{o}C for 30 minutes provides the most attractive fuel by means of ash content. Volatile matter content of raw, torrefied and carbonized SOMR is illustrated in Figure 48. Both torrefaction and carbonization of SOMR results with a solid fuel with reduced volatile matter content. Results showed CSOMR has lowest volatile matter content where T30 has highest volatile matter content. Nevertheless, it must be stated that volatile matter content of T30 and T120 do not deviate more than 8%. Figure 49 demonstrates fixed carbon content of raw, torrefied and carbonized SOMR. Higher Fixed carbon content is an indicator of more qualified fuel. Results indicated that the variation of fixed carbon content of SOMR torrefied at 280^{o}C for 30 minutes and for 120 minutes is not more than 7%. Calculated fixed carbon contents of SOMR, T30, T120 and CSOMR showed that CSOMR contains highest amount of fixed carbon. The fixed carbon content of CSOMR is approximately 38% more than T30 and 28% more than T120.

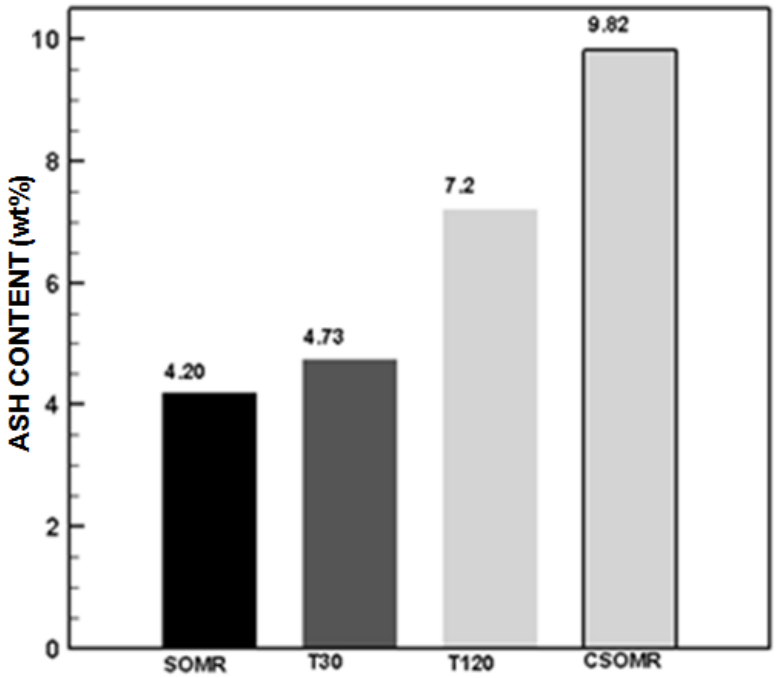

Figure 47. Ash content of raw, torrefied and carbonized SOMR.

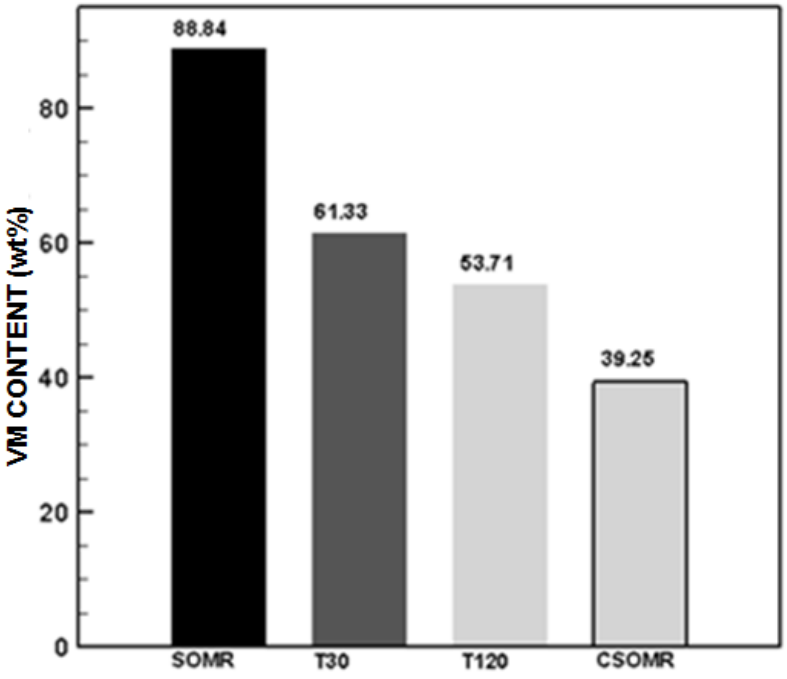

Figure 48. Volatile Matter content of raw, torrefied and carbonized SOMR.

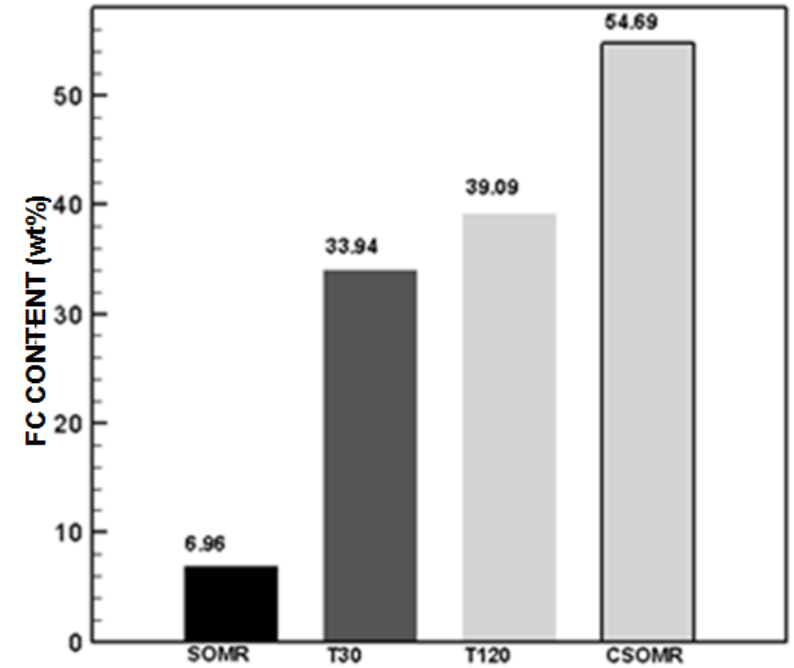

Figure 49. Fixed carbon content of raw, torrefied and carbonized SOMR.

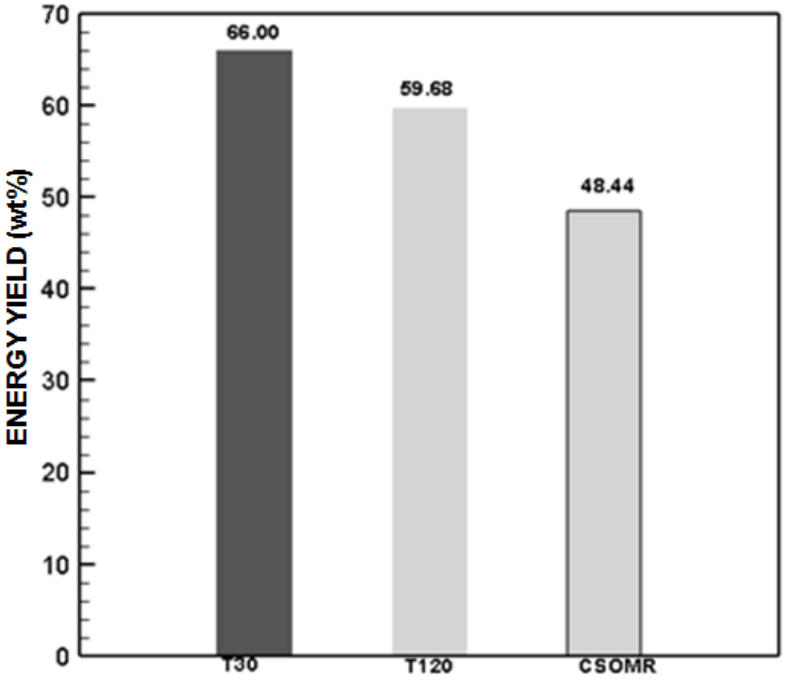

Figure 50. Energy yield of torrefied and carbonized SOMR.

5.4.4 HHV and Energy Yield of Torrefied and Carbonized Solid Olive Mill Residue

Figure 50 demonstrates energy yield of carbonized and torrefied SOMR. The mass yield of CSOMR was 37.15%, where its HHV is 25.18 MJ/kg. Energy yield calculations reveals that, more than 50% of energy is lost during carbonization. There exists a remarkable difference in energy yield of SOMR torrefied for 30 minutes and 120 minutes. Results showed that torrefaction at 280^{o}C for 30 minutes saves 66% of biomass energy where torrefaction at 280^{o}C for 120 minutes saves approximately 59.68% of energy.

5.4.5 Comparison of Carbonized and Torrefied Solid Olive Mill Residue

Ultimate analysis results showed that carbon content of both carbonized and torrefied SOMR were almost same. A considerable difference(compared to carbon and hydrogen) was observed in oxygen content. Results showed that CSOMR contains 5.19% less oxygen compared to torrefied SOMR (30 minutes). H/C ratio of products revealed that, the process efficiency of carbonization is higher than the torrefaction as expected. However, it must be pointed out that the difference in H/C ratio does not exceed 0.15. Similarly O/C ratio of products demonstrated that carbonization yields to a more hydrophobic fuel.

Proximate analysis of products revealed that torrefaction for 30 minutes results with minimum ash content and maximum volatile matter content. The most significant difference between carbonization and torrefaction is observed in volatile matter and fixed carbon content. Energy yield calculations of products showed that, almost half of energy is lost during carbonization where approximately 66% of energy is saved during torrefaction at 280^{o}C for 30 minutes.

Experimental results demonstrated that, carbonization and torrefaction yields a very similar solid end product by means of elemental composition. Comparison of torrefied and carbonized SOMR showed that torrefied SOMR yields to less qualified fuel compared to carbonization of SOMR by means of proximate composition. However, the fuel properties of T30 and CSOMR showed that torrefaction is more feasible by means of process input energy.

5.5 Effects Of Torrefaction On Carbonization Characteristics Of Solid Olive Mill Residue

Biomass pretreatment methods listed in Section 4.3.1 are generally used before treatment methods either for increasing efficiency or quality of energy carriers obtained at the end of treatment. As a pretreatment method, torrefaction yields to a solid fuel which can directly be combusted for energy generation. Nevertheless, the effects of torrefaction on gasification and fast pyrolysis has been investigated.

Neupane *et al.* [90] and Zheng *et al.* [91] tested the effect of torrefaction on fast pyrolysis characteristics of biomass. Also, Sarkar *et al*. [113] and Daniyanto *et al*. [114] studied the effect of torrefaction on gasification of biomass.

The proven merits of torrefaction, on gasification [113, 114] and fast pyrolysis [90, 91] motivated investigation of the effect of process on carbonization. The similarities and differences of torrefaction and carbonization (slow pyrolysis) is explained in section 5.4 in detail. Also the similarities and differences of their products were given in section 5.4.2.

In this study, effects of torrefaction on carbonization characteristics of biomass is also investigated by using Solid Olive Mill Residue (SOMR). The effect of torrefaction on carbonization characteristics of SOMR is tested by conducting carbonization experiments with both raw SOMR and torrefied SOMR (tSOMR). The produced biochars from SOMR and tSOMR were characterized by ultimate and proximate analysis for clarifing effect of torrefaction on carbonization characteristics of SOMR.

5.5.1 Carbonization of raw SOMR and Torrefied SOMR

The torrefaction/carbonization equipment shown in Figure 23 is used for clarifying the effects of torrefaction, on carbonization characteristics of SOMR as well. Each torrefaction/carbonization experiment was conducted with 5 g of dry SOMR. Torrefaction/carbonization processes were carried out under the flow of 20 mL/ min Nitrogen. The oxygen inside the glass tube was taken out by flowing 50 mL/min Nitrogen for 10 minutes before each experiment.

Carbonization experiments were conducted in two different sets for clarifying the effect of torrefaction on carbonization characteristics of SOMR. The first set of experiments was direct carbonization experiments. Direct carbonization experiments were conducted with dry SOMR at CT; 350^{o}C, 400^{o}C and 450^{o}C where, holding time was stated to 20 minutes. It must be pointed out that, the holding time refers to time that SOMR held at associated carbonization temperature (CT) and do not include heating time. The second set of carbonization experiments were conducted with torrefied SOMR. Dry SOMR were first torrefied at 240^{o}C for 10 minutes. At the end of torrefaction period, the process temperature was risen to associated CT. During this process CT is kept at 350^{o}C, 400^{o}C and 450^{o}C and holding time was set to 10 minutes for each carbonization process. Each carbonization experiment was repeated

twice and average of analysis results was presented. Biochars obtained from direct carbonization of SOMR at 350^{o}C, 400^{o}C and 450^{o}C are represented by 350, 400 and 450 respectively in figures and tables. Similarly, biochars produced from tSOMR at 350^{o}C, 400^{o}C and 450^{o}C are represented by 240+350, 240+400 and 240+450 respectively in figures and tables.The Costech ECS 4010 Series Element Analyzer (Italy) was used for ultimate analysis of produced biochars to obtain elemental composition in dry basis. In addition, the proximate analysis was carried out in a muffle furnace and gave the volatile matter (VM), fixed carbon (FC), and ash content composition of the sample in wt% in dry basis as described in section 5.3.1.

5.5.2 Mass Yield

The biochar yield of each carbonization process is given in Figure 51 in dry basis. Mass yield measurements showed that during direct carbonization processes; the mass yield decreases with increased CT. The mass yield decreases to 33.18 wt% from 38.00 wt% when CT rises from 350^{o}C to 450^{o}C.

Results showed that biochar yield of tSOMR is higher than directly carbonized SOMR. The difference in mass yield of SOMR and tSOMR decreases to 4.4% from 6% when CT rised to 400^{o}C from 350^{o}C. Also, at CT of 450^{o}C, the biochar yield of tSOMR is 2.62% higher than the biochar yield of SOMR. The reduced mass yield during carbonization is mainly based on the loss of moisture which is followed by the depolymarization of hemicellulose, cellulose and lignin [115]. During depolymerization of hemicellulose, cellulose and lignin; CO, CO_2 H_2O, are released [68]. In this study at CT of 350 and 400^{o}C reduction in mass yield is mainly attributed to degradation of cellulose and hemicellulose. In addition to that, at CT of 450^{o}C, decomposition of lignin occurs and results with reduced mass yield. The

reasons of reduced mass yield during the torrefaction process is well explained in section 5.3.3.

During the carbonization of tSOMR, removal of light volatiles and decomposition of xylan and hemicellulose results with mass loss at torrefaction stage. Rise in CT to 350, 400 and 450^{o}C results with more effective decomposition of cellulose and hemicellulose during carbonization of tSOMR. Carbonization experiments done by different biomass have shown that the increased holding time results with lower mass yield during carbonization [116].

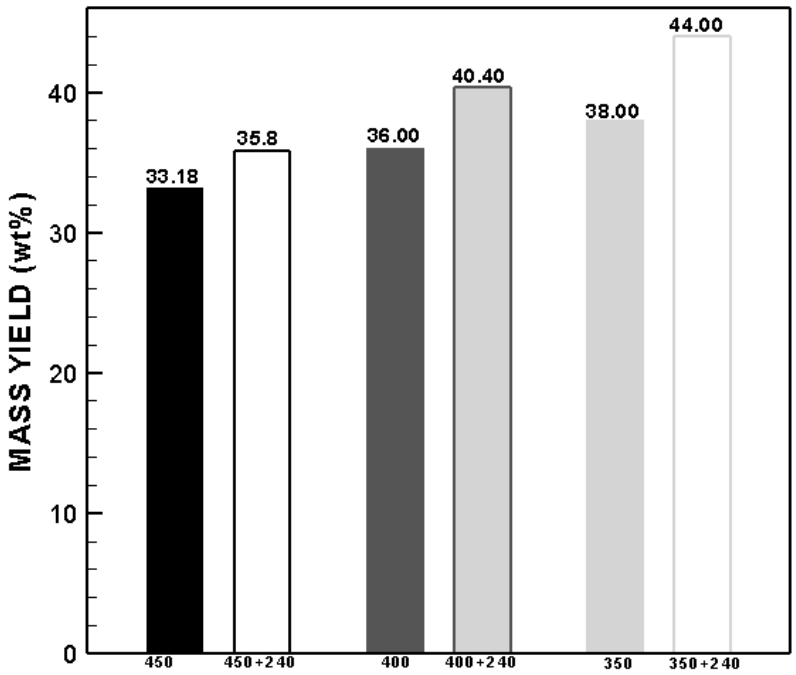

Figure 51. Mass Yield of biochar produced from SOMR and tSOMR.

In this study SOMR carbonized for 20 minutes where tSOMR carbonized for 10 minutes at CT of 350^{o}C ,400^{o}C and 450^{o}C. Higher mass yield during carbonization of tSOMR is associated with less holding time used during the carbonization process.

5.5.3 Carbon (C), Hydrogen (H), Nitrogen (N) and Oxygen (O) Content of SOMR and tSOMR Biochars

Ultimate analysis results of carbonized SOMR and tSOMR are given in Figure 52, 53 and 54. Carbonization of SOMR results biochar with reduced hydrogen and oxygen contents compared to raw SOMR. Also, carbonization yields to biochar with higher carbon content. Elemental composition of carbonized SOMR shows that reduction in hydrogen and oxygen content increases, where rise in carbon content increases with increased CT. Both torrefaction and carbonization results with reduced hydrogen and oxygen content which mainly associated with destroyed hydroxyl group (-OH) of the biomass [82,101,117] . Ultimate analysis results of raw SOMR biochars and tSOMR biochars, showed that tSOMR biochars have less hydrogen content at all CTs. The carbon content measurements showed that, although there was no significant difference, tSOMR biochars had higher carbon content compared to SOMR biochars at CT of 350°C and 400^{o}C. However, the carbon content of tSOMR biochars at CT of 450^{o}C have less carbon content where the difference was around 1.29%.

The oxygen content of SOMR and tSOMR biochars were compared. At a CT of 350°C, tSOMR yielded biochar with 1.02 wt% higher oxygen content than SOMR. The opposite trend was obtained at a CT of 400°C and 450°C. Results showed that tSOMR biochar have 0.02% and 0.73% less oxygen content relative to SOMR biochar 400°C and 450°C, respectively.

Ultimate analysis results demonstrated that both direct carbonization of SOMR and tSOMR remarkably changed the elemental composition of raw SOMR. Furthermore, carbonization of both SOMR and tSOMR yielded changes in the H/C and O/C ratios

of raw SOMR. The H/C and O/C ratios of SOMR and tSOMR biochars are demonstrated in Figures 55 and 56, respectively.

Experimental results showed that tSOMR biochars have lower H/C ratio. The H/C ratio of tSOMR biochars was 0.82, whereas the H/C ratio of SOMR biochars was 0.89 at a CT of 450°C. At a CT of 400°C, SOMR biochar had an H/C ratio of 1.12, whereas the H/C ratio of tSOMR biochar was 1.10. A similar effect was observed on the H/C ratios of biochars at the CT of 350°C. The H/C ratio of biochar from tSOMR was 1.13, whereas the H/C ratio of directly carbonized SOMR was 1.17 at the CT of 350°C.

Carbonization experiments also revealed that, tSOMR biochars have higher O/C ratio. At CT of 350^{o}C, the O/C ratio of tSOMR biochar is 0.23 and O/C ratio of SOMR biochar is 0.21. Also, at CT of 400^{o}C, SOMR biochars have O/C ratio of 0.20 where O/C ratio of tSOMR biochar is 0.21. The reduced H/C ratio indicates higher structural stability in biochars [118,119] where decreased O/C ratio denotes the higher-degree of carbonization [119,120]. Carbonization experiments also revealed that tSOMR biochars had a higher O/C ratio at CT of 350°C and 400°C. At a CT of 350°C, the O/C ratio of tSOMR biochar was 0.23, and the O/C ratio of SOMR biochar was 0.21. At a CT of 400°C, SOMR biochars had an O/C ratio of 0.20, whereas the O/C ratio of tSOMR biochar was 0.21. However, the O/C ratio of both tSOMR and SOMR biochars were the same (0.18).

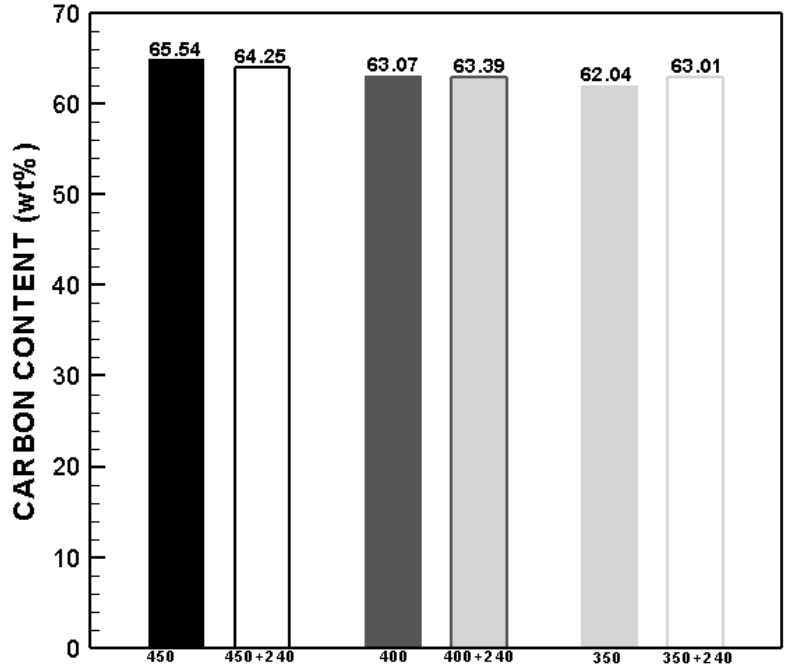

Figure 52. Carbon content of SOMR and TSOMR biochars.

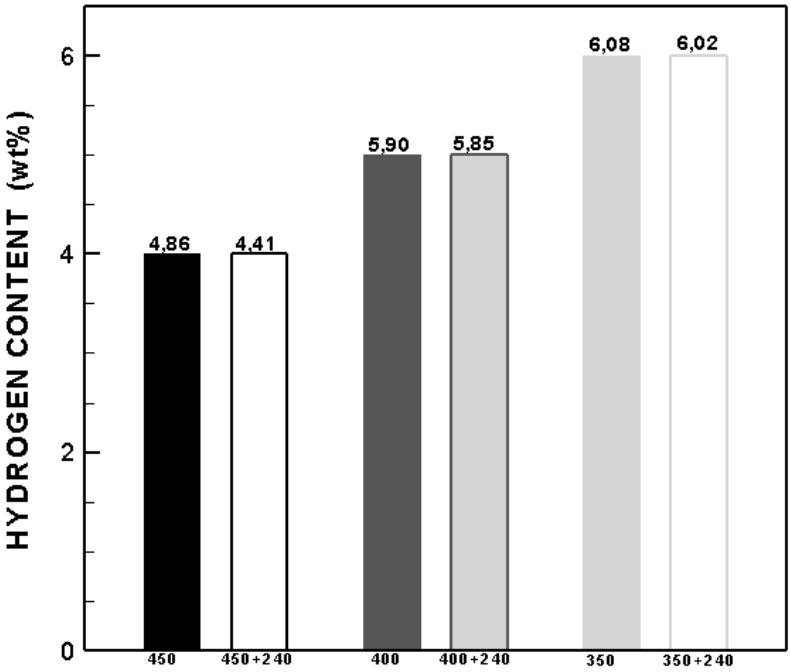

Figure 53. Hydrogen content of SOMR and tSOMR biochars.

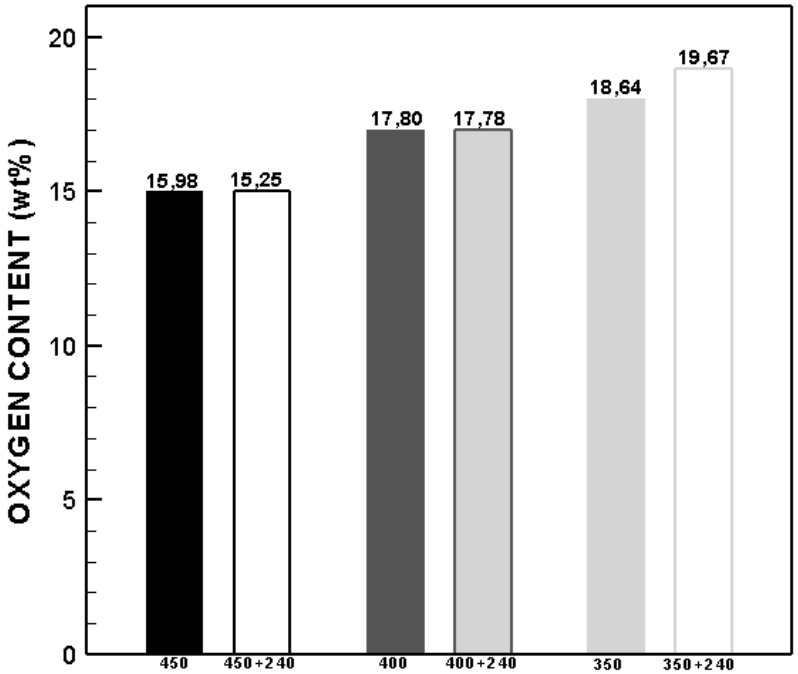

Figure 54. Oxygen content of SOMR and tSOMR biochars.

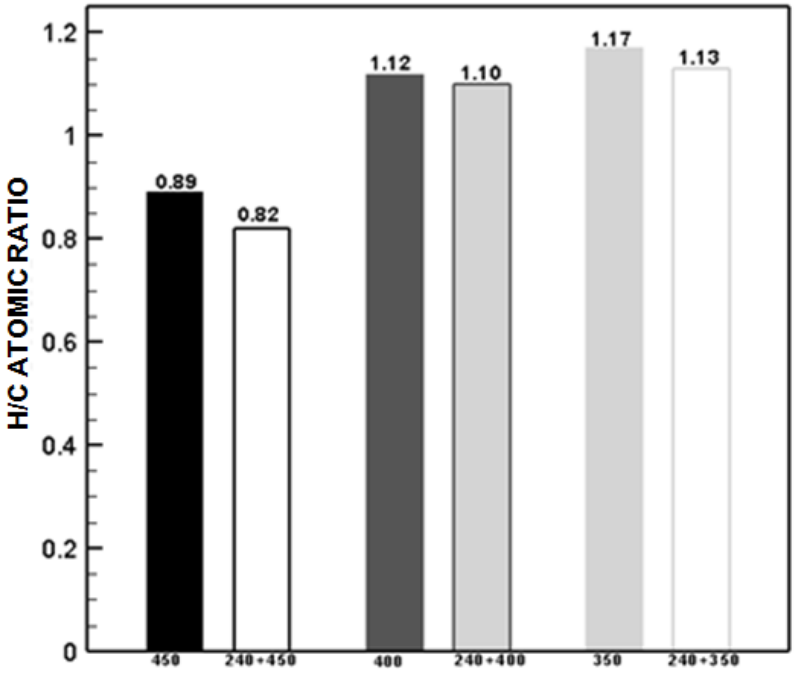

Figure 55. H/C ratio of biochar produced from SOMR and tSOMR.

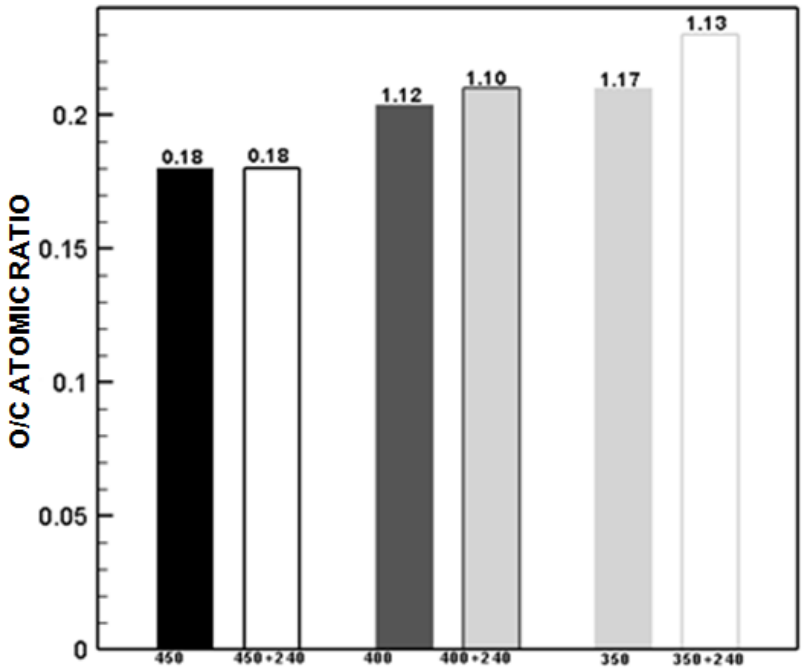

Figure 56. O/C ratio of biochar produced from SOMR and tSOMR.

5.5.4 Volatile Matter (VM), Fixed Carbon (FC) and Ash Content of SOMR and tSOMR Biochars

The proximate analysis results of biochars produced from raw SOMR and tSOMR are given in Figures 57, 58 and 59. The ash and fixed carbon content of biochars increased with an increased CT. However, the volatile matter content of biochars showed a different trend. tSOMR yielded biochar with less ash at CT of 350^{o}C and 400^{o}C. However, the biochar produced from carbonization of tSOMR at 450^{o}C have more ash compared to SOMR. It is estimated that higher ash content of tSOMR carbonized at 450^{o}C is a result of non-homogenous structure of SOMR. The ash content measurements showed that torrefaction of SOMR before carbonization ameliorated combustion problems at lower CT. Proximate analysis results also demonstrated that tSOMR yielded biochar with increased VM. Complete combustion of VM leads to dark smoke, heat loss, and pollution hazards [110].

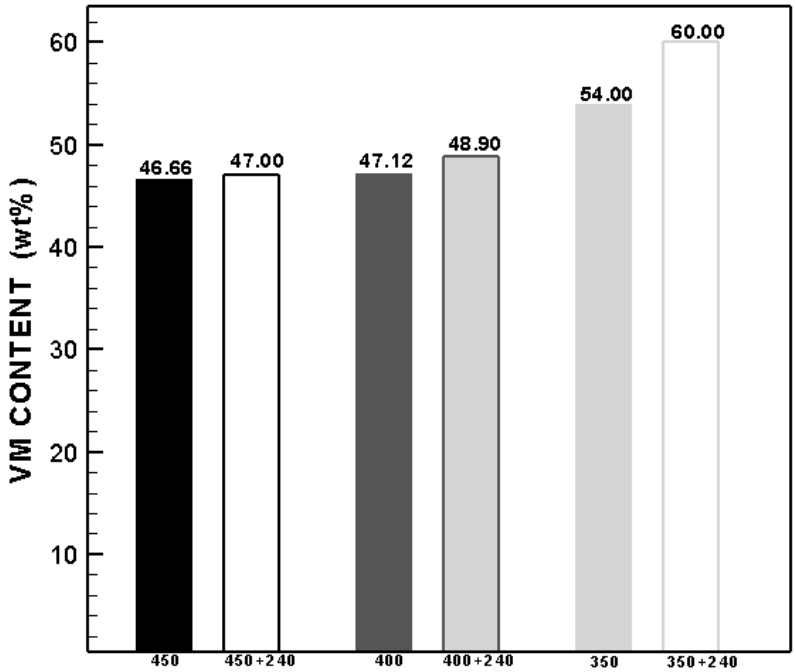

Figure 57. Volatile Matter content of SOMR and tSOMR biochars.

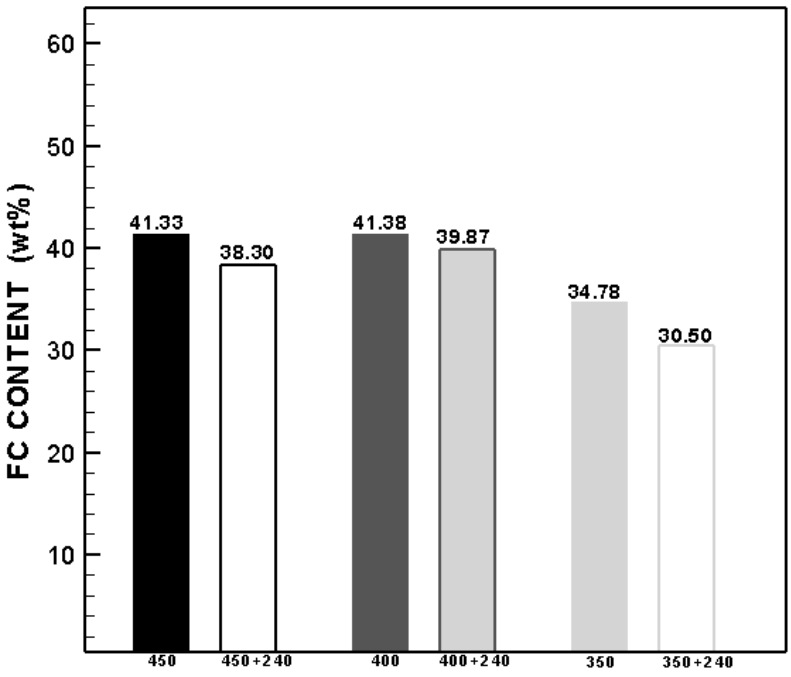

Figure 58. Fixed Carbon content of SOMR and tSOMR biochars.

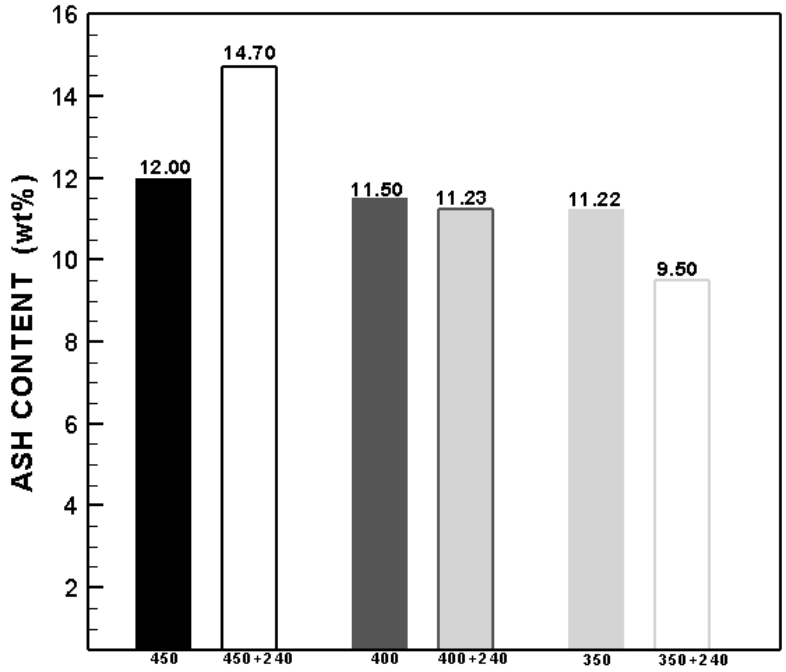

Figure 59. Ash content of SOMR and tSOMR biochars.

The FC content of tSOMR, which is the amount of the carbon present in the biochar sample [122] followed a trend similar to ash content. tSOMR carbonization resulted in biochar with less FC content than SOMR at all CTs.

5.5.5 Energy Yield and Higher Heating Value

The HHV of all produced biochars (in dry basis) are given in Figure 6. HHV is one of the important parameters which determines the potential of biochar as fuel [123]. Carbonization experiments done by Volpe et al. [121] showed that, at carbonization temperatures exceeding 400°C, the gross calorific value of biochar produced from olive pomace decreased. Consistent with the study of Volpe et al. [121] the HHV of biochar increased when the CT risen to 400°C from 350°C. Nevertheless, biochar with the lower HHV of 26.16 MJ/kg was obtained at the CT of 450°C. At the CT of 350°C, the HHV of tSOMR biochar was 26.30 MJ/kg, and the HHV of SOMR biochar was 26.54 MJ/kg. However, at the CT of 400°C, the HHV of tSOMR biochar was 26.65 MJ/kg, and the SOMR biochar was 26.61 MJ/kg at 400°C.

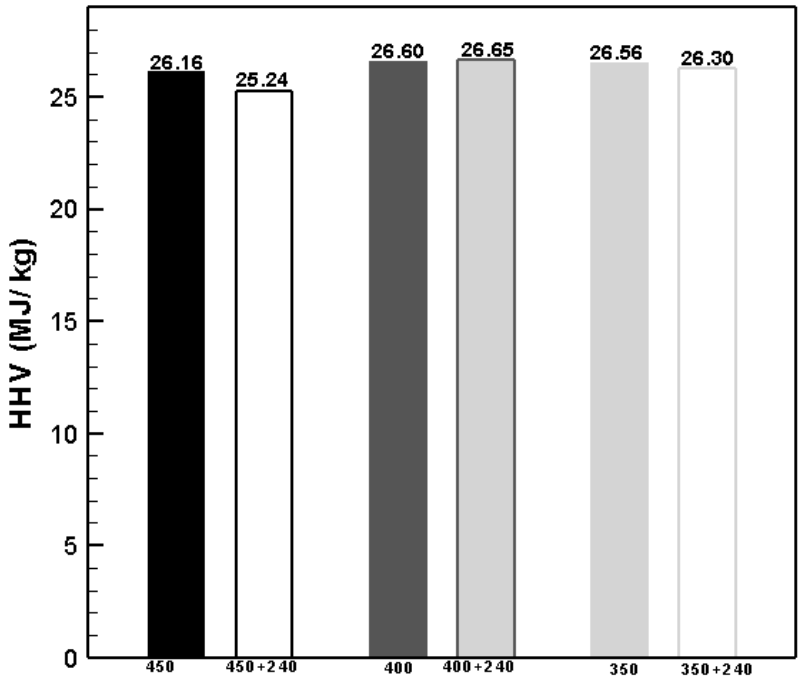

Figure 60. HHV of biochars produced from SOMR and tSOMR.

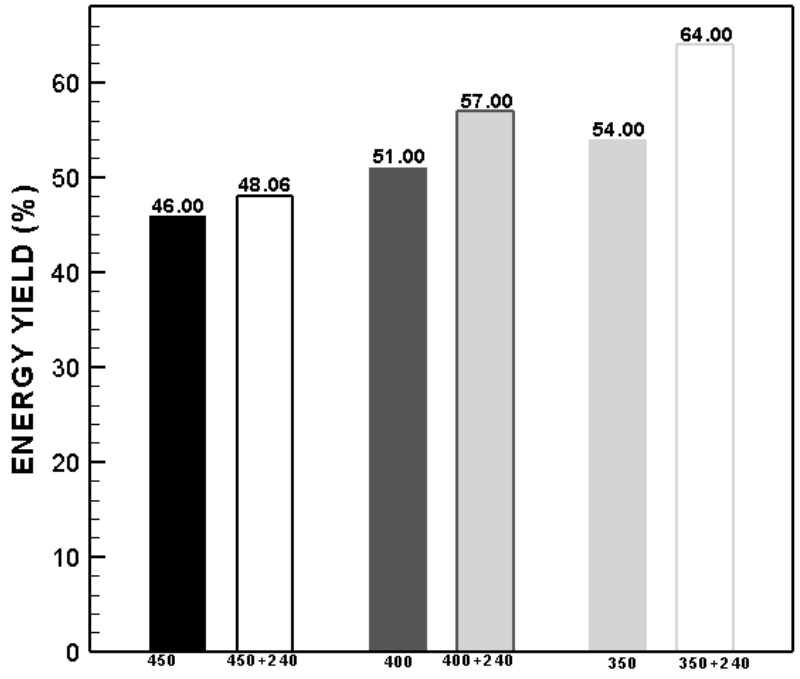

Figure 61. Energy yield of biochars produced from SOMR and tSOMR.

Also, biochar with lower HHV was obtained from tSOMR compared to SOMR at 450°C. Besides HHV, the energy yield was calculated in dry basis and shown in Figure 61 energy yield is the main indicator of the amount of energy saved in biochar after the thermal process [112]. The energy yield of biochars decreased with increased CT, from 54% to 46% when the CT was raised to 450°C from 350°C. tSOMR biochars had a higher energy yield. At a CT of 350°C, the energy yield of tSOMR biochar was 64% and the SOMR biochar was 54%, whereas at 400°C, the energy yield of tSOMR and SOMR were 57% and 51%, respectively. Similar behavior in energy yield also were observed at a CT of 450°C. Higher energy yield from carbonization of tSOMR is a result of higher mass yield from carbonization of tSOMR compared to SOMR.

5.5.6 Effects of Torrefaction on the Carbonization Characteristics of SOMR

The effect of torrefaction on the carbonization characteristics of SOMR was investigated at three carbonization temperatures. Elemental analysis showed that torrefaction of SOMR before carbonization yielded a solid fuel with higher carbon at lower CT and less hydrogen content at all the studied CT values. The effect of torrefaction on the elemental composition of SOMR was more remarkable at lower CT.

The H/C and O/C ratios are two important parameters associated with biochars produced by carbonization. Ultimate analysis results revealed that torrefaction contributed to reduce H/C ratio. Also, the O/C ratios of tSOMR biochars produced were very close to the O/C ratios of SOMR biochars. Generally, lignocellulose with low H/C and O/C ratios is a good fuel because it has low energy loss and emits little smoke or water vapor during combustion [124]. Proximate analysis of produced biochars demonstrated that tSOMR biochars have less ash content when they had

been prepared at lower carbonization temperatures. Lower ash content provided more efficient combustion for tSOMR biochar compared with SOMR biochar. tSOMR yielded biochar with higher volatile matter content, where the difference did not exceed 6% with SOMR biochar. Beyond the ultimate and proximate analysis results, torrefaction had considerable effect on the energy yield of produced biochars. Energy yield calculations showed that more energy was retained in biochar if the SOMR was torrefied before carbonization.

In this study, the holding time used for carbonization of tSOMR for all CTs was half of the holding time used for the carbonization of SOMR. Sadaka et al. [116] and Shaaban et al. [125] have shown that, holding time significantly changes the elemental composition of biomass. However, the produced biochars from SOMR and tSOMR had very similar ultimate and proximate analysis characteristics. Thus, torrefaction significantly contributes to improve fuel characteristics of biomass during carbonization. Nevertheless, torrefaction, can be used to reduce the holding time during carbonization, which then requires less energy input to the carbonization system.

Chapter 6

SOLAR TORREFACTION OF SOLID OLIVE MILL RESIDUE

6.1 Solar Torrefaction

In this study, torrefaction characteristics of SOMR [128] and effects of torrefaction on carbonization characteristics of SOMR [129] have been investigated. Results showed that torrefaction significantly contributes to upgrade fuel characteristics of raw SOMR and yields to more qualified solid fuel. Also it has been shown that; torrefaction can be used as a pretreatment for carbonization of SOMR and reduces the input energy during carbonization. Proven impacts of torrefaction on fuel characteristics of biomass motivated commercial investments on wood torrefaction plants.The torrefaction process is conducted with natural gas or biomass in pilot torrefaction plants [92].

SOMR is mainly produced in Mediterranean Basin. It is estimated that 900 million olive trees cover 10 million hectares worldwide where 98% are located in the Mediterranean Basin [94]. Mediterranean countries produce approximately 2.5 million metric tons/year olive oil [127]. During olive oil extraction process 200 kg of oil and 400 kg of SOMR is produced from each ton of olive [126]. Statistics showed that considerable amount of SOMR is produced in Mediterrenean Basin. Besides SOMR, Mediterrenean Basin have high solar energy potential.

In this work, proven effects of torrefaction on SOMR and being produced in Mediterrenean Basin, motivated use of solar thermal energy as input energy for torrefaction of SOMR. Furthermore, the low process temperature and ease of process control, relative to other biomass treatment methods, makes use of solar energy very attractive for torrefaction (solar torrefaction). In this study, a solar furnace which is named as "parabolic dish solar torrefier" is constructed. The parabolic dish torrefier was tested on October 8 to 10 in 2014. Properties of parabolic dish torrefier and solar torrefaction results are demonstrated below.

6.2 Parabolic Dish Torrefier and Solar Torrefaction Experiments

In this study, solar torrefaction experiments were conducted with dry SOMR. Also, ultimate and proximate analysis results are expresses in dry basis. The parabolic dish torrefier was constructed by using a parabolic dish antenna as shown in Figure 62. Geometrical characteristics of parabolic dish are given in Table 11. The parabolic dish was covered with a reflective film which reflectivity is given as 1 from producer Company (Magic Plant, Turkey). The surface of parabolic dish was completely covered by 10 triangular pieces of reflective film.

Solar torrefaction process was conducted in a cylindrical receiver tube made up of stainless steel as shown in Figure 63. The receiver tube was fixed to focus of parabolic dish by using copper wires. The receiver-tube has a circular-flat base with diameter 0.035 m and height of 0.1 m. Receiver tube is painted black by using a heat resistant paint (up to 300^{o}C) for increasing amount of absorbed solar thermal energy. The schematic representation of parabolic dish torrefier is shown in Figure 64.

Table 11. Geometrical Characteristics of Parabolic Dish Collector.

Geometrical Characteristics	Value
Diameter (d)	0.87m
Focal Length (f)	0.59 m
(d/f) Ratio	1.47
Rim Angle (Φ)	40.35^{o}
Surface Area (S)	0.59 m^2

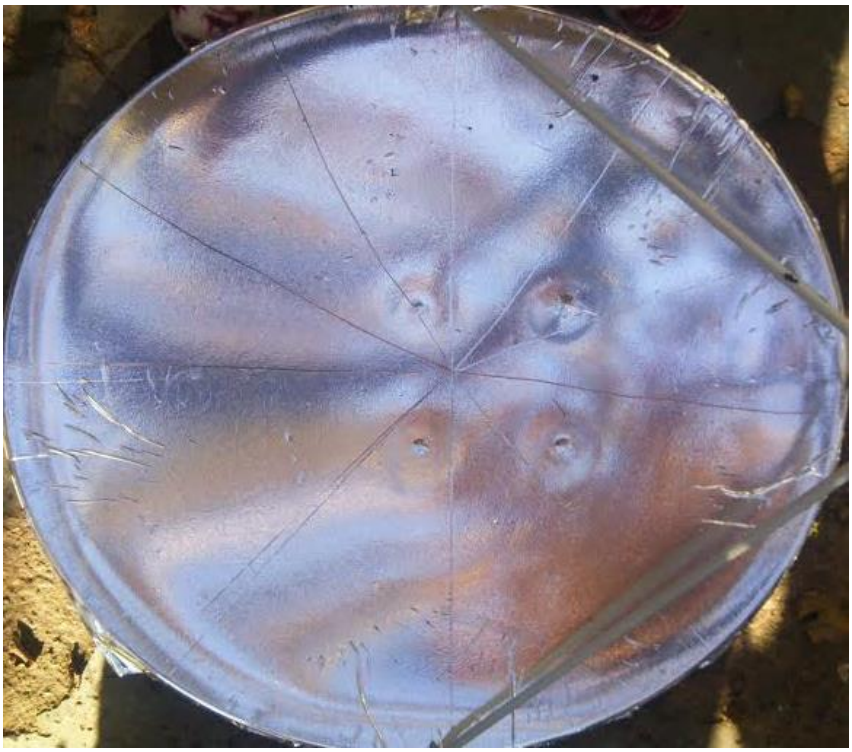

Figure 62. Parabolic dish antenna covered by reflective material for concentration of solar thermal energy.

Figure 63. Cylindrical receiver-tube used in solar torrefaction process.

The receiver tube is fed by nitrogen (20 mL/min) through the pipes as shown in Figure 64 to provide an inert medium. Also 50 mL/min nitrogen was flowed for 10 minutes for removal of oxygen in receiver-tube before each solar torrefaction process.

Gas produced by process is also brought out from other stainless steel pipe, connected to another plastic pipe. The plastic pipes used in parabolic dish torrefier were covered with aluminum foil in order to prevent melting. The solar torrefaction process was conducted at 250^{o}C. The holding time was adjusted to 10 minutes which do not include the heating time. It is observed that the stainless steel reactor were heated with maximum rate of 50^{o}C/min and reached to torrefaction temperature in 5-10 minutes. Each solar torrefaction experiment was conducted with 5 gr of SOMR and solar torrefaction products were represented by S1, S2 and S3 in figures.

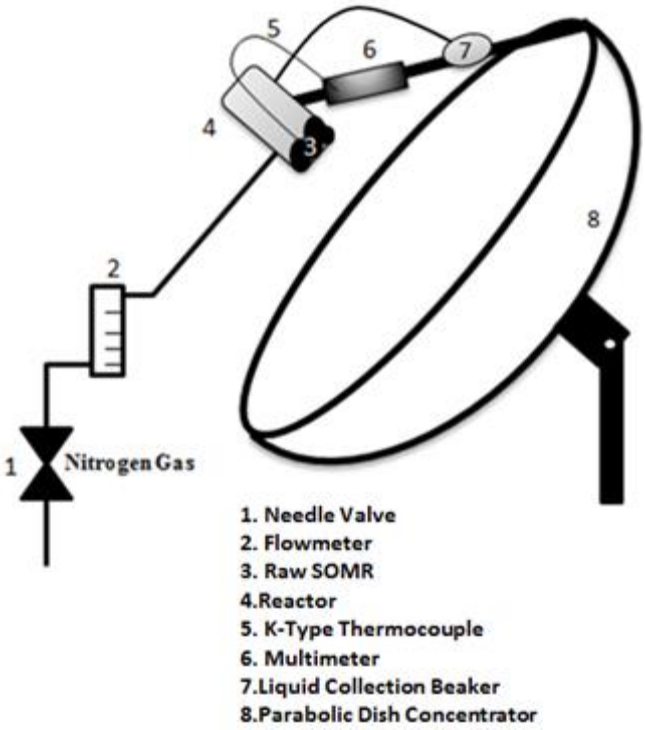

Figure 64. Schematic representation of parabolic dish torrefier.


Figure 65. Parabolic dish solar torrefier.

6.3 Appearance of Solar Torrefaction Products

The appearance of raw SOMR and three solar torrefied SOMR are given in Figure 66 (a), (b), (c), (d). Similar to torrefaction process conducted by electrical heater-glass tube system shown in Figure 23, solar torrefaction results with darker solid fuel. Also, it is observed that solar torrefaction yields a solid fuel which is much more brittle compared to raw SOMR.

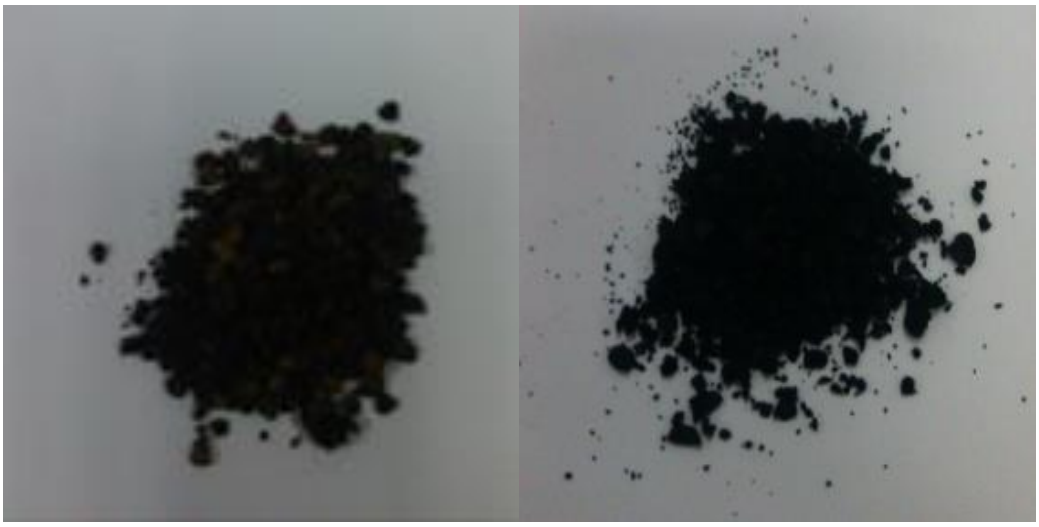

(a) (b)

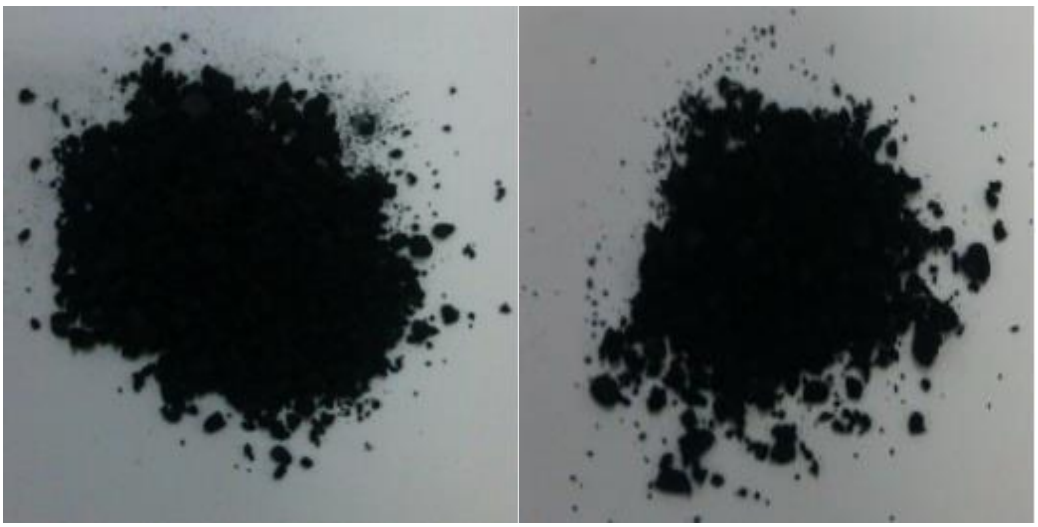

(c) (d)

Figure 66. Appearance of raw and solar torrefied SOMR.

6.4 Mass Yield

Figure 67 shows the mass yield results of solar torrefaction products. The average mass yield of solar torrefaction treatment of SOMR is 57.74%. Isothermal [99] and non-isothermal [67] torrefaction experiments showed that at torrefaction temperature of 250^{o}C, hemicellulose and xylan are thermally degraded to form volatile products [78]. In this study the mass loss during solar torrefaction was attributed to degradation of hemicellulose, xylan and also to removal of bounded water.

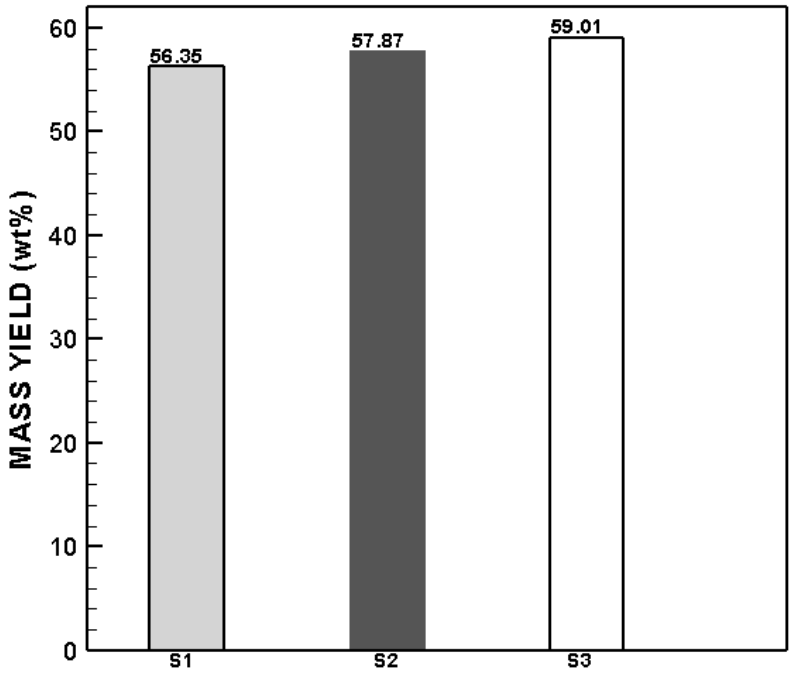

Figure 67. Mass yield of solar torrefaction products; S1, S2, S3.

6.5 Carbon (C), Hydrogen (H), Nitrogen (N) and Oxygen (O) Content of Solar Torrefied SOMR

The elemental composition of solar torrefied SOMR is demonstrated in Figure 68 to 70. Results indicated that, the carbon content of raw SOMR increased by average rate of 7.65% after solar torrefaction process. Hydrogen content of solar torrefied samples are reduced similar to torrefaction process. The average amount of change in

Hydrogen content of solar torrefied SOMR is around 0.41%. Also, results indicated that solar torrefied SOMR have lower oxygen content. The average rate of change in oxygen content is 15.01%.

Torrefaction process is associated with destroyed hydroxyl group (-OH) [105, 85] and destroyed hydroxyl group (-OH) results in a solid fuel with reduced hydrogen and oxygen contents. Ultimate analysis results revealed that solar torrefied SOMR well obeys the carbon, hydrogen and oxygen content change behavior of torrefaction process.

Also; the H/C and O/C atomic ratios of S1, S2 and S3 were calculated. H/C ratio is an indicator of pyrolysis efficiency where O/C ratio is a measure of degree of oxidation [102, 103]. Besides all, reduced O/C ratio is a potential indicator of both hydrophilicity and polarity. The reduced polar surface groups results in a reduction of affinity of the fuel with water molecules [104].

Figure 71 shows O/C atomic ratios of raw and solar torrefied samples S1, S2 and S3. Results revealed that average O/C ratio of solar torrefaction products is 0.28 where O/C ratio of SOMR is 0.50. Figure 72 shows H/C atomic ratio of raw SOMR and solar torrefied samples S1, S2 and S3. The average H/C ratio of solar torrefaction products is 1.27 and the H/C ratio of SOMR is 1.53.

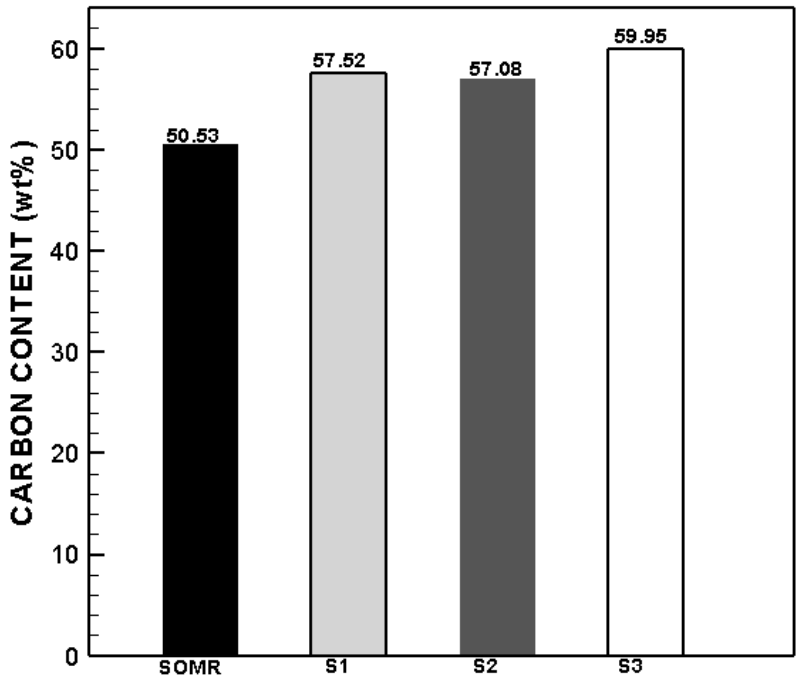

Figure 68. Carbon content of raw SOMR and solar torrefied SOMR; S1, S2 ,S3.

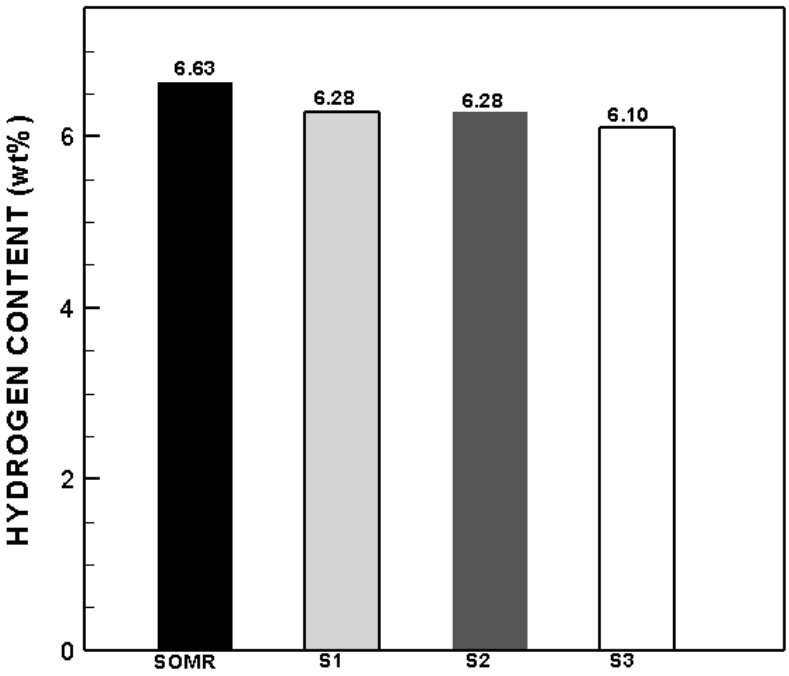

Figure 69. Hydrogen content of raw SOMR and solar torrefied SOMR; S1, S2, S3.

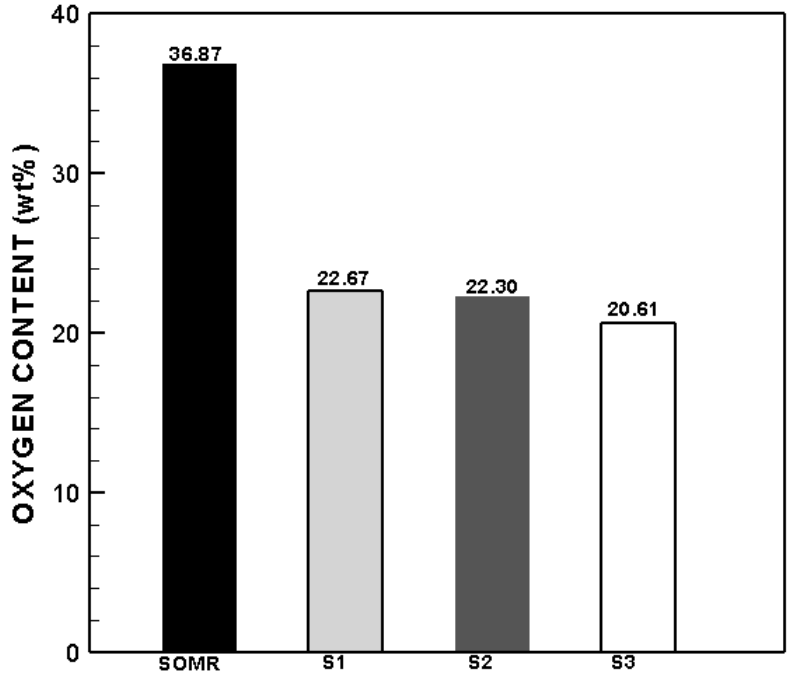

Figure 70. Oxygen content of raw SOMR and solar torrefied SOMR; S1, S2, S3.

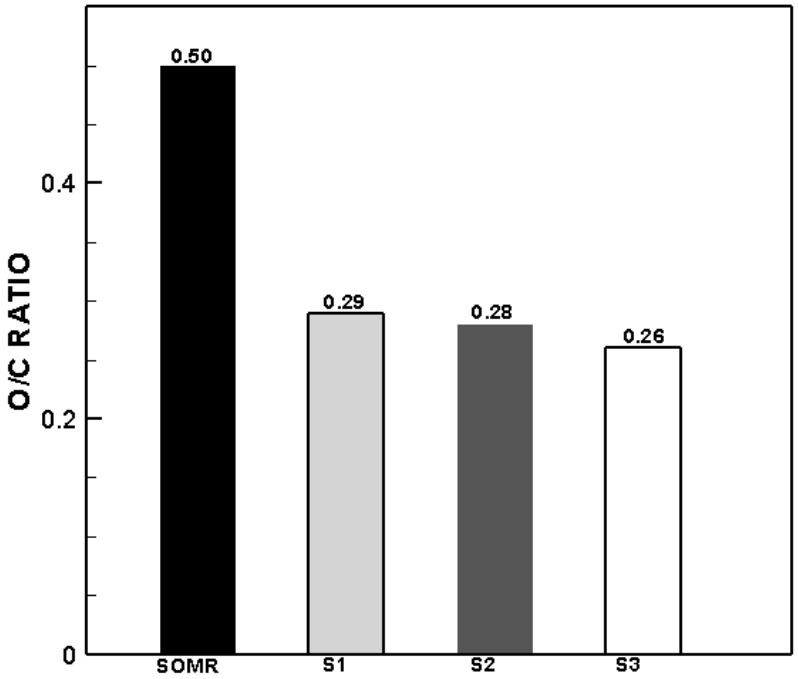

Figure 71. O/C atomic ratio of raw and solar torrefied SOMR; S1, S2, S3.

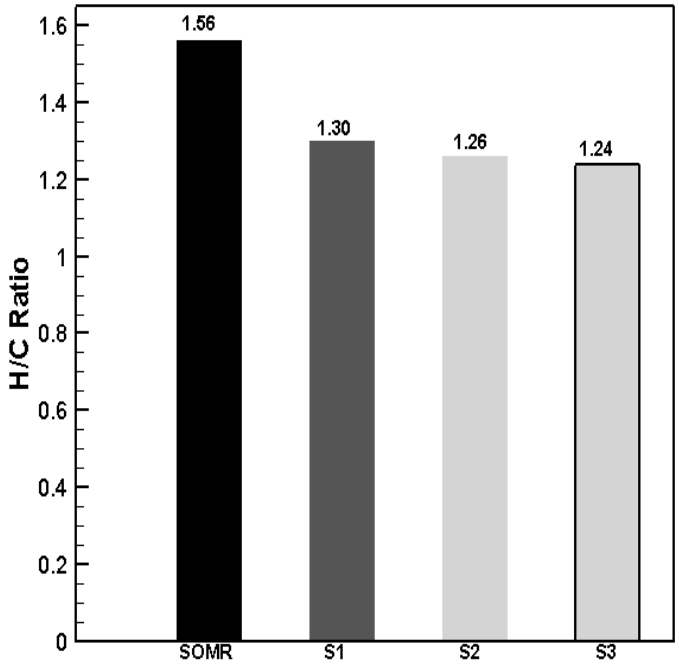

Figure 72. H/C ratio of raw and solar torrefied SOMR; S1, S2, S3.

6.6 Volatile Matter (VM), Fixed Carbon (FC) and Ash Content of Raw and Solar Torrefied SOMR

The volatile matter and fixed carbon composition of solar torrefied SOMR is obtained by proximate analysis. Torrefaction studies done for varius biomass studies and SOMR showed that torrefaction results a solid fuel with reduced volatile matter content and increased ash and fixed carbon content. Figure 73 demonstrated volatile matter content of raw SOMR and solar torrefied SOMR. Volatile matter change behavior of solar torrefaction products are consistent with torrefaction process.

Results showed that volatile matter content of samples changed by rate of 14.83% after solar torrefaction. Reduced volatile matter of a solid fuel is an indicator of more qualified fuel with less smoke during combustion [110]. Fixed carbon content of solar torrefaction products were given in Figure 74. The average rate of change in fixed carbon content of samples S1, S2 and S3 is 7.50% wt.

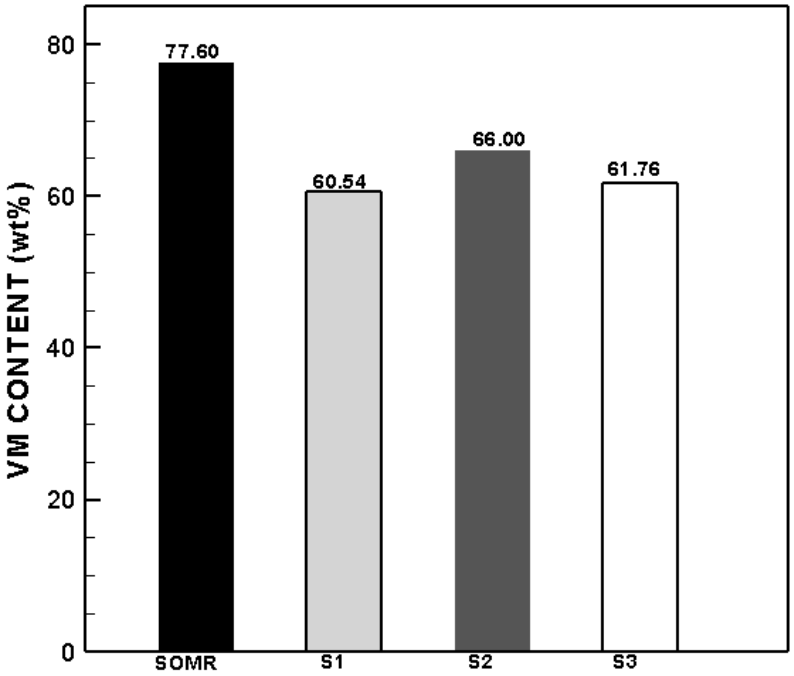

Figure 73. Volatile Matter Content of raw SOMR and solar torrefied SOMR.

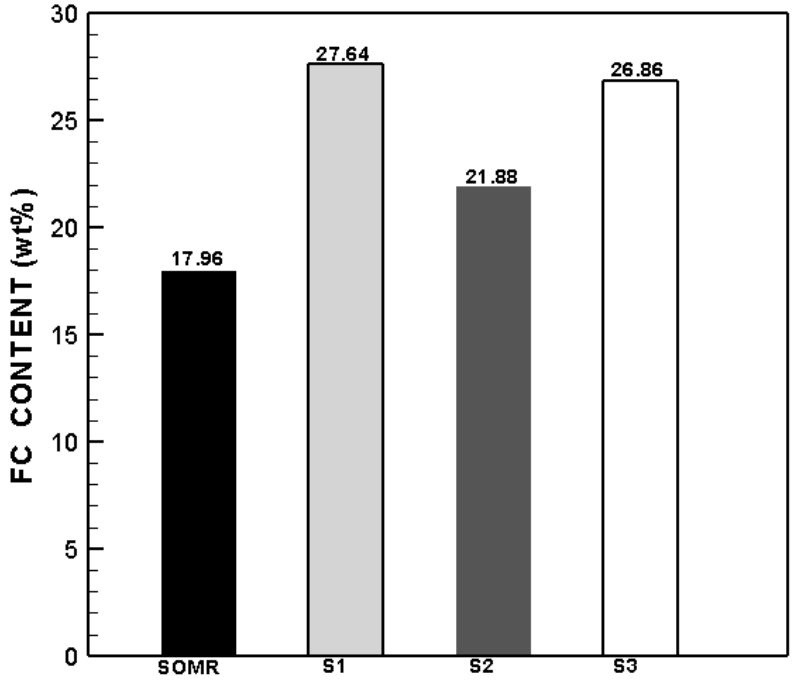

Figure 74. Fixed carbon content of raw SOMR and solar torrefied SOMR.

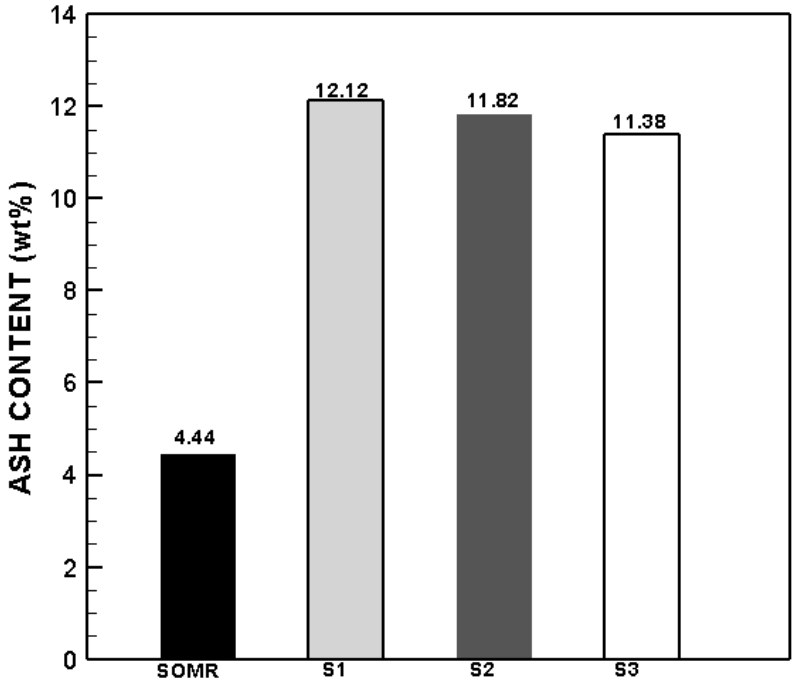

Figure 75. Ash Content of raw and solar torrefied SOMR S1, S2 and S3.

Ash content of solar torrefaction products is given in Figure 75. Results showed that solar torrefaction yields higher ash content similar to torrefaction process. Results indicated that; the average ash content of torrefaction products is 11.77% where the ash content of raw SOMR is 4.44%.

6.7 Higher Heating Value of Solar Torrefied SOMR

Torrefaction studies conducted with different biomass have shown that, torrefaction yields a solid fuel with higher HHV [83]. HHV value of solar torrefaction products are demonstrated in Figure 76 in dry basis. Results have shown that solar torrefaction also yields a solid fuel with 15.30% higher HHV than raw SOMR. Also the energy yield of solar torrefaction products given in Figure 77. Energy yield calculations showed that 67.25% of energy is retained in products after solar torrefaction.

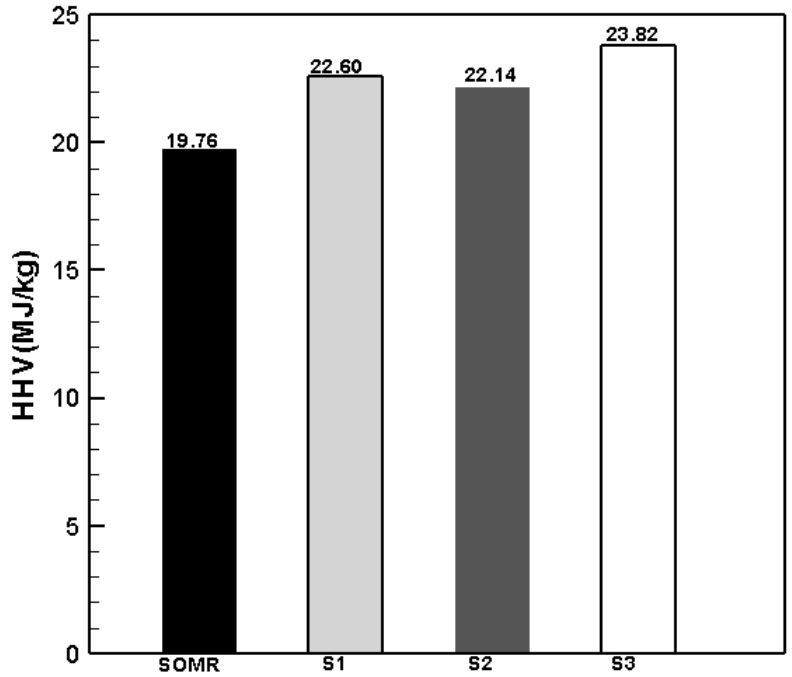

Figure 76. HHV of of raw and solar torrefied SOMR S1, S2 and S3.

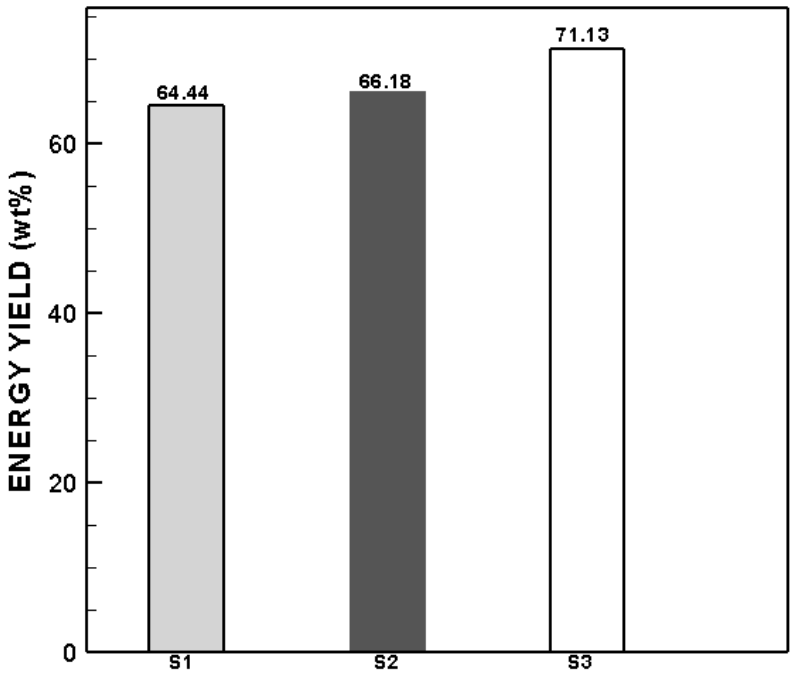

Figure 77. Energy yield of raw and solar torrefied SOMR S1, S2 and S3.

6.8 Thermal Performance of Parabolic Dish Solar Torrefier and Solar Torrefaction

The thermal efficiency of parabolic dish solar torrefier is defined as; the ratio of the useful thermal energy transferred to the receiver, to the energy incident on the parabolic dish collector aperture. The thermal efficiency (η) of parabolic dish torreffier was calculated according to;

$$\eta = \dot{Q}_{useful} \Big/ \dot{Q}_{aperture} \tag{6.1}$$

Where $\dot{Q}_{useful}$ the amount of solar thermal energy per second, transferred to the stainless steel receiver and $\dot{Q}_{aperture}$ is the energy incident on the parabolic dish collector per second.

$$\dot{Q}_{useful} = \dot{m}c(T - T_O) \tag{6.2}$$

$$\dot{Q}_{aperture} = \alpha I_B S \tag{6.3}$$

Where m is the mass of stainless steel receiver, c is the specific heat capacity of stainless steel, T is the torrefaction temperature, T_O is the ambient temperature, α is the, reflectivity parabolic dish, I_B is the beam radiation on parabolic dish collector, S is the aperture area of parabolic dish collector. In this study the mass of stainless steel receiver is 0.380 kg where mass of used SOMR in each run is 0.005 kg. The mass of SOMR used for solar torrefaction is neglected for thermal efficiency calculations. The thermal characteristics of solar torrefier is given in Table 12. The thermal efficiency calculations showed that, parabolic dish solar torrefaction system is working with 24.22% thermal efficiency.

Table 12. Thermal characteristics of Parabolic Dish Torrefier.

Parameter	Value
$\dot{m}$	0.00063 (kg/s)
c	510 (J/kg K)*
T	250°C
T_O	24°C
α	1
I_B	508 (W/m^2)**

*Average of maximum (530 J/kg K) and minimum (490 J/kg K) specific heat capacities associated with stainless steel.

** Average direct beam radiation in Northern Cyprus during October (Northern Cyprus Ministry of Public Tourism and Environment, Meteorology Department)

6.9 Solar Torrefaction of SOMR

This study showed that torrefaction of SOMR can be conducted by using solar energy. Furthermore, it has been shown that solar torrefaction results with similar changes on biomass such as higher carbon content, less oxygen and hydrogen content and higher HHV, similar to torrefaction of SOMR [128].

The effect of torrefaction on fast pyrolysis [90, 91], gasification [113, 114] and carbonization [129] has been studied. Results showed that, besides being directly used solid fuel, torrefied biomass can be used as fuel for listed biomass treatment methods. Similar to torrefied SOMR, solar torrefied SOMR can be directly used as fuel. Also, can be used for producing more qualified bio-oil, syngas or charcoal via fast pyrolysis, gasification or carbonization respectively.

Chapter 7

CONCLUSION

This study was mainly set to investigate, the possibility of solar torrefaction by designing a solar furnace for conducting mild carbonization (torrefaction) process. Solid Olive Mill Residue is used as biomass, by considering the fact that SOMR is mainly produced in places with high solar energy potential. However, before solar torrefaction, torrefaction characteristics of SOMR was investigated for checking suitability of this biomass for process.

The torrefaction characteristics of SOMR was studied at three different torrefaction temperatures and three different holding times. The mass yield, elementel composition, proximate composition, Higher Heating Value and energy yield of products were compared for specifiying optimum torrefaction conditions of SOMR.

Experimental results indicate that the effect of temperature is much more significant than the effect of holding time, especially at severe torrefaction conditions. Results also showed that, holding time do not have any considerable effect at severe torrefaction conditions. Torrefaction of SOMR showed that, the most qualified product is obtained at severe torrefaction conditions of, 280^{o}C. Torrefied SOMR is also compared with other torrefied biomass with the Van-Krevelen diagram. The Van-Krevelen diagram showed that, SOMR is very suitable biomass for torrefaction process.

The torrefaction process converts biomass to solid fuel. Besides torrefaction, carbonization which is also known as slow pyrolysis is the unique biomass, thermochemical treatment method which results with solid fuel (as main product). The main difference between torrefaction and carbonization is the process temperature. The torrefied and carbonized SOMR were compared by means of elemental and proximate composition. Torrefaction and carbonization experiments demonstrated that carbonization and torrefaction yields a very similar solid end product by means of elemental composition. However; the proximate analysis results showed that, significant difference occurs in volatile matter and fixed carbon contents of torrefaction and carbonization products.

In this study; the effect of torrefaction on fast pyrolysis and gasification motivated investigation of the, effect of process on carbonization characteristics of SOMR. Ultimate analysis results of SOMR and tSOMR biochars demonstrated that, there is no significant difference in elementel composition of both biochars. The results also showed that torrefaction contibutes to rise the pyrolysis efficiency. Also results showed that; tSOMR biochars have almost same degree of oxidation with raw SOMR biochars. Besides the ultimate and proximate composition, energy yield calculations showed that; torrefaction remarkably contributes to retain more energy in biochar during carbonization. Carbonization experiments with SOMR and tSOMR demonstrated that, torrefaction can be used to reduce the holding time during carbonization.

Proven effects of torrefaction on solid olive mill residue as fuel motivated solar torrefaction of SOMR. A parabolic dish solar torreffier was desinged and solar torrefaction was tested on 8 October 2014 to 10 October 2014. The torrefaction

temperature of 250^{o}C had been reached and SOMR was torrefied for 10 minutes with parabolic dish solar torrefier. Ultimate and proximate analysis results showed that, solar torrefaction well obeys the changes associated with torrefaction process and solar energy can be used as input energy for process.

This study showed that; solar torrefaction of SOMR yields to more valuable solid fuel than raw SOMR. Besides producing more qualified solid fuel, solar torrefaction contributes to prevent fossil fuel usage and inefficient combustion of biomass for torrefaction. Also, solar torrefaction obliquely results storege and transportation of solar energy, with solid fuel rather than Hydrogen.

REFERENCES

[1] Indicators of Sustainable Development: Guidelines and Methodologies, (2007), Third Edition, United Nations, New York.

[2] Asif, M. & Munee, T. (2007) Energy Supply, Its Demand and Security Issues For Developed And Emerging Economies, *Renewable and Sustainable Energy Reviews.* 11, 1388–1413.

[3] Renewables 2014: Global Status Report; REN 21 Renewable Energy Policy Network for the 21st Century.

[4] http://www.bp.com/en/global/corporate/energy-economics/statistical-review

[5] Shafiee, S. & Topal, E. (2009). When Will Fossil Fuel Reserves Be Diminished? *Energy Policy.* 37, 181–189.

[6] Chiari, L. & Zecca, A. (2011).Constraints Of Fossil Fuels Depletion On Global Warming Projections. *Energy Policy*. 39 ,5026–5034.

[7] Demirbas, A.(2008). Energy Issues and Energy Priorities. *Energy Sources, Part B: Economics, Planning and Policy*. 3, 41–49.

[8] Şen, Z. (2008). Solar Energy Fundamentals and Modeling Techniques: Atmosphere, Environment, Climate Change and Renewable Energy. Springer

[9] Kalogirou, A. S. (2004) Solar Thermal Collectors and Applications. *Progress in Energy and Combustion Science.* 30, 231–295.

[10] Intergovernmental Panel on Climate Change (IPCC), 2007. Climate change 2007: the Physical Science Basis. In: Solomon, S., Qin, D., Manning, M., Chen, Z., Marquis, M., Averyt, K.B., Tignor, M., Miller, H.L. (Eds.).

[11] Şen, Z. (2004). Solar Energy In Progress And Future Research Trends. Progres in Energy and Combustion Science. 30, 367–416.

[12] Kalogirou, S. (2007). Recent Patents in Solar Energy Collectors and Applications. Recent Patents on Engineering. 1, 23-33.

[13] Goswami, D.Y., Kreith ,F. & Kreider, J. F. (2000). Principles of Solar Engineering. Second Edition. Taylor & Francis.

[14] Tian, Y. & Zhao, C.Y. (2013). A Review of Solar Collectors And Thermal Energy Storage In Solar Thermal Applications. Applied Energy. 104, 538–553.

[15] Vendan, S.P., Shunmuganathan, L.P.A., Manojkumar, T. & Thanu, C.S. (2012). Study on Design of an Evacuated Tube Solar Collector for High Temperature Steam Generation. International Journal of Emerging Technology and Advanced Engineering. 2, 539-541.

[16] Arora,S., Chitkara,S., Udayakum, R. & Ali, M. (2011). Thermal Analysis of Evacuated Solar Tube Collectors. Journal of Petroleum and Gas Engineering. 2, 74-82.

[17] Sheth, M. G. & Shah, P. (2013). Design And Development Of Compound Parabolic Concentrating Solar Collector With Flat Plate Absorber, *International Journal of Innovative Research in Science, Engineering and Technology*. 2, 3884-3889.

[18] Salomoni, V. A. , Majorana, C.E. , Giannuzzi, G. M. , Miliozzi A. & Nicolini, D. (2010). New Trends in Designing Parabolic trough Solar Concentrators and Heat Storage Concrete Systems in Solar Power Plants. New Trends in Designing Parabolic trough Solar Concentrators and Heat Storage Concrete Systems in Solar Power Plants, Solar Energy, Radu D Rugescu (Ed.), InTech.

[19] Sorenson, B. & Breez, P. (2009). Renewable Energy Focus Handbook, Academic Press.

[20] Hobeika, S., Alexander, B. , Benmarrazea, S. , Itskhokine, D., Yang F. &. Benmarraze M. (2015). Case study: Linear Fresnel Reflectors (LFR) solar systems for industrial applications. Energy Procedia. 00 ,000–000.

[21] Demirbaş, M. F. (2007). Electricity Production Using Solar Energy, *Energy Sources, Part A: Recovery, Utilization, and Environmental Effects*. 29, 563-569.

[22] Reddy, V.S. , Kaushik, S.C. , Ranjan, K.R. & Tyagi S.K. (2013). State-of-the-art of solar thermal power plants—A review. Renewable and Sustainable Energy Reviews. 27, 258–273.

[23] Joshi, A. S., Dincer, I. & Reddy, B. V. (2011). Solar Hydrogen Production: A Comparative Performance Assessment. *International Journal of Hydrogen Energy*.36, 11246-11257.

[24] Özalp, N., Kogan, A. & Epstein,M. (2009). Solar Decomposition of Fossil Fuels as an Option for Sustainability. *International Journal of Hydrogen Energy*. 34, 710 – 720.

[25] Steinfeld, A. (2005). Solar Thermochemical Production Of Hydrogen—A Review. *Solar Energy*. 78, 603–615.

[26] http://www.dlr.de/sf/en/desktopdefault.aspx/tabid-8683/12090_read-34677/

[27] Mohamed, M.F., Jassim, A. S., Mahmood, H.Y. & Ahmed, A.K.M. (2012) Design and Study of Portable Solar Dish Concentrator.*International Journal of Recent Research and Review*.III; 52-59.

[28] Radiation Protection Standard: Occupational Exposure to Ultraviolet Radiation, Radiation Protection Series no.12. *Australian Radiation Protection and Nuclear Safety Agency* (ARPANSA). December 2006.

[29] Li, H., Huang, W., Huang, F., Hu, P. &Chen, Z. (2013). Optical Analysis and Optimization of Parabolic Dish Solar Concentrator With A Cavity Receiver. *Solar Energy*. 92, 288–297.

[30] Bendt, P.& Rabl, A. (1981). Optical Analysis of Point Parabolic Radiation. *Applied Optics.* 20, 674–683.

[31] Rabl, A. (1976). Comparison of Solar Concentrators. *Solar Energy*. 18, 93-111.

[32] Steinfeld, A. & Palumbo, R. (2001). Solar Thermochemical Process Technology, Meyers, R. A. (Ed.). *Encyclopedia of Physical Science & Technology*, Academic Press, 15: 237-256.

[33] Steinfeld, A., and Schubnell, M. (1993). Optimum Aperture Size and Operating Temperature of a Solar Cavity-Receiver. *Solar Energy.* 50, 19-25.

[34] Abuelnuor, A.A.A., Wahida , M.A. , S.E. Hosseini , Saat, A. , Saqr, K. M. , Sait, H. H. & Osman, M. (2014). Characteristics of biomass in flameless combustion: A review. *Renewable and Sustainable Energy Reviews.* 33, 363–370.

[35] Demirbas A. (2005). Potential applications of renewable energy sources, biomass combustion problems in boiler power systems and combustion related environmental issues. *Progress in Energy and Combustion Science.* 31,171–92.

[36] Longa, H., Li, X., Wanga, H.& Jia, J. (2013). Biomass Resources and Their Bioenergy Potential Estimation: A review, *Renewable and Sustainable Energy Reviews*.26, 344–352.

[37] Jenkins, B.M., Baxter, L.L., Miles, Jr.T.R. & Miles,T.R. (1998). Combustion Properties of Biomass, *Fuel Processing Technology*. 54, 17–46.

[38] Demirbas, A. (2007). Combustion of Biomass. *Energy Sources Part A: Recovery Utilization Environmental Effects.* 29, 549–61.

[39] World Energy Council (WEC) (2010). Survey Of Energy Resources Executive Summary. /http://www.worldenergy.org/documents/ser2010exsumsept8.pdfS

[40] Gera, D., Mathur, M. P., Freeman, M. C. & Robinson, A. (2002). Effect of Large Aspect Ratio of Biomass Particles on Carbon Burnout in a Utility Boiler. *Energy & Fuels*. 16, 1523–1532.

[41] Karekezi, S., Lata, K. &Coelho, S.T. (2004). Traditional Biomass Energy-Improving Its Use And Moving To Modern Energy Use. In: Secretariat of the International Conference for Renewable Energies, Bonn, June 1–4.

[42] Strezov, V., Patterson, M., Zymla, V., Fisher, K., Evans, T. J &. Nelson, P. F. (2007). Fundamental Aspects of Biomass Carbonization. *Journal of Analytical and Applied Pyrolysis.*79, 91–100.

[43] ASTM. Standard E1705, 1995 (2002). Standard Technology Relating To Biotechnology ASTM International. 1995; West Conshohocken, PA:www.astm.org.

[44] Agbor, V.B., Cicek, N., Sparling, R., Berlin, A. & Levin, D. B. (2011). Biomass Pretreatment: Fundamentals Toward Application. *Biotechnology Advances.* 29, 675–685.

[45] Sun, Y. & Cheng, J. (2002): Hydrolysis of Lignocellulosic Materials For Ethanol Production: A review. *Bioresource Technology*. 83, 1-11.

[46] Harmsen, P.F.H., Huijgen, W.J.J., Bermúdez López, L.M. & Bakker, R.R.C. (2010). Literature Review of Physical and Chemical Pretreatment Processes for Lignocellulosic Biomass. *ECN Report*.

[47] Yang, H., Yan, R., Chen, H., Lee, D.H. & Zheng, C. (2007). Characteristics of Hemicellulose, Cellulose and Lignin Pyrolysis. *Fuel*. 86, 1781.

[48] Shang, L. (2013) Upgrading Fuel Properties of Biomass by Torrefaction, Department of Chemical and Biochemical Engineering, Technical University of Denmark, doctoral thesis.

[49] http://www.engin.umich.edu/dept/che/research/savage/energy.html.

[50] Sun, Y-C., Wen, J-L., Xu, F. & Sun, R-C. (2011). Structural and Thermal Characterization Of Hemicelluloses Isolated By Organic Solvents and Alkaline

solutions from Tamarix austromongolica. *Bioresource Technology*. 102, 5947–51.

[51] Palma,C. F., (2013). Modelling of Tar Formation and Evolution for Biomass Gasification: A review. *Applied Energy*. 111, 129–141.

[52] Ghose, T.K., Selvam, P.V. & Ghosh, P. (1983). Catalytic Solvent Delignification of Agricultural Residues: Organic Catalysts. *Biotechnology and Bioengineering.* 25, 2577–2590.

[53] Chew, J.J. & Doshi, V. (2011). Recent Advances in Biomass Pretreatment – Torrefaction Fundamentals and Technology. *Renewable and Sustainable Energy Reviews.* 15, 4212–4222.

[54] Chaturvedi, V. & Verma, P. (2013). An Overview of Key Pretreatment Processes Employed for Bioconversion of Lignocellulosic Biomass Into Biofuels and Value Added Products. *Biotechology*. 3:415–431.

[55] Palmowski, L. & Muller, J. (1999). Influence of The Size Reduction Of Organic Waste On Their Anaerobic Digestion. *In II. International Symposium on anaerobic digestion of solid waste*. 137–44 Barcelona.

[56] Inoue, H., Yano, S., Endo, T., Sakaki, T. & Sawayama, S. (2008). Combining Hot-Compressed Water And Ball Milling Pretreatments To Improve The Efficiency of the Enzymatic Hydrolysis Of Eucalyptus. *Biotechnology and Biofuels.* 1, 1-9.

[57] Delgenes, J.P., Penaud, V.& Moletta R. Pretreatment for the Enhancement Of Anaerobic Digestion Of Solid Waste, Chapter 8. In Biomethanization of the organic fraction of municipal solid waste IWA publishing. 2002:201–28.

[58] Hendricks, A.T. & Zeeman, G. (2009).Pretreatments To Enhance the Digestibility of Lignocellulosic Biomass. *Bioresource Technology*.100,10–8.

[59] Hammel, K.E., Kapich A.N., Jensen Jr K.A.& Ryan, Z.C. (2002). Reactive Oxygen Species as Agents of Wood Decay By Fungi. *Enzyme and Microbial Technology*. 30, 445–453.

[60] Nakamura, Y., Daidai , M. & Kobayashi, F. (2004). Ozonolysis Mechanism Of Lignin Model Compounds And Microbial Treatment Of Organic Acids Produced. *Water Science and Technology.* 50, 167–172.

[61] Wan, C.& Li, Y. (2012). Fungal Pretreatment of Lignocellulosic Biomass. *Biotechnology Advances*. 30, 1447–1457.

[62] Karkania,V. , Fanara,E. & Zabaniotou,A. (2012). Review of Sustainable Biomass Pellets Production- A Study for Agricultural Residues Pellets' Market in Greece. *Renewable and Sustainable Energy Reviews.*161426-2536.

[63] Peksa-Blanchard M., Dolzan P., Grasssi A., Heinimö J., Junginger M., Ranta T. & Walter A. (2007). Global Wood Pellets Markets and Industry: Policy Drivers, Market Status and Raw Material, Potential IRRA Bioenergy Task 40.

[64] Sultana, A. & Kumar, A. (2012). Ranking of Biomass Pellets by Integration of Economic, Environmental and Technical Factors. *Biomass & Bioenergy*. 39, 344-355.

[65] Nordin, A. & Kjellström, B. (1996). Biomass for Heat and Electricity Production Engineering Aspects in Farming for Fuel. Murphy(Ed), 253-315.

[66] Stelte,W.,Sanadi,A. R. ,Shang, L. , Holm ,J. K., Ahrenfeldt, J.& Henriksen, U. (2012). Recent Developments in Biomass Pelletization-A review. *Bioresources*. 7, 4451-4490.

[67] Chen, W-H.&Kuo, P-C. (2011).Torrefaction and Co-Torrefaction Characterization of Hemicellulose, Cellulose And Lignin As Well As Torrefaction Of Some Basic Constitients In Biomass. *Energy.* 36, 803-811.

[68] Balat, M., Balat, M., Kırtay, E.&Balat,H. (2009). Main routes for the thermo-conversion of biomass into fuels and chemicals. Part 1: Pyrolysis Systems. *Energy Conversion and Management.* 50, 3147-3157.

[69] Dutschke M. ,Kapp G., Lehmann A, Schafer V, Risks And Chance Of Combined Forestry And Biomass Projects Under The Clean Development Mechanism.CD4CDM working paper series, working paper no.1.Hamburg Institute of International Economics: UNEP RISO Centre: June 2006.

[70] Umeki, K., Moilanen, A., Gómez-Barea,A., Konttinen,J. (2012). A Model of Biomass Char Gasification Describing The Change In Catalytic Activity of Ash, *Chemical Engineering Journal*, *207-208*, 616–624.

[71] Bahn, M.-K. , Mukarate, C. , Robichaud, D. J. &Nimlos, M.R. (2009). Current Technologies for Analysis of Biomass Thermochemical Processing: A review. *Analytica Chimica Acta*. 651, 117-138.

[72] Quang-Vu, B., Roger, A. K., Khanh-Quang, T. & Oyvind, S. (2014). Torrefaction Kinetics of Norwegian Biomass Fuels. *Chemical Engineering Transactions* 37, 49-54.

[73] Van der Stelt, M.J.C., Gerhauser, H., Kiel, J.H.A. & Ptasinski, K.J. (2011). Biomass Upgrading By Torrefaction for the Production Of Biofuels: A Review. *Biomass Bioenergy.* 35, 3748-3762.

[74] Deng, J., Wang G., J., Kuang, J.H., Zhang, Y.L. & Luo, Y.H. (2009). Pretreatment of Agricultural Residues for Co-Gasification via Torrefaction. *Journal of Analitical and Applied Pyrolysis.* 86, 331-337.

[75] Li, H., Liu, X., Legros, R., Xiaotao, B. T., and Lim, C. J. & Sokhansanj, S. (2012). Torrefaction of sawdust in a fluidized bed reactor. *Bioresource Technology.* 103, 453–458.

[76] Fang Z. (ed) (2013) Pretreatment Techniques for Biofuels and Biorefineries, Springer Science & Business Media.

[77] Rousset, P., Aguiar, C., Labbe, N. & Commandre, J-M. (2011). Enhancing the Combustible Properties of Bamboo by Torrefaction. *Bioresource Technology.* 102, 8225–8231.

[78] Prins, J.M., Ptasinski, J.K., and Janssen, J.J.G.F. (2006a). Torrefaction of wood Part 1. Weight kinetics. *Journal of Analytical and Applied Pyrolysis.* 77, 28–34.

[79] Prins, M. J., Ptasinski, J. K., and Janssen, J.J.G.F. (2006b). Torrefaction of Wood Part 2. Analysis of Products. *Journal of Analytical and Applied Pyrolysis.* 77, 35–40.

[80] Eseltine, D., Thanapal, S. S., Annamalai, K. & Ranjan, D. (2013). Torrefaction of Woody Biomass (Juniper and Mesquite) Using Inert And Non-Inert Gases. *Fuel.* 113, 379–388.

[81] Uemura, Y., Omar, W. N., Tsutsui, T. &Yusup Bt, S. (2011). Torrefaction of Oil Palm Wastes. *Fuel.* 8, 2585–2591.

[82] Phanphanich, M. & Mani, S. (2011). Impact of torrefaction on the grindability and fuel characteristics of forest biomass. *Bioresource Technology*. 102, 1246–1253.

[83] Bridgeman, T.G., Jones, J.M., Williams, A. &Waldron, D.J. (2010). An Investigation of the Grindability of Two Torrefied Energy Crops. *Fuel*. 89, 3911–3918.

[84] Chen, W-H. , Hsu, H.-C. ,Lu, K.-M. Lee, W.-J. & Lin, T.-C. (2011). Thermal Pretreatment Of Wood (Lauan) Block By Torrefaction And Its Influence On The Properties Of The Biomass. *Energy*. 5, 3012–3021.

[85] Chen, W-H. & Kuo, P.-C. (2010). A Study on Torrefaction of Various Biomass Materials and Its Impact on Lignocellulosic Structure Simulated by a Thermogravimetry. *Energy*.35, 2580-2586.

[86] Bridgeman, T.G. , Jones , J.M. Shield, I. & Williams, P.T. (2008). Torrefaction of Reed Canary Grass, Wheat Straw and Willow to Enhance Solid Fuel Qualities and Combustion Properties. *Fuel.* 87, 844–856.

[87] Arias, B., Pevida, C., Fermoso, J., Plaza, M.G., Rubiera, F. & Pis, J.J. (2008). Influence of Torrefaction on the Grindability and Reactivity of Woody Biomass, *Fuel Processing Technology.* 89, 169–175.

[88] Chen, W.-H. , Cheng, W.-Y. , Lu, K-M., Huang Y.-P. (2011). An Evaluation On Improvement of Pulverized Biomass Property For Solid Fuel Through Torrefaction. *Applied Energy.* 88, 3636–3644.

[89] Couhert, C., Salvador, S .& Commandre, J-M. (2009). Impact of Torrefaction On Syngas Production From Wood. *Fuel*. 88,2286-2290

[90] Neupane, S., Adhikari,S. , Wang Z, Ragauskas, A. J. & Pu, Y. (2015). Effect of Torrefaction on Biomass Structure and Hydrocarbon Production from Fast Pyrolysis. *Green Chemistry.* 17, 2406-2417.

[91] Zheng, A., Zhao, Z., Sheng, C., Huang, Z., Wang, X., He, F.& Li, H. (2013). Effect Of Torrefaction On Structure And Fast Pyrolysis Behaviour of Corncobs. *Bioresource Technology* 128, 370-377.

[92] Koppejan, J., Sokhansanj, N. S., Melin, S., Madrali, Ş., Status Overview of Torrefaction Technologies IEA Bioenergy Task 32 report Final Report.

[93] Evans, G. (2010). Techno-Economic Assessment of Biomass 'Densification' Technologies. *A project Report from NNFCC*. NNFCC Project 08-15.

[94] Sesli, M. & Yeğenoğlu, E.D. (2009). RAPD-PCR Analysis Of Cultured Type Olives in Turkey. *African Journal of Biotechnology.* 8, 3418–23.

[95] Özveren, U. & Özdoğan, Z. S. (2013). Investigation of the Slow Pyrolysis Kinetics Of Olive Oil Pomace Using Thermo-Gravimetric Analysis Coupled with Mass Spectrometry. *Biomass & Bioenergy*.58, 168-17.

[96] Vera, D., Jurado, F. & Carpio, J. (2011).Study of a Downdraft Gasifier and Externally Fired Gas Turbine for Olive Industry Wastes. *Fuel Processing Technol*ogies. 92, 1970–1979.

[97] Demirbaş, A., Güllü, D. , Çaglar, A. & Akdeniz, F. (1996). Estimation of Calorific Values Of Fuels From Lignocellulosics. *Energy Sources.* 19(8), 765-770.

[98] Prins, M.J., Ptasinski, J. K. & Frans J.J.G.F. (2006c). More Efficient Biomass Gasification via Torrefaction. *Energy*. 31, 3458–3470.

[99] Chen, W-H. & Kuo, P-C. (2011b). Isothermal Torrefaction Kinetics Of Hemicellulose, Cellulose, Lignin And Xylan Using Thermogravimetric Analysis. *Energy*. 36, 64-51.

[100] Bhaskar, T. & Pandey, A. (2015). Advances in Thermochemical Conversion of Biomass, *Ashok Pandey (Ed),* Recent Advances in Thermochemical Conversion of Biomass, Pages 3-30, Elsevier B.V.

[101] Bergman, P.C.A., Boersma, A.R.,Zwart, R.W.R. & Kiel, J.H.A. (2005). Torrefaction for Biomass Cofiring In Existing Coal-Fired Power Station, European Competition Network (ECN)Report, ECN-C–05–013.

[102] Schmidt, M.W.I., Skjemstad, J.O., Czimczik, C.I., Glaser, B. Prentice, K.M., Gelinas, Y. & Kuhlbusch, T.A.J. (2001). Comparative analysis of black carbon in soils. *Global Biogeochemical Cycles.* 15, 163–167.

[103] Nguyen, T.H., Brown, R.A., Ball & Ball W.P. (2004). An evaluation of thermal resistance as a measure of black carbon content in diesel soot, wood char, and sediment. *Organic Geochem*istry. 35, 217-234.

[104] Manyà, J.J. (2012). Pyrolysis for biochar purposes: a review to establish current knowledge gaps and research needs. *Environmental Science & Technology*. 46, 7939

[105] Jinliang, M. (1996). Soot formation during coal pyrolysis. PhD. Dissertation, Brigham Young University, Provo, UT.

[106] Kim, Y-H., Lee, S-M., Lee, H-W & Lee. J-W. (2012). Physical and chemical characteristics of products from the torrefaction of yellow poplar (Liriodendron tulipifera). *Bioresource Technology*. 116, 120–125.

[107] Capareda, S. C. (2011). Biomass Energy Conversion," Sustainable Growth and Applications in Renewable Energy Sources, Dr. Majid Nayeripour (Ed.), ISBN: 978-953-307-408-5, InTech.

[108] Syamsiro, M., Saptoadi, H., Tambunan, B.H. & Pambudi, N.A. (2012). A Preliminary Study On Use Of Cocoa Pod Husk As A Renewable Source Of Energy in Indonesia. *Energy for Sustainable Development.* 16, 74-77.

[109] European Standards (2005). Appliances, Solid Fuels and Fire Lighters For Barbecuing Part 2: Barbecue Charcoal and Barbecue Charcoal Briquettes. Requirements and Test Methods. BSEN 1860-2:2005.

[110] Patel, B. & Gami, B. (2012). Biomass Characterization and Its Use as Solid Fuel for Combustion. *Iranica Journal of Energy & Environment*. 3, 123-128.

[111] Wu, K-T., Tsai, C-J., Chen, C-S. & Chen, H-W. (2012). The Characteristics of Torrefied Microalgae. Applied Energy. 100, 52–57.

[112] Wannapeera, J., Fungtammasan, B. & Worasuwannarak, N. (2011). Effects of Temperature and Holding Time During Torrefaction on The Pyrolysis Behaviors of Woody Biomass, *Journal of Analytical and Applied Pyrolysis* 92, 99–105.

[113] Sarkar, M., Kumar, A., Tumuluru, J.S., Patil K.N. & Bellmer, D. D. (2014). Gasification Performance of Switchgrass Pretreatment with Torrefaction and Densification. *Applied Energy.* 127, 194-201.

[114] Daniyanto, Sutidjan, Deendarlianto & Budiman A. (2015). Torrefaction of Indonesian Sugar-Cane Bagasse to Improve Bio-Syngas Quality For Gasification Process. *Energy Procedia.* 68, 157 – 166.

[115] Yang, H., Yan, R., Chen, H., Zheng, C., Lee, D.H. & Liang, D.T. (2006). In-Depth Investigation Of Biomass Pyrolysis Based on Three Major Components: Hemicellulose, cellulose and lignin. *Energy Fuels.* 20, 388–393.

[116] Sadaka , S., Sharara, M. A. , Ashworth, A., Keyser, P. , Allen F. & Wright A. (2014). Characterization of Biochar From Switchgrass Carbonization. *Energies. 7,* 548-567.

[117] Giudicianni, P., Cardone, G. & Ragucci, R. (2013). Cellulose, Hemicellulose And Lignin Slow Steam Pyrolysis: Thermal Decomposition Of Biomass Components Mixtures, *Journal of Analytical and Applied Pyrolysis.* 100, 213–222.

[118] Kloss, S., Zehetner, F., Dellantonio, A., Hamid,R., Ottner, F., Liedtke, V., Schwanninger, M., Gerzabek, M. H. & Soja, G. (2012). Characterization of Slow Pyrolysis Biochars: Effects of Feedstocks and Pyrolysis Temperature On Biochar Properties. *Journal of Environmental Quality*. 41, 990–1000.

[119] Schimmelpfennig, S. & Glaser, B. (2012). One Step Forward Toward Characterization: Some Important Material Properties to Distinguish Biochars. *Journal of Environmental Quality*. 41, 1001–1013.

[120] Keiluweit, M., Nico, P.S., Johnson, M.G. & Kleber, M. (2010). Dynamic Molecular Structure of Plant Biomass-Derived Black Carbon (Biochar). *Environmental Science& Technology*. 44, 1247–1253.

[121] Volpe, M., D'Anna, C., Messineo, S., Volpe, R. & Messineo, A. (2014). Sustainable Production of Bio-Combustibles from Pyrolysis of Agro-Industrial wastes. *Sustainability*. 6, 7866-7882.

[122] Pandey, S. & Dhakal, R. P. (2013). Pine Needle Briquettes: A Renewable Source of Energy. *International Journal of Energy Sci*ence. 3, 254-260.

[123] Hmid, A., Mondelli, D., Fiore, S., Fanizzi, F. P., Chami, Z. A. & Dumontet, S. (2014). Production and Characterization Of Biochar From Three-Phase Olive Mill Waste Through Slow Pyrolysis. *Biomass & Bioenergy*. 71, 330-339.

[124] Liu, Z. G., Quek, A., Hoekman, S. K. & Balasubramanian, R. (2013). Production of Solid Biochar Fuel from Waste Biomass By Hydrothermal Carbonization. *Fuel*. 103, 943-949.

[125] Shaaban, A, Se, S.-M. Dimin, M. F., Juoi, J. M., Husin, M. H. M. & Mitan N. M. M. (2014). Influence of Heating Temperature and Holding Time on Biochar Derived from Rubber Wood Sawdust via Slow Pyrolysis. *Journal of Analytical and Applied Pyrolysis*. 107, 31-39.

[126] Sadeghi, H., Akbarpour, V. & Movaghatnezhad, K. (2010). Investigation of Olive Stones as Lignocellulose Material For Bioethanol Production. American-Eurasian Journal of Agricultural & Environmental Sciences. 8, 520-524.

[127] Dermechea, S., Nadour, M, Larroche, C., Moulti-Mati, F. & Michaud, P. (2013). Olive mill wastes: Biochemical Characterizations And Valorization Strategies. *Process Biochemistry* 48, 1532-1552.

[128] Cellatoğlu, N. & İlkan, M. (2015). Torrefaction of Solid Olive Mill Residue. *BioResources*. 10, 5876-5889.

[129] Cellatoğlu, N. & İlkan, M. (2016). Effects of Torrefaction on Carbonization Characteristics Of Solid Olive Mill Residue. *BioResources*. 11, 6286-6298.